Analysis and design of microwave components using metamaterials

A Dissertation submitted towards the partial fulfilment of
the requirement for the award of degree of

Master of Technology in
Microwave and Optical Communication Engineering

Submitted by
Gaurav Gupta
2K14/MOC/07

Under the supervision of
Dr. Priyanka Jain
Assistant Professor

Department of Electronics & Communication Engineering
and
Department of Applied Physics

Delhi Technological University
(Formerly Delhi College of Engineering)

JUNE 2016

DELHI TECHNOLOGICAL UNIVERSITY

Established by Govt. of Delhi vide Act 6 of 2009
(*Formerly Delhi College of Engineering)*
SHAHBAD DAULATPUR, BAWANA ROAD, DELHI-110042

CERTIFICATE

This is to certify that the work which is being presented in the dissertation entitled " **Analysis and design of microwave components using metamaterials** " is the authentic work of **Gaurav Gupta** under my guidance and supervision in the partial fulfillment of requirement towards the degree of Master of Technology in Microwave and Optical Communication Engineering jointly run by Department of Electronics & Communication and Department of Applied Physics in Delhi Technological University during the year 2014-16.

As per the candidate declaration this work has not been submitted elsewhere for the award of any other degree.

Dr. Priyanka Jain (Supervisor)
Assistant Professor
Department of Electronics & Communication

Prof. S. C. Sharma
(Head of Department)
Department of Applied Physics

Prof. Rajesh. Rohilla
(Head of Department)
Department of Electronics & Communication

DECLARATION

I hereby declare that all the information in this document has been obtained and presented in accordance with academic rules and ethical conduct. This report is my own, unaided work. I have fully cited and referenced all the material and results that are not original to this work. It is being submitted for the degree of Master of Technology in Microwave and Optical Communication Engineering at Delhi Technological University. It has not been submitted for any degree or examination in any other university.

Gaurav Gupta
M. Tech, MOCE
2K14/MOC/07

ABSTRACT

A theoretical investigation of the design of the basic unit cell structure for metamaterial has been carried out in this thesis work which shows a negative refractive index in a particular range of frequency. The basic unit cell structure for the metamaterial was studied and designed using a split-ring resonator which affected the permeability of the medium and the wire structure which affected the permittivity of the medium. This designed metamaterial structure showed a negative refractive index in the frequency range of 2.25 GHz to 2.5 GHz.

With this basic knowledge of metamaterials, a complementary split ring resonator (CSRR) loaded microstrip patch antenna was designed with a resonant frequency of 4 GHz. An array of CSRR is etched at the ground plane of the antenna affected the permittivity of the medium and helped in achieving size miniaturization of a microstrip patch antenna. The CSRR loaded patch antenna showed a size reduction of 33% when compared to the size of a conventional microstrip patch antenna designed at 4 GHz. Then a double-superstrate configuration (DSC) was used to enhance the directivity and the gain of the designed CSRR loaded microstrip patch antenna at 4 GHz. The thickness of two superstrates and the air gaps were optimized which increased the directivity of the antenna by 2.51 dBi and its gain increased by 1.87 dB. Thus the CSRR loaded patch antenna with DSC helped in achieving size miniaturization as well as improving the performance parameters of the designed patch antenna.

Then a CSRR loaded wideband bandpass filter with a capacitive gap in the transmission line was analyzed and designed. The designed bandpass filter has its lower cut-off frequency equal to 2.026 GHz and the upper cut-off frequency equal to 4.775 GHz. The bandwidth of the designed filter was calculated equal to 2.750 GHz and its central frequency equal to 3.375 GHz.

LIST OF PUBLICATION

- Gaurav Gupta, Priyanka Jain, "Miniaturization and directivity enhancement of a microstrip patch antenna using complementary split ring resonators and double-superstrate configuration", IEEE First International Conference on Power Electronics, Intelligent Control and Energy systems, IEEE ICPEICES 2016, DTU, 4-6 July, 2016.

ACKNOWLEDGEMENT

I take this opportunity as a privilege to thank all the individuals without whose support and guidance I could not have completed my project successfully in this stipulated period of time.

First and foremost I would like to express my deepest gratitude to my supervisor **Dr. Priyanka Jain**, Asst. Professor, Department of Electronics and Communication, for her valuable support, patience, guidance, motivation and encouragement throughout the period this work was carried out. I would also like to thank **Kamlesh Patel**, Asst. Professor, DU for his valuable time and interest in this project. I am grateful to both for closely monitoring my progress and providing me with timely and important advice, their valued suggestions and inputs during the course of the project work.

I am deeply grateful to the **Prof. S. C. Sharma** (Head of the Applied Physics Department) and **Prof. Prem R. Chadha** (Head of the Electronics and Communication Engineering Department) for their support and providing best educational facilities.

I also wish to express my heartfelt thanks to the classmates as well as staff at Department of Electronics & Communication and Department of Applied Physics of Delhi Technological University for their goodwill and support that helped me a lot in successful completion of this project.

Finally, I want to thank my parents and friends for always believing in my abilities and for always showering their invaluable love and support.

Gaurav Gupta
M. Tech. MOC
2K14/MOC/07

LIST OF CONTENTS

LIST OF FIGURES

LIST OF TABLES

CHAPTER 1
Introduction

1.1 Overview and motivation

In the last few decades, there has been an increased interest for the study of metamaterials and its related application in the scientific community. These metamaterials components are made artificially to exhibit exceptional properties which are not readily found in the nature materials. The materials exhibits a property characterized by the negative permittivity and negative permeability simultaneously in a particular range of microwave as well as optical frequencies. This type of medium which showed negative refractive index for a particular range of frequency was first discovered and proposed in 1968 and were termed as left-handed medium as they followed a left-hand rule for the wave propagation instead of right-hand rule for the wave equation formed by the E (electric field), H (magnetic field) and k (propagation constant) vectors. These left-handed materials showed a number of unique properties using a negative refractive index which supported backward wave propagation. Recently, metamaterials have been in great interest for the upcoming technologies and these properties of metamaterials have been very useful in designing of microwave components like antennas, filters, couplers, power dividers, etc. The property exhibited by the left-handed materials have also been used in designing invisible cloaks, light and sound filtering devices, superlenses, wave absorbers and various other microwave passive components which are being developed using the current technology. Also, these metamaterials are being used to enhance the performance, design approach and characteristics of the microwave components in the wireless communication systems.

In the last few decades mobile radio and wireless communication have been developed rapidly and widely in the modern world. The demand for high performance in mobile and wireless communication systems and in applications like aircraft, spacecraft, satellite and missile applications where the size, cost, weight, performance, ease of installation and low profile antennas are required. Many applications require similar specifications for wireless and radio communication systems. Thus to meet these requirements, microstrip patch antennas were designed for the communication systems. These microstrip antennas are conformable to planar and non-planar surfaces, low profile, simple and inexpensive to manufacture using printed circuit technology, compatible with MMIC designs, mechanically robust when mounted in rigid surfaces and very versatile in terms of resonant frequency, pattern and impedance. As the demand for wireless communication is rapidly increasing, the need for the smaller size microstrip patch antennas with better performance characteristics like gain, directivity and bandwidth are also required in the systems. The various technologies and methods have been proposed in the past few years for improving the performance characteristics and reducing the size of antennas for increasing the packing efficiency along with the better performance of the whole radio/wireless device used. This in turn saves the materials required by the device and thus the cost for manufacturing a device. Also metamaterial concepts are widely being used in current technology for designing a small size patch antennas with better performance result.

Nowadays, filters play a very important role in many radio frequency circuits and in wireless communication systems such as radar, radio devices for communication, navigation systems, sensing and medical instruments. These filters are used to pass a certain band of frequency and reject the remaining band of frequency based on the filter response and the communication needs. Thus more practically, filters are designed to select and reject or to separate and combine the signals at various frequencies. Filters which are generally designed by using lumped elements like capacitor and inductors are bulky, costly and difficult to use practically and thus making them hard to implement in wireless devices. To solve these problems, filters were implemented using microstrip technologies which were cheap, easy to manufacture and can be easily integrated with the different compact circuits. With the emerging wireless communication technologies, the increasing numbers of user have led to greater demand for bandwidth and the data rates. Thus in wireless communication system, the wider range of frequency is required to support high data rates and large number of users, has led to the growth of wideband band-pass, band-stop, low-pass and high-pass filters in the emerging technology for the various wireless and radio communication systems. Also, as the application of filters are being increased in the various microwave components, the filters with more stringent requirements such as low insertion loss, linear phase, high selectivity, low cost for manufacture, light weight and small size has increased. Thus compact size microstrip filters are required so that the designed communication devices are small in size having a high packing efficiency and thus reducing the cost and material required for manufacturing the component. The introduction of metamaterial concepts has also allowed conventional approach of designing a microstrip filter to a newer technology design filters with improved performance characteristics and smaller size.

1.2 Thesis objectives

The main objective of the thesis are given as follows:

- Study the basics of metamaterials, understanding the unique properties exhibited by them and how these materials are practically realized with their applications.
- Design a basic unit cell structure for a metamaterial and analysing the simulation result to obtain negative refractive index region for the unit cell where the metamaterials exhibit left-hand property.
- Study the basic concepts of microstrip patch antennas with their advantages and disadvantages, the various method of analyzing and their feeding techniques.
- Design a conventional patch antenna with inset feeding mechanism and simulate the design to obtain the various performance parameters like resonant frequency, directivity, gain, bandwidth, power pattern and voltage standing wave ratio (VSWR).
- Understanding the concept of complementary split-ring resonators.
- Design and simulation of a CSRR loaded microstrip patch antenna and obtain various performance parameters.
- Improving the characteristic of a CSRR loaded microstrip patch antenna using double-superstrate configuration (DSC).
- Design and simulation of a CSRR loaded microstrip patch antenna with DSC and obtaining performance parameters.

- Fabrication and testing of a CSRR loaded microstrip patch antenna and verify the results obtained during simulation.
- Study different types of filters and their characteristics response.
- Design and analysis of a CSRR loaded bandpass filter and the equivalent lumped element model for the designed bandpass filter.
- Simulation of a CSRR loaded bandpass filter to compute the passband and stopband and hence the bandwidth of the designed filter.
- Fabrication and testing of a CSRR loaded wideband bandpass filter and verify the result obtained during simulation.

1.3 Thesis organisation

The outcome of the work carried out in this thesis is divided into 5 chapters. Chapter 1 is titled as "Introduction" and consists of overview and motivation for the thesis work along with the objectives of the thesis.

Chapter 2 is titled as the "Basic unit cell structure for a metamaterial" and consists of introduction to metamaterials, defining the left-handed materials, realizing the metamaterials using symmetric wire structure and split-ring resonators (SRR), and the designing and simulated result of unit cell structure.

Chapter 3 of the thesis is titled as "Microstrip patch antenna based on metamaterials" which includes the basic introduction to microstrip patch antennas with their advantages and disadvantages, the methods for analyzing and the different feeding techniques used for feeding microstrip patch antennas. The next section deals with the designing and simulation of a conventional microstrip patch antenna at 4 GHz. The various performance characteristic are measured for the designed patch antenna. The next section deals with the designing of a patch antenna using CSRR at the same resonant frequency, i.e. 4 GHz. The simulation results are shown to measure the performance parameters of the proposed antenna. The next section of this chapter deals with the designing and simulation result of a CSRR loaded patch antenna with DSC to improve the performance parameters like gain and directivity of the antenna. The comparative analysis of the results obtained by simulating various designed patch antennas are formulated in the form of a table with the conclusions made from the comparison table. Finally, the CSRR loaded microstrip patch antenna is fabricated and tested experimentally whose resonant frequency is 4 GHz.

Chapter 4 of the thesis is titled as "Microstrip bandpass filter based on metamaterials" which gives a brief introduction to the filters and their characteristic responses. The lumped equivalent models for the filters are discussed in this chapter. The next section of this chapter deals with the designing of the bandpass filter using a CSRR. The simulated result for the designed bandpass filters is used to find the lower and upper cutoff frequency using S-parameter and hence the bandwidth of the filter. Finally, the CSRR loaded bandpass filter is fabricated and tested experimentally to verify the results obtained during simulation.

Chapter 5 is the conclusion of the work done in this thesis with some suggestion to the future work that can be done related to this field of microwave.

CHAPTER 2
Basic unit cell structure for a metamaterial

2.1 Introduction

Left-handed materials which are also called as metamaterials are recently being studied because of their unique physical properties and exceptional behaviors. These metamaterials are recently used in many novel applications like compact and efficient antennas, waveguides and microwave components like filter, negative refractive index lenses, invisibility cloaks, invisible submarines, and many other microwave and optical devices. Negative refractive index of the EM waves is a very extraordinary phenomenon exhibited by left-handed metamaterial structures which make them more useful for designing the microwave components. The backward Cerenkov radiation and the Doppler shift are also some exceptional properties which arises from a left-handed metamaterials. The magnetic and the electric properties are determined by the magnetic permeability and electric permittivity of the material respectively. The permittivity 'ε' and the permeability 'μ' together determine the property of a material. Generally, 'ε' and 'μ' are both positive for an ordinary material, while permittivity can be negative in some materials like metals where the permittivity has a negative value below the plasma frequency and some ferrites material have negative permeability for certain range of frequency. However, for metamaterials which are called left-handed materials (LHM), both the effective permeability 'μ_{eff}' and the effective permittivity 'ε_{eff}' possess a negative value. In these materials, the refractive index 'n' is less than zero and thus the phase velocity of the wave is in opposite direction of the group velocity of a wave such that the direction of propagation of the wave is reversed with respect to the energy flow of the wave [1]. This property of negative refractive index was first proposed by a Prof. Veselago in the year 1968 who also figured various interesting and unique optical properties for negative index mediums [1].

The negative effective permittivity of a medium in microwave frequency range can be realized using an array of symmetric thin wire structure. Dielectric permittivity can take a negative value where EM waves cannot propagate below the plasma frequency in the medium [2-4]. Electric charges are responsible for electrical response in a dielectric medium but due to lack of magnetic charges which are analogous to electric charges are more difficult to obtain in a medium which has negative magnetic permeability. Pendry et al. suggested that a periodic array of split-ring resonators can exhibit a negative permeability in the frequency range close to the magnetic resonant frequency of the material [5]. In 2000, Smith et al. demonstrated that a left-handed material can be implemented by stacking a split ring resonator (SRR) and an array of thin wire structure which was called as composite metamaterials [6,7].

The analyses and theoretical calculation have showed that the refractive index for the medium is negative when both permittivity and permeability are simultaneously negative [8]. Also, Shelby et al. [9] experimentally verified the negative refraction in the left-handed materials. Composite metamaterials shown in Fig. 2.1 (a) are the materials which can give rise to negative refractive index medium. Negative refractive index medium can be achieved

using 2D photonic crystals as shown in Fig. 2.1 (b). The experimental observations [10-12] and the theoretical studies [13-15] confirm the existence of a negative refractive index.

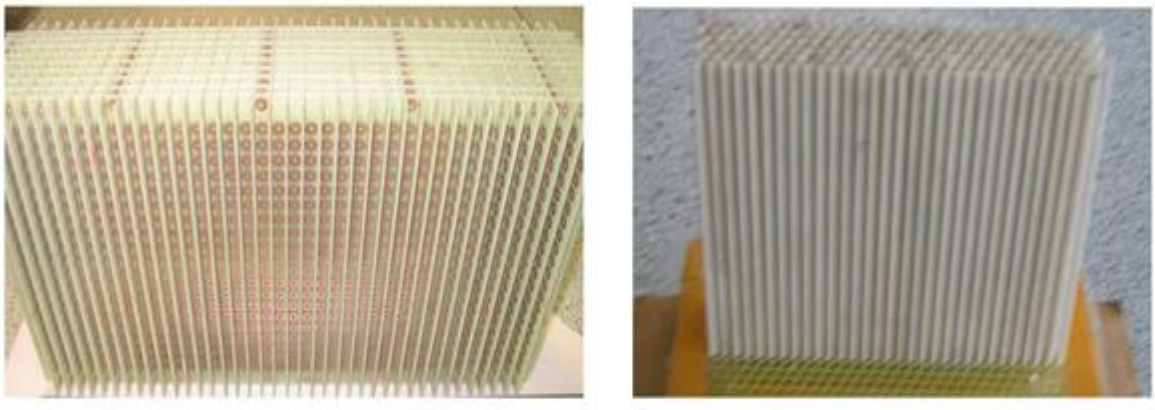

(a) ***(b)***

Fig 2.1: *Examples of Negative refractive media* ***(a)*** *Left-handed metamaterials,* ***(b)*** *2D Photonic Crystals. (Taken from Ref. [16])*

Reversal of Doppler effect [17], Cerenkov radiation [18] and backward wave propagation [19] are some of the interesting physical phenomena which are exhibited by a negative refractive index medium and can be used in several applications like filter design[20,21], enhancing the performance of antenna [22,23], electromagnetic absorption reduction [24,25], invisibility cloaking [26,27], polarization rotator [28], etc. Moreover, structures which has negative permeability have been used for magnetic resonance imaging [29]. These metamaterials which tend to exhibit negative refractive index are also called as double-negative materials (DNG) because they possess negative permeability and negative permittivity simultaneously for a certain range of frequency and hence are very useful for upcoming technologies in the designing better microwave devices and components.

2.2 Defining left-handed metamaterials

To have a clear understanding of left-handed medium or metamaterials, we should first have a clear knowledge of right-hand rule in the electromagnetism. The right-hand rule for EM waves states that when the direction of the electric field '*E*' is represented by the thumb and the magnetic field '*H*' by the index finger of the right hand placed at 90˚ to each other, then the middle finger perpendicular to both the fingers will give the direction of the propagation of the wave, thus normal to both the E-field and the H-field. All electromagnetic waves follow this rule and is given by the Eq. 2.1:

$$\vec{E} \times \vec{H} = \vec{S} \tag{2.1}$$

$\vec{E}$ is the electric field intensity, $\vec{H}$ is the magnetic field intensity and $\vec{P}$ represents the Poynting vector and the direction of propagation of energy and the wave.

The Maxwell's equations which describe the electromagnetic wave are given in Eq. 2.2 through Eq. 2.5:

$$\nabla \times \vec{E} = -\frac{\partial \vec{B}}{\partial t} \tag{2.2}$$

$$\nabla \text{ x } \vec{H} = J_c + \frac{\partial \vec{D}}{\partial t} \tag{2.3}$$

$$\nabla . \vec{D} = \rho \tag{2.4}$$

$$\nabla . \vec{B} = 0 \tag{2.5}$$

Here $\vec{B}$ is the magnetic flux density, $\vec{D}$ is the electric flux density and J_c is the electric current density.

The first two equations Eq.2.2 and Eq. 2.3 take the form:

$$\vec{k}\text{x}\vec{E} = -\frac{\omega}{c}\mu\vec{H} \tag{2.6}$$

$$\vec{k}\text{x}\vec{H} = \frac{\omega}{c}\mu\vec{E} \tag{2.7}$$

Where '$\vec{k}$' is the propagation constant vector along the direction of phase velocity of the wave, c is the speed of light and ω is the angular frequency of the wave.

It is evident that when a medium has negative permittivity and negative permeability, the wave will have its phase velocity anti-parallel to the direction of wave propagation or in the direction of flow of energy. Thus we can say that the wave has a negative phase velocity in that medium. Although, the direction of the energy propagated is from the sender to the receiver, the phase moves in the opposite direction and is illustrated by the Fig. 2.2 shown.

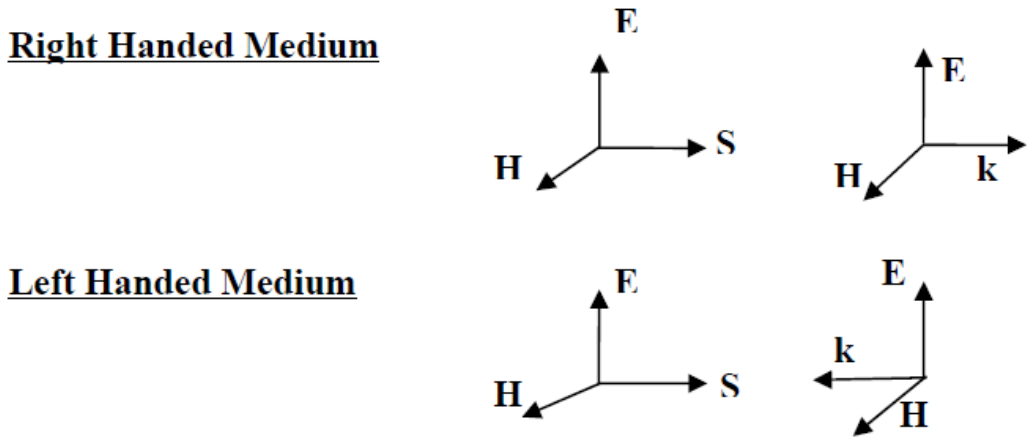

Fig. 2.2: *The wave propagation in Right handed and Left Handed System.*

As we know that the refractive index of any material can be defined by the square root of the product of its permeability and the permittivity and is given by Eq. 2.8:

$$n = \sqrt{\mu\varepsilon} \tag{2.8}$$

Here, 'n' is the refractive index of the material while 'μ' is the permeability of the material and 'ε' is the permittivity of the material.

From the above expression it might be thought that the negative permeability and negative permittivity will not give rise to negative refractive index medium. However, the negative refractive index is due to the square root of the product in this case and has been

proved by Ziolkowski [30] that the square root of the product of permittivity and permeability is correct and leads to give negative refractive index. The mathematical proof is briefly given in this section below. As we know that the expression for wave number 'k', the wave speed 'v' and the wave impedance can be represented in the following equations:

$$k = \omega\sqrt{\mu\varepsilon} = k_o n \tag{2.9}$$

$$k_o = \omega\sqrt{\mu_o\varepsilon_o} \tag{2.10}$$

$$n = \pm\sqrt{\mu_r\varepsilon_r} \tag{2.11}$$

$$\vartheta = \frac{\omega}{k} = \frac{1}{\sqrt{\mu\varepsilon}} = \frac{1}{\sqrt{\mu_r\varepsilon_r}\sqrt{\mu_o \in_o}} = \frac{c}{\sqrt{\mu_r\varepsilon_r}} = \frac{c}{n} \tag{2.12}$$

$$Z = \frac{E_o}{H_o} = \frac{k}{\omega\varepsilon} = \sqrt{\frac{\mu}{\varepsilon}} = \xi Z_o \tag{2.13}$$

$$\xi = \sqrt{\frac{\mu_r}{\varepsilon_r}} \tag{2.14}$$

Here we may notice that the refractive index 'n' will be positive even though μ and ε being negative. But for double negative material (DNG), the refractive index is negative and can be proved when the permittivity and the permeability of the medium is calculated in terms of magnitude and phase as:

$$\varepsilon_r = |\varepsilon_r| e^{j\emptyset_\in} \text{ , where } \emptyset_\varepsilon = \left(\frac{\pi}{2}, \pi\right] \tag{2.15}$$

$$\mu_r = |\mu_r| e^{j\emptyset_\mu} \text{ , where } \emptyset_\mu = \left(\frac{\pi}{2}, \pi\right] \tag{2.16}$$

Then the wave impedance and the refractive index of the medium can be written as:

$$n = \sqrt{|\mu_r\varepsilon_r|}\, e^{j\emptyset_n} \tag{2.17}$$

$$\xi = \sqrt{|\frac{\mu_r}{\in_r}|}\, e^{j\emptyset_\xi} \tag{2.18}$$

Where the phase for n and ξ would be:

$$\emptyset_n = \frac{1}{2}(\emptyset_\mu + \emptyset_\varepsilon) \in \left(\frac{\pi}{2}, \pi\right] \tag{2.19}$$

$$\emptyset_\xi = \frac{1}{2}(\emptyset_\mu - \emptyset_\varepsilon) \in \left(-\frac{\pi}{4}, \frac{\pi}{4}\right] \tag{2.20}$$

For a positive square root choice.

$$\emptyset_n = \frac{1}{2}(\emptyset_\mu + \emptyset_\varepsilon) - \pi \in \left(-\frac{\pi}{2}, 0\right] \tag{2.21}$$

$$\emptyset_\xi = \frac{1}{2}(\emptyset_\mu - \emptyset_\varepsilon) + \pi \in \left(\frac{3\pi}{4}, \frac{5\pi}{4}\right] \tag{2.22}$$

For a negative square root choice.

Irrespective of the choice of the root, the refractive index for the medium turns out to be negative. Upon substituting the negative refractive index in the wave equation, we find that the poynting vector and the wave vector for a wave in this type of medium will be anti-parallel and hence will be exhibiting left-handed properties. In these medium or materials, where refractive index is negative, the wave travelling from air into the medium will bend towards the same side of the normal as the incident ray. This phenomenon is shown in the Fig. 2.3 below.

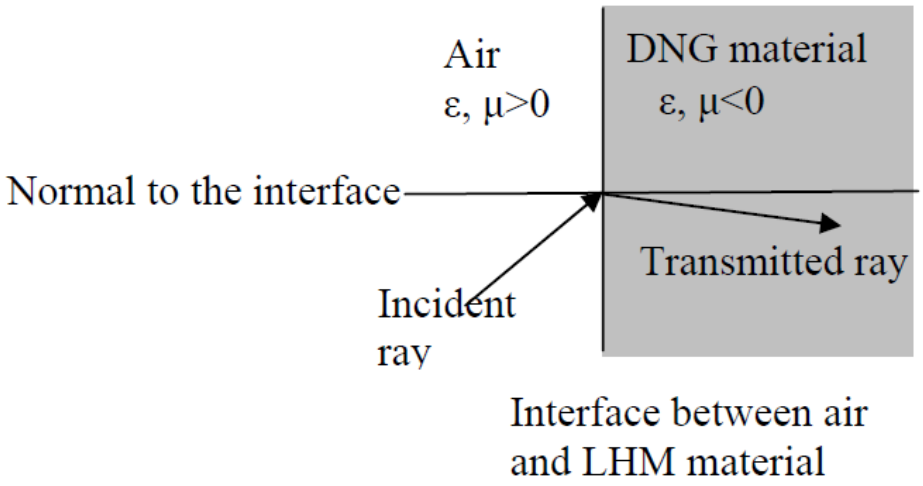

Fig. 2.3: *Refraction at DPS-DNG interface.*

This property of negative refractive index materials was very useful in realizing a perfect lens as suggested by Pendry et al. [31]. Veselago said that it was important for a material to have both the permeability and permittivity of the material to be either negative or positive. However, recent research has proved the mediums with only one parameter (permittivity or permeability) are realizable and the utility of the mediums with only one parameter can have a real negative value. These materials are called as single negative materials (SNG) and can have a negative permittivity or a negative permeability value. Some examples of negative permittivity materials are plasmonic materials like noble metals in the visible or infrared region. While materials like ferromagnets and anti-ferromagnets can have negative permeability near the ferromagnetic resonance region. The dispersion relation in an isotropic medium can be given as:

$$k^2 = \omega^2 \mu \varepsilon \tag{2.23}$$

The dispersion relation shows that a wave can propagate or decay depending upon the signs of ε and μ. The Fig. 2.4 shows the four quadrants and defines the classification of the materials based upon the value of permittivity and permeability.

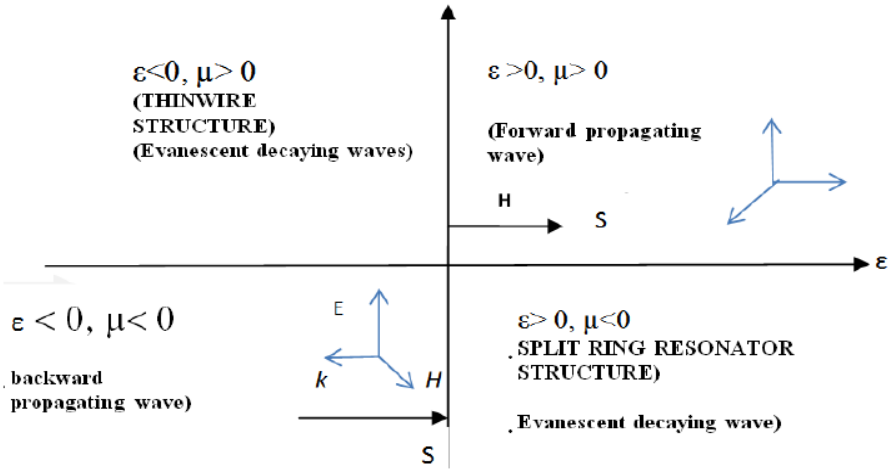

Fig. 2.4: *Classification of materials based on ε and μ.*

The first quadrant shows a medium in which both the permittivity and permeability is positive and the medium exhibits a forward propagating wave. The second quadrant shows a material in which the permittivity is negative with positive permeability where the waves are evanescent in nature and decay as they propagate. They are generally implemented by thin wire structure using some noble metals. The third quadrant defines the materials which has both negative permittivity and negative permeability and exhibits a property of backward wave propagation. The fourth quadrant represents the materials which show negative permeability and are generally implemented artificially using a split-ring resonators or some naturally occurring materials like ferromagnets and anti-ferromagnets. The fourth quadrant also has an evanescent decaying wave as the wave propagates in the particular direction.

2.3 Realization of left-handed metamaterials

Metamaterials are artificially designed materials as they don't exist in nature. These materials are realized by embedding periodic metallic structures in a dielectric substrate. Metamaterials are complex structure which alters the properties of a bulk composite medium and tends to exhibit negative permittivity and negative permeability for a certain range of frequency band. Left-handed materials (metamaterials) were first practically realized by Schultz et al. [6] by using a periodic array of spaced conducting non-magnetic split ring resonators and an array of symmetric continuous wires that showed negative permeability 'μ_{eff}' and negative permittivity 'ε_{eff}' respectively in a particular rang of microwave frequency.

Earlier, some attempts were made to realize materials which showed negative permittivity. A mesh of conducting wires was realized as a structure which gave negative permittivity for a certain range of frequency. Pendry et al. [5] in the year 1999 showed that an array of conducting non-magnetic SRR can modify the permeability of the host medium to give a negative permeability as a function frequency. Schultz et al. [6] combined the array of composite wire structures and an array of SRR to construct a negative refractive index medium in which both the permittivity and permeability parameters had a negative value which varied as a function of frequency. By combining the wire structure and split ring resonators, a formula was proposed which showed the variation of propagation constant 'k' as a function of frequency is given in Eq. 2.24.

$$k^2 = \frac{(\omega^2 - \omega_p^2)(\omega^2 - \omega_b^2)}{c^2 - (\omega^2 - \omega_o^2)} \tag{2.24}$$

The above equation showed that the range of propagation constant 'k' which is real extends from ω_o to $\omega_b = \omega_o/\sqrt{(1-F)}$. Here '$F$' is the fractional area enclosed by the rings and ω_o is the resonant frequency of the split ring resonator and ω_b is the plasmonic frequency of the ring resonator. The periodic structure can give a uniform isotropic alteration in the properties of the base material if the size of the designed unit cell for these periodic structures is kept smaller than the smallest wavelength in the bandwidth which is kept under consideration for a medium. Thus for a typical electromagnetic wave of frequency 'ω', the constraint on the dimension of the unit cell structure is given in Eq. 2.25 as:

$$a \ll \frac{2\pi c}{\omega} \tag{2.25}$$

Several attempts were made to establish a theory and build materials based on the composite material concept [32-34]. Since the concept of composite material gives a high degree of freedom to design the material for various applications, numerous new designs were explored for these composite material structures. 2-D and 3-D structures were designed and their properties were analyzed along with their effect on the bulk composite medium were also studied based on various crucial parameters like the size of lattice, arrangement of structures, spacing between the structures, compositions, material used etc [35]. The Fig. 2.5 shown shows a generic view of metamaterials made up of periodic structures which results in an effective bulk permeability and permittivity for a composite medium.

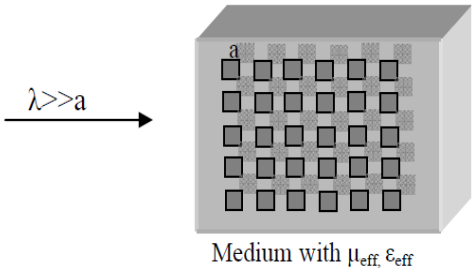

Fig. 2.5: *Generic view of a composite medium with periodically place structures constituting metamaterials. (Taken from Ref. [36])*

The array of wire strips causes negative permittivity and the split ring resonators which exhibit negative permeability are discussed in the coming section in this chapter. This section also deals that how the split ring resonator and the wire strips contribute in understanding and designing of a composite medium.

2.3.1 Negative permittivity in the medium using metal wire geometry

Thin metallic wires can be used to alter the effective permittivity of the host medium when the medium is excited appropriately with proper boundary conditions. In the year 1998, Pendry [5] calculated the long wavelength limit for transverse dielectric as a function of a composite medium made up of long metallic cylinders in homogeneous medium based on photonic gap structures. The geometry for the periodically placed wire strips and the variation

of the real part of the electric permittivity as a function of frequency is shown in the Fig. 2.6 in a composite medium.

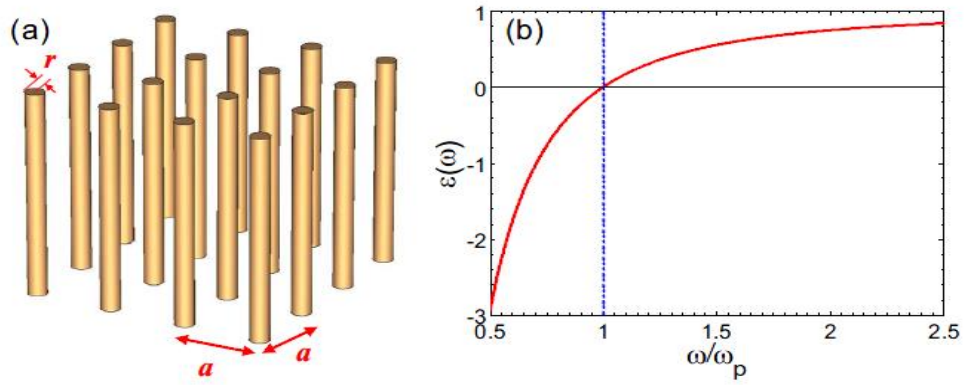

Fig. 2.6: (a) *Geometry for a medium with metallic wire strips,* ***(b)*** *Variation of real part of electric permittivity as a function of frequency. (Taken from Ref. [37])*

It was proposed and then proved that the composite structure can be replaced by an effective homogeneous medium that gives the dispersion relation of the effective permittivity for the composite medium can be derived from Eq. 2.26 as mentioned in [38]:

$$\varepsilon_{eff}(\omega) = \frac{k^2 c^2}{\omega^2} \tag{2.26}$$

The effective permittivity can be represented by a Drude dielectric function which varies as a function of frequency and can be controlled by geometry of the wire. The Drude dielectric function is given in Eq. 2.27:

$$\varepsilon_{eff}(\omega) = 1 - \frac{\omega_p^2}{\omega^2 + i\omega\gamma} \tag{2.27}$$

Here 'ω_p' is the bulk plasma frequency of the metal and 'γ' represents the inverse electron relaxation time. The plasma bulk frequency 'ω_p' for the metal wire structure is given by the Eq. 2.28:

$$\omega_p^2 = \frac{ne^2}{\varepsilon_o m_{eff}} \tag{2.28}$$

Where 'n' is the electron density, 'm_{eff}' is the effective mass of the electron and 'e' is the electronic charge and 'ε_o' is the relative permittivity of free space.

Considering the wire geometry for calculating the effective permittivity as a function of frequency, the plasma frequency of the wire structure used in the designing of a composite material is given in the Eq. 2.29 as:

$$\omega_p^2 = \frac{2\pi c_o^2}{a^2 \ln\left(\frac{a}{r}\right)} \tag{2.29}$$

Here 'r' is the radius of the wire structure, 'a' is the spacing between the wire strip and 'c_o' is the speed of light in free space, i.e. 3×10^8 m/s.

2.3.2 Negative permeability in the medium using split ring resonators

As we have already discussed, that the split-ring resonators are kept in the host medium which causes the permeability of the bulk composite medium to vary as a function of frequency. This variation of permeability as a function of frequency becomes negative for a certain range of frequency. This region of negative permeability is generally observed between the resonant the resonant frequency and the plasma frequency of the SRR. The design and geometry of the SRR is simple and has a split in the rings of a resonator, as the name suggest. The splits causes the ring to resonate at a much higher frequency than the closed ring of the same shape and size. Generally, a closed ring is a quarter wavelength in size at its resonant frequency. However, introducing a split in the ring causes the size to be reduced to one-tenth of the wavelength and thus enables the rings to resonate at a much higher frequency than the closed rings. The magnetic effect produced by the split ring resonators is enhanced by the capacitive elements. The splits in the ring structure gives the desired capacitive effect in the resonator circuit although the current in rings of the split ring resonator does not have a closed patch for current to flow, however the strong capacitance between the two concentric rings allows the flow of current. Since the split ring resonator has a capacitance and inductance in the structure, the effective permeability shows a resonant form. The resonant frequency arises due to the resonant interaction between the inductance of the structure and the capacitance which arises due to the gap in the structure. During resonance, the electromagnetic energy is being shared between the electrostatic field and the magnetic field with the capacitive and inductive elements in the structure respectively. This gives an idea that the effective permeability of the structure is above and around the resonance frequency. The Fig. 2.7 shows a typical structure of a split-ring resonator with its dimension specifications. In a square split-ring resonator, 'a' is the length of the outer-most dimension, while for a circular split-ring resonator 'r_{ext}' is the external radius. The 'r_o' of the split-ring resonator is the average radius of the two concentric rings. The width of the each rings is represented by 'c' and their separation is represented as 'd'. The split in the two rings in represented by 'g'.

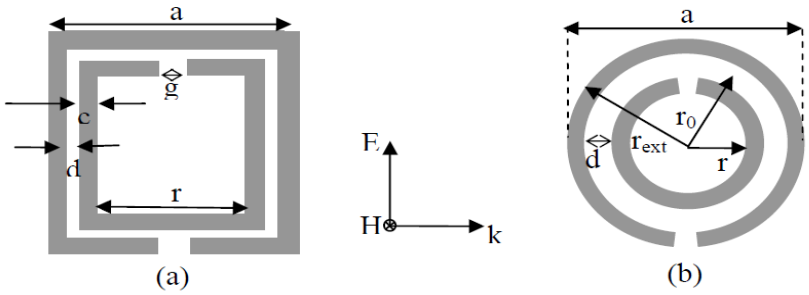

Fig. 2.7: *Split Ring Resonator (SRR) Configurations.*
(a) *Typical square split ring resonator*
(b) *Circular split ring resonator*

The effective permeability 'μ_{eff}' of the split ring resonator can be expressed using the Eq 2.30 [5]:

$$\mu_{eff} = 1 - \frac{F}{1 + \frac{j2\sigma}{\omega r \mu_o} - \frac{3}{\pi^2 \mu_o \omega^2 C r^3}} \tag{2.30}$$

Here '*F*' is the fractional volume given by the Eq. 2.31 of the unit cell which is defined as the ratio of the area covered by the interior of the concentric rings having a radius 'r' and the capacitance '*C*' to the lattice dimension.

$$F = \frac{\pi r^2}{a} \tag{2.31}$$

The capacitance 'C' for the split ring resonator is given by the Eq. 2.32 given below.

$$C = \frac{\varepsilon_o}{d} = \frac{1}{dc_o^2 \mu_o} \tag{2.32}$$

The effective permeability for the structure begins to diverge from a certain resonant frequency 'ω_o' and is given by the Eq. 2.33 below.

$$\omega_o = \sqrt{\frac{3}{\pi^2 \mu_o C r^3}} = \sqrt{\frac{3dc_o^2}{\pi^2 r^3}} \tag{2.33}$$

And the plasmonic frequency for the resonator structure is given by the Eq. 2.34 given below.

$$\omega_{mp} = \sqrt{\frac{3}{\pi^2 \mu_o C r^3 (1 - F)}} = \sqrt{\frac{3dc_o^2}{\pi^2 r^3 \left(1 - \frac{\pi r^2}{a^2}\right)}} \tag{2.34}$$

From the above equation it can be seen that the plamonic frequency of the structure depends upon the fractional volume not enclosed by the inner ring. The dispersion relation of the effective permeability of the split ting resonators has a gap in the range between the resonant frequency and the plasmonic frequency where the effective permeability of the medium is negative. Also, the square geometries has greater area than the circular one having the same dimension, thus square geometries are generally used for designing the split ring resonator. The variation of the permeability for the split ring resonator over a range of frequency is shown in the Fig. 2.8.

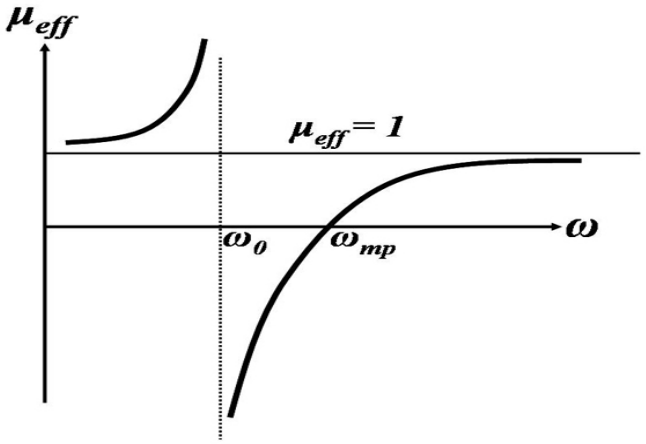

Fig. 2.8: *Variation of effective permeability as a function of frequency.(Taken from Ref. [39])*

From the figure it is evident that the split ring resonators designed exhibits a negative permeability over a range of frequency which is between the resonant frequency 'ω_o' and the magnetic plasma frequency 'ω_{mp}'. This property of the split ring resonators is used in designing a composite medium which shows the properties of left-handed materials and has a negative refractive index region which varies as a function frequency.

2.3.3 Composite DNG medium using split ring resonators and wire structures

A double negative material can be fabricated using split ring resonators and the metal wire structures in a lattice design which shows a negative refractive index. The implemented unit cell structure which exhibit double negative medium is shown in the Fig. 2.9 below.

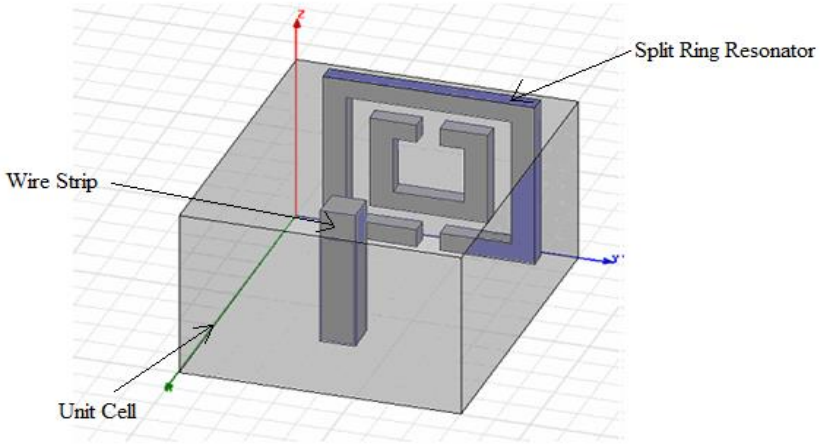

Fig. 2.9: *Unit cell structure for metamaterials. (Taken from Ref. [40])*

The wire strip in the unit cell of the metamaterial structure is placed in such a way that the electric field passes along its axis, while the split-ring resonators are placed in such a way that the magnetic field is parallel to the axis of the rings. The figure above generally deals with the 1-D structure of the composite medium. But in general, the composite medium can be 1-D, 2-D and 3-D structures which are illustrated in the Fig. 2.10 below.

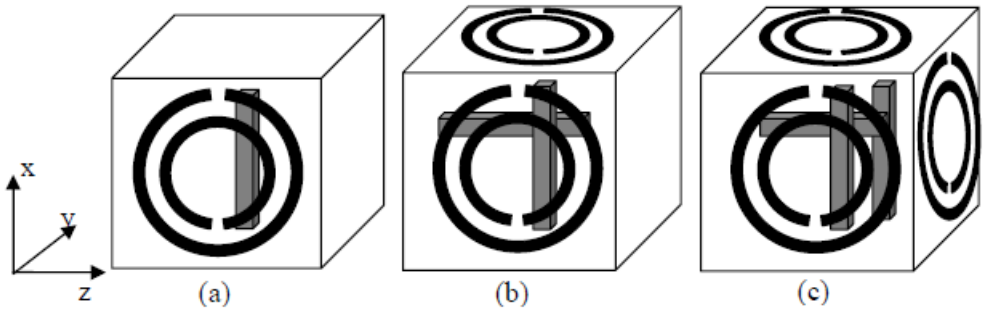

Fig. 2.10: (a) *1-D structure,* ***(b)*** *2-D structure,* ***(c)*** *3-D structure for composite medium. (Taken from Ref. [41])*

These composite medium can be realized artificially and can be used for wide number of microwave applications like in designing of filters, absorbers, superlens, cloaking devices, couplers, antennas with the enhanced properties and compact size.

2.4 Design and simulation of a metamaterial unit cell structure

A basic unit cell structure for a metamaterial is designed in the CST Microwave Studio and its simulation is done which shows the range of frequencies in which the permeability and the permittivity of the structure is negative which resembles the property of a metamaterial and thus showing the negative refractive index in a particular range of frequency. Sir J.B Pendry proposed that a split ring resonators (SRRs) designed can be used to exhibit negative permeability 'μ' around its resonance frequency. The continuous wires array structure exhibit a negative permittivity 'ε' up to the plasma frequency due to the plasmas response in the composite structure. SRR along with the wire structure gives a negative refractive index 'n'. The formulas for calculating the dimension of SRR and the wire structure are used to design the unit cell structure of metamaterial. The simulation result of the unit cell structure is done on CST Microwave Studio and various S-parameter's magnitude, phase, the real part and the imaginary part for the unit cell are computed which are further used to calculate the impedance, permittivity, permeability and the refractive index of the composite medium as a function of frequency. The graphs for the various parameters are plotted in MATLAB which varies as a function of frequency. The unit cell structure has a cell dimension 'a' which is a cubical structure in which a metamaterial is made. The metamaterial is made using a FR-4 (Lossy) substrate having the relative permittivity 'ε_r' value equal to 4.4 and height 'h' of the substrate being 1.6 mm with a loss tangent '$tan\delta$' value equal to 0.025. The copper is used for making the split ring resonator and the wire structure at the front and back side of the substrate respectively whose dimension are specified below. The copper used has a thickness 't' of 0.035 mm and has the electrical conductivity (σ) equal to 5.8×10^7 S/m.

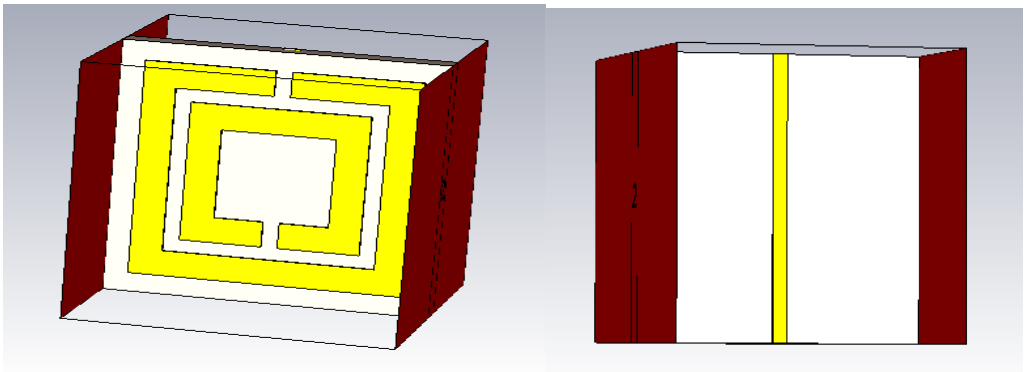

***(a)** Front view* ***(b)** Back view*

***Fig. 2.11:** Basic unit cell structure designed in CST Studio Suite.*

The split-ring resonator which is artificially designed on the FR-4 (lossy) substrate is responsible for negative permeability in the composite medium. The schematic for the designed split ring resonator in the CST Microwave Studio is shown in the Fig. 2.12

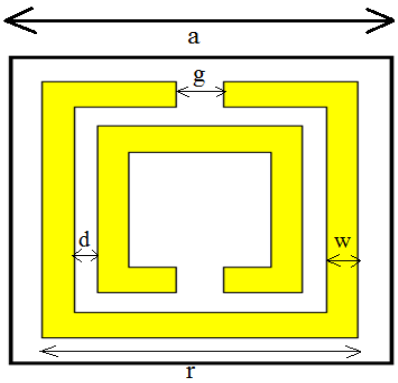

Fig. 2.12: *Schematic of the designed split-ring resonator for a unit cell structure.*

Here, '*a*' is the lattice dimension of the unit cell, '*r*' is the length of the outer ring of the designed SRR, 'w' is the width of the wire placed behind the substrate, '*d*' is the distance between the two rings and '*g*' is the slit gap in the rings. The Eq. 2.30 through Eq. 2.34 mentioned previously can be used for designing and verifying the designed split ring resonator and finding the resonant frequency and the plasmonic frequency of the SRR. The dimensions of the designed SRR are given in the Table 2.1.

Table 2.1. Dimensions of a designed split ring resonator for a unit cell structure.

Split Ring Resonator Parameters	Dimensions
Lattice Dimension (a)	12.5 mm
Outer length of ring (r)	10.0 mm
Width of ring (w)	1.0 mm
Distance between the two rings (d)	0.75 mm
Slit gap (g)	1.5 mm

The metal wire structure made up of copper is placed on the opposite face of the substrate on which the split ring resonator is designed. The copper wire strip in the unit cell is responsible for the negative permittivity in the composite medium. The Fig. 2.13 shows the designed symmetric wire structure on the back side of the substrate.

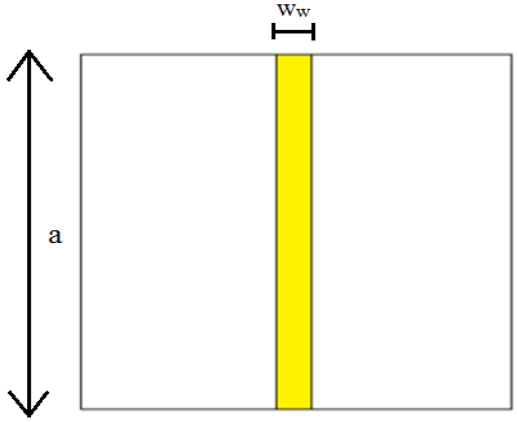

Fig. 2.13: *Designed symmetric wire structure for unit cell of metamaterial.*

The metallic wire has its wire width 'w_w' of 1.0 mm, the copper thickness 't' of 0.035 mm and the conductivity 'σ' of 5.8×10^7 S/m. The Eq. 2.29 mentioned previously in this

chapter can be used to determine plasma frequency of the metal wire and thus find the region in which the material exhibits a negative permittivity.

The two waveguide ports shown in the Fig. 2.14 are used as input and output port which are excited by TEM wave to calculate the S-parameters across the designed structure.

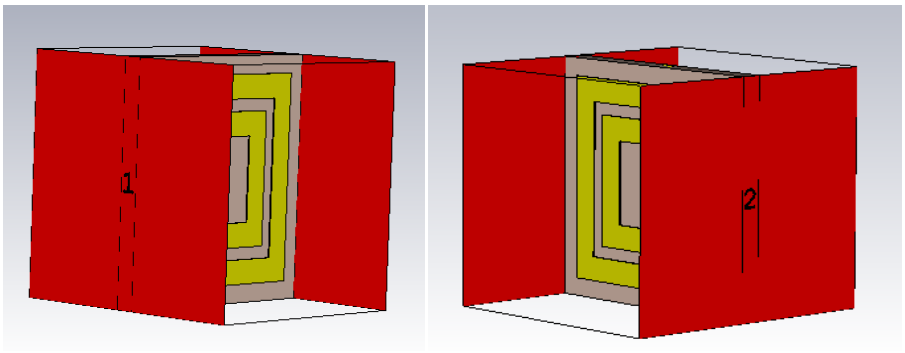

Fig.2.14: *Two waveguide ports for Unit Cell Structure.*

The two waveguide ports are used for the input and output excited by TEM wave in which the port 1 is directed along positive X-axis while the port 2 is directed along negative X-axis. The time domain solver is used in CST Microwave Studio is used to find the 1-D results of S(1,1), S(2,1) which vary as a function of frequency. The simulation is done by applying some boundary conditions to the unit cell structure, i.e. the front and back side of the structure are bounded by a perfect magnetic conductor while the top and bottom side of the structure are bounded by a perfect electric conductor while the two waveguide port sides are kept open. The Fig. 2.15 shown below is the boundary conditions applied to the structure.

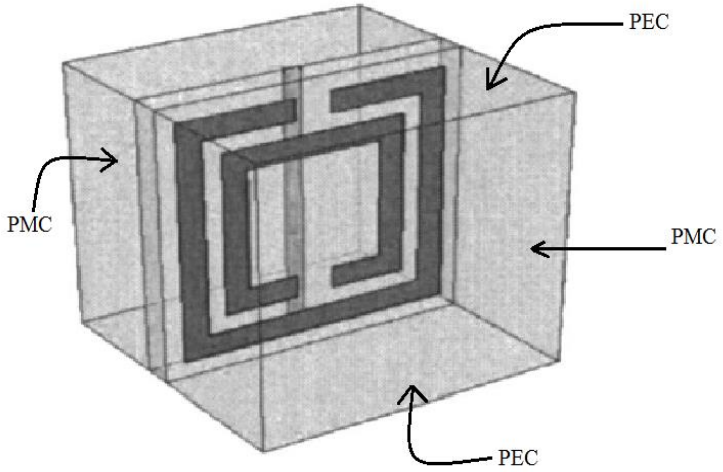

Fig.2.15: *Applied boundary conditions on a unit cell structure.*

Here the PMC stands for perfect magnetic conductor which implies that the tangential component of the magnetic field is zero along it, and the PEC stands for perfect electric conductor implies that the tangential component of the electric field is zero along it. While the rest two sides are kept open and used as waveguide ports for the unit cell.

2.5 Simulation result for a unit cell structure

The basic unit cell structure of metamaterial comprising of split-ring resonator and the symmetric wire structure is simulated on CST Microwave Studio and the various S-parameters results along with the impedance, permittivity, permeability and refractive index are shown in this section. The magnitude and phase response of the S(1,1) and S(2,1) are measured during simulation which is used to calculate the impedance and refractive index of the unit cell structure using the S-parameter retrieval techniques as proposed by Soukoulis et al [42]. The refractive index and the impedance of the designed composite medium is used to find the real and imaginary part of the relative permittivity and relative permeability. The impedance, permittivity, permeability and the refractive index of the medium is calculated using MATLAB and their corresponding graphs are plotted.

The Fig. 2.16 shows the magnitude plot of S(1,1) and S(2,1) parameters as a function of frequency.

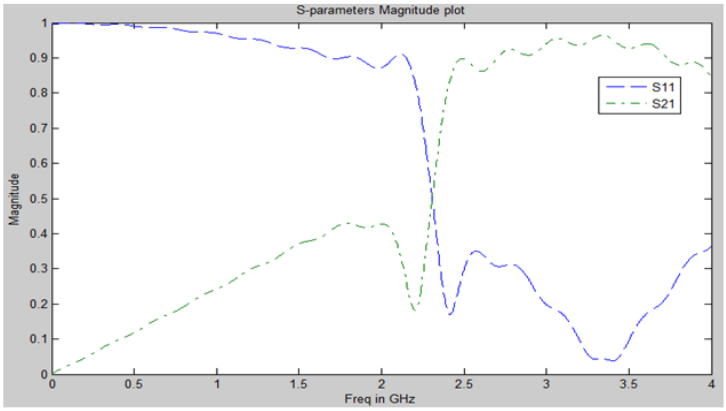

Fig. 2.16: *Magnitude plot for S(1,1) and S(2,1) parameters for the unit cell as a function of frequency.*

Here, S(1,1) is the reflection coefficient at the port 1 of the unit cell structure while S(2,1) is the transmission coefficient from port 1 to the port 2 of the waveguide structure. From the above S-parameters magnitude plot, it can be concluded that the reflection coefficient and the transmission coefficient of the composite structure has same magnitude and cut each other at nearly 2.35 GHz, after this the frequency the transmission coefficient value increases while the reflection coefficient value decreases.

The Fig. 2.17 shows the phase plot of the reflection and transmission coefficient of the designed unit cell structure.

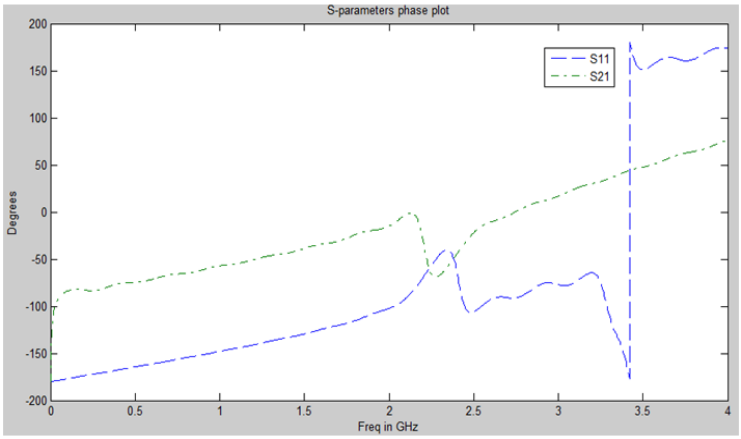

Fig. 2.17: *Variation of phase plot for S(1,1) and S(2,1) as a function of frequency.*

From the phase plot for the designed unit cell structure, it can be seen that the phase of the reflection coefficient '*S(1,1)*' and the transmission coefficient '*S(2,1)*' undergoes a 180^o phase reversal in the frequency range between 2.25 GHz to 2.4 GHz.

Further, the magnitude and phase plot of the reflection and transmission coefficient is used to calculate the impedance for the unit cell metamaterial structure. The impedance of the structure is calculated in the MATLAB using the Eq. 2.35 given below [42].

$$Z = \sqrt{\frac{(1+S_{11})^2 - S_{21}^2}{(1-S_{11})^2 - S_{21}^2}} \tag{2.35}$$

Here, 'S_{11}' is the reflection coefficient having magnitude and phase which varies as a function of frequency, similarly 'S_{21}' is the transmission coefficient with magnitude and phase and 'Z' is the impedance of the unit cell structure.

The Fig. 2.18 shows the variation of the impedance in the medium as a function of frequency.

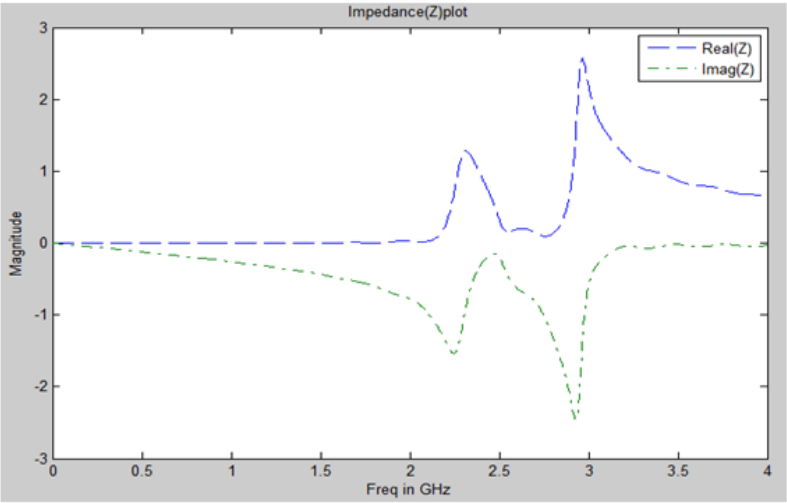

Fig. 2.18: *Variation of real and imaginary part of impedance as a function of frequency.*

From the above plot, it is seen that the real part of the impedance takes a non-zero value in the frequency range from 2.2 GHz to 2.5 GHz which is close to the resonant and plasmonic frequency of the split ring resonator. The real part of impedance attains a maximum peak value at 3 GHz and then starts decreasing to zero beyond it. The real part of the impedance signifies a resistance offered by the medium in the range 2.2 GHz to 2.5 GHz and thus power absorption takes place in this region. Also, the imaginary part of the impedance continuously decreases to a certain value till 2.25 GHz and then starts increasing till 2.5 GHz, thereafter the imaginary part decreases till a frequency of 2.9 GHz and then increases to a zero value at 3.1 GHz. The real part of the impedance is the resistive part of the composite medium while the imaginary part of the impedance is the reactance part which is basically a capacitance shown by the unit cell structure. The impedance for the structure is used to calculate the effective relative permittivity and the effective relative permeability of the composite structure using the Eq. 2.36.

$$\mu_r = n.Z \qquad \varepsilon_r = \frac{n}{Z} \tag{2.36}$$

Where 'n' is the refractive index and 'Z' is the impedance of the composite unit cell structure. The refractive index 'n' is calculated using the Eq. 2.37.

$$n = \frac{1}{ka} cos^{-1}\left(\frac{1-S_{11}^2+S_{21}^2}{2*S_{21}}\right) \tag{2.37}$$

The Fig. 2.19 shows the variation of real and imaginary part of the refractive index as a function of frequency.

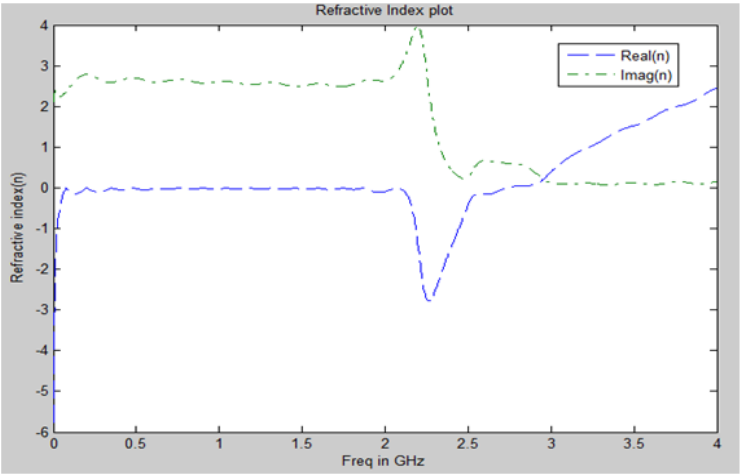

Fig. 2.19: *Variation of real and imaginary part of refractive index as a function of frequency.*

From the above plot, it is evident that the real part of the refractive index is negative in a frequency range of 2.2 GHz to 2.5 GHz and thus the medium acts as a double negative metamaterial. This negative refractive index region lies in the S-band of the microwave frequency which can be used in various microwave components like filters and antennas. The imaginary part of the refractive index in always positive and attains a zero value beyond 2.9 GHz where the real part of the refractive index starts to increase. The real part of the refractive index accounts for refraction in the medium while the imaginary part of the handles the attenuation in the wave.

The real and imaginary part of the permittivity and the permeability of the unit cell is calculated using the Eq. 2.36 and the variation of the permittivity and permeability as a function of frequency is plotted and shown in the Fig. 2.18 and Fig. 2.19 respectively.

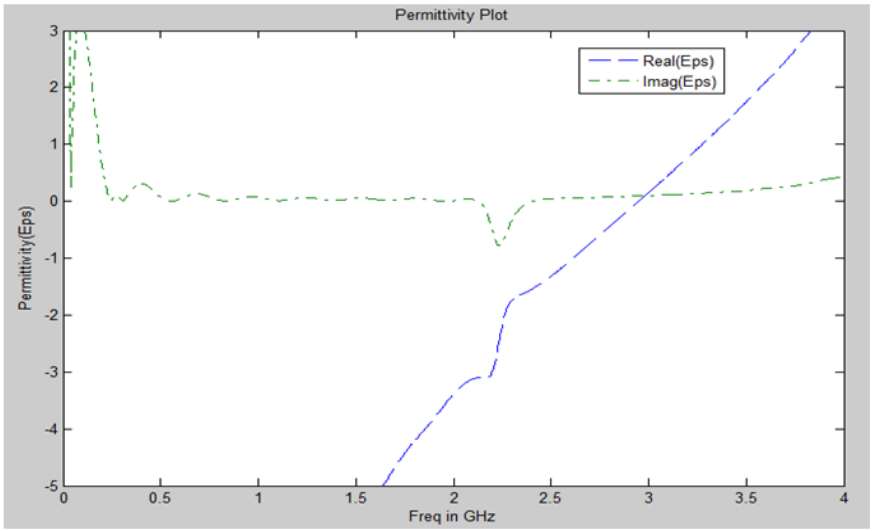

Fig. 2.20: *Variation of real and imaginary part of the permittivity as a function of frequency.*

From the Fig. 2.20 of relative permittivity, it can be seen that the real part of the permittivity is negative below 3 GHz which is the plasma frequency of the metal wire structure used in designing a unit cell. The real part of the permittivity deals with the energy stored in the medium and a negative value of permittivity implies that reflection and transmission depends upon the frequency. The imaginary part of the permittivity is positive which implies that the energy absorption takes place in the medium.

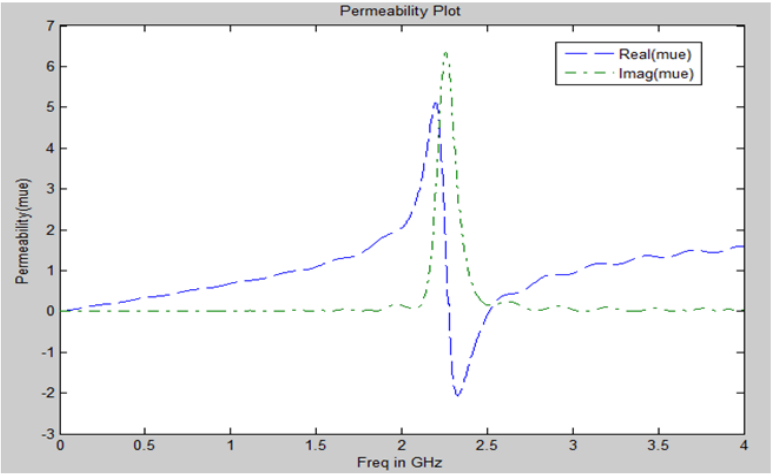

Fig. 2.21: *Variation of real and imaginary part of the permeability as a function of frequency.*

From the Fig. 2.21 of permeability variations as a function of frequency, it is seen that the real part of the permeability for the medium increases up to the resonant frequency 'ω_o' and then attains a negative value from the resonant frequency to the plasmonic frequency 'ω_{mp}'. The ratio of imaginary part and the real part of the permeability can give us the loss tangent of the medium which defines the amount of power lost in the material to the amount of power stored in the medium. The real part of the permeability defines the amount of power stored in the medium, and it is seen that the medium gives away energy in between resonant frequency and plasmonic frequency for the designed structure. The above graph shows that the imaginary part of the permeability attains a value between 2.2 GHz to 2.5 GHz with its maximum value at 2.3 GHz. The imaginary part tells that the energy is getting absorbed in the medium. Also from the above graph, it is evident that the resonant frequency of the designed split ring resonator is 2.2 GHz and a plasmonic frequency of 2.6 GHz.

Hence, in this chapter a basic 1-D unit cell structure is designed which shows a negative refractive index property of a metamaterial. The composite structure designed on a FR-4 (lossy) substrate and copper conductor has a split-ring resonator which confines magnetic energy is responsible for negative permeability, and a symmetric wire structure which confines electric field and is responsible for negative permittivity. The various S-parameters magnitude and phase plot are shown which as used to find the impedance, the refractive index, the relative permittivity and the relative permeability of the composite medium. The simulation result obtained in CST Microwave studio and MATLAB shows that the designed unit cell structure shows a negative refractive index in the frequency region 2.25 GHz to 2.5GHz and hence shows a property of left-handed medium.

CHAPTER 3
Microstrip patch antenna based on metamaterials

3.1 Introduction to microstrip patch antenna

3.1.1 Introduction

Nowadays, microstrip antennas have become very popular due to their small size, low cost for fabrication, light weight, conformable to various structures and are versatile in nature [43]. These antennas can also be integrated with the active devices and components and printed strip-line feed networks. The microstrip patch antennas have various radiation properties which are known since mid-1950's [44]. The application of such type of microstrip antennas started in the year 1970's when the antennas where required for missiles and their communication systems. Circular and rectangular patch antennas have been in demand and are commonly used in many types of array configuration. Also, the manufacturing of microstrip antennas in the current revolution has bought circuit miniaturization and helped in large scale integration. Since the conventional antennas which are being used are bulky, costly and large in size, microstrip patch antennas have become popular and are fabricated using the photolithographic technology which is seen as a major breakthrough in the engineering technology.

A microstrip patch antenna in a fundamental form is designed on a dielectric substrate which has a radiating patch on one side of the substrate and a ground plane on the other side of the substrate. The Fig. 3.1 shows a fundamental structure of a microstrip patch antenna.

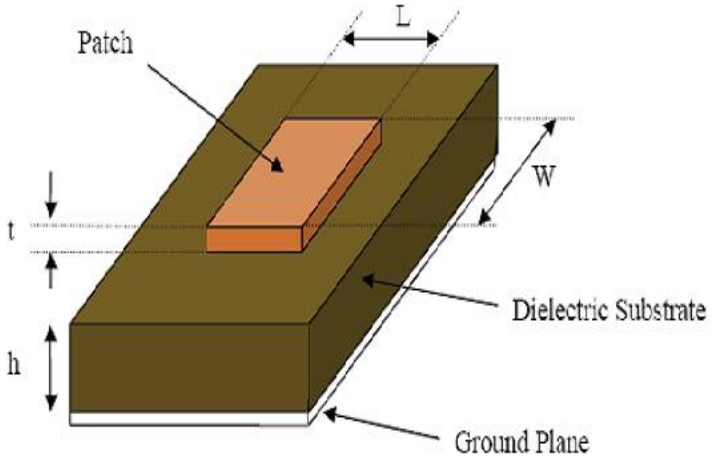

Fig. 3.1: *Fundamental structure of microstrip patch antenna. (Taken from Ref. [45])*

The patch is usually made up of conducting material like copper or gold and can take variety of shapes and configuration. The radiating patch of the antenna and the feed lines for the feeding mechanism are photo etched on the dielectric substrate. For simple analysis and prediction of the antenna performance, the patch is generally chosen to be a rectangular, square, circular, triangular, elliptical and some other common shapes as shown in the Fig. 3.2.

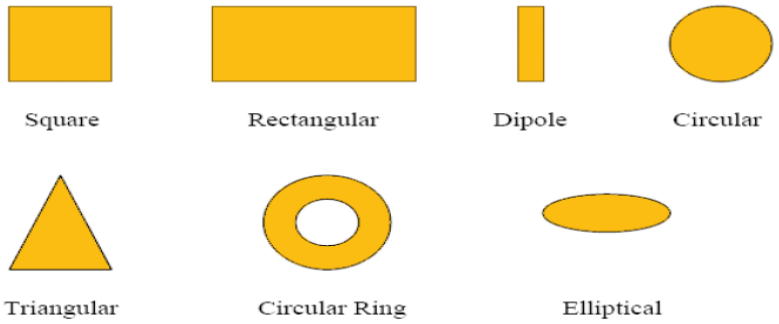

Fig. 3.2: *Shapes for a microstrip patch antenna. (Taken from Ref. [43])*

Generally a rectangular patch antenna is analysed due to its simplicity in designing and calculation of the performance. For a rectangular patch, the length 'L' of the patch is usually taken as $0.33\lambda_o < L < 0.5\lambda_o$, where λ_o is the wavelength in free space. The thickness of the patch 't' is selected to be very thin such that $t << \lambda_o$. The height 'h' of the dielectric substrate is usually considered in the range, $0.003\lambda_o < h < 0.05\lambda_o$. The dielectric constant that is also called as relative permittivity of the substrate 'ε_r' is selected in the range $2.2 \leq \varepsilon_r \leq 12$. Microstrip patch antennas radiate mainly due to the fringing fields between the patch edge and the ground plane. For the good performance of the antenna, a thick dielectric substrate with a low dielectric constant is desirable to give a large bandwidth, better efficiency and better radiation, but these kinds of antenna configuration leads to a larger size of an antenna. Thus in order to design a compact size antenna, substrate having a large relative permittivity is selected which provides a less efficiency and a narrow bandwidth. Hence there is a trade-off between the performance parameters of an antenna and its dimension.

3.1.2 Advantages and disadvantages of microstrip patch antenna

Microstrip patch antennas are gaining their popularity in wireless applications because of their low profile structure. These antennas are compatible for embedding antennas in the handheld devices like pagers, cell phones, etc. These antennas have found their applications in missiles as they are thin and conformal and have been successful in the satellite communication due to their small size and planar structure. The various advantages are given below [43]:

- Low cost for fabrication.
- Low profile with a planar configuration.
- Light in weight and has small size.
- Supports linear and circular polarization for radiation.
- Easy to combine with the microwave integrated circuits.
- Can support up to three frequencies of operations.
- Mechanically robust and can be mounted on rigid surfaces.

Microstrip patch antennas have certain drawbacks as compared to the conventional antennas used for wireless communication systems. Some of these major disadvantages are given below [46]:

- Efficiency is low.
- Bandwidth is narrow.

- Gain of the antenna is low.
- Spurious radiations are emitted from feeds and junctions.
- End fire radiation is poor.
- Low power handling capacity.
- Surface wave excitation exhibits.

The quality factor '*Q*' of the microstrip patch antenna is very high. The quality factor can be used to express the losses associated with the antenna where a large value of *Q* gives a low efficiency and narrow bandwidth. The quality factor can be decreased using the thickness of the dielectric substrate, but as the thickness of the substrate increases, a fraction of total power delivered by the sources into the surface waves increases. These surface waves can be considered as an undesired power loss and leads to the degradation of the antenna characteristics. The problems like low gain and lower power handling capability can be overcome with the help of array configuration for the antenna elements.

3.1.3 Method of analyzing a microstrip patch antenna

The transmission line model and cavity models are the two models which are preferred for the analysis of the microstrip patch antennas. The transmission line model is simple and gives a very good insight for analyzing a patch antenna but has a drawback of less accuracy in its solution. The cavity model is more accurate but the method of analyzing is complex in nature. We also have a full wave models which are extremely accurate, versatile in its approach and can be applied to single element, stacked elements, finite and infinite arrays as well as random shaped elements. This type of model gives a less insight as compared to the transmission line model and cavity model and is very complex in nature. In this section we will discuss about the transmission line model and then cover cavity model for the analysis of patch antennas.

(a) Transmission line model

In transmission line model, it represents a microstrip patch antenna with a two slots of width '*W*' and height '*h*' separated by a transmission line having a length 'L'. The microstrip is basically a non-homogenous line having two dielectrics, i.e. the air and substrate.

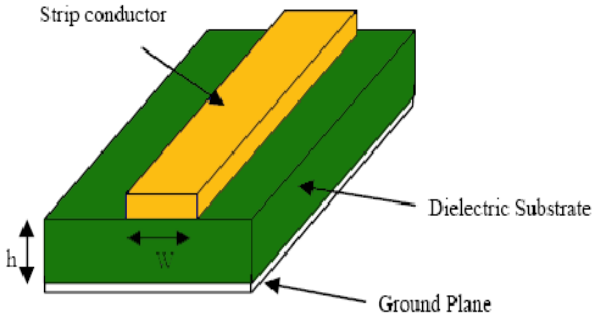

Fig. 3.3: *Microstrip Line. (Ref. [43])*

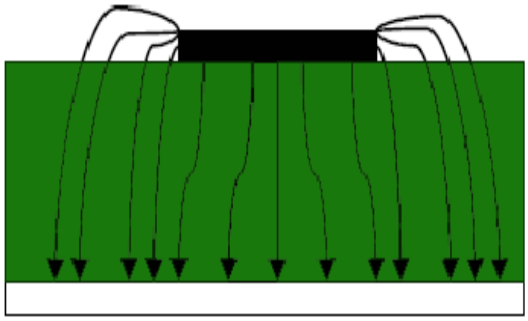

Fig.3.4: *Electric field lines.(Ref. [43])*

The Fig. 3.3 shows a microstrip line on a dielectric substrate and the Fig. 3.4 shows the electric field lines which lies mostly in the substrate and some part of it lies in the air. Thus as a result the transmission line does not support pure transverse-electromagnetic

(TEM) mode of transmission. The phase velocities being different in the substrate and the air, the dominant mode of propagation in the transmission line would be a quasi-TEM mode instead of a pure TEM mode. Thus an effective dielectric constant 'ε_{reff}' for the medium is calculated which considers the fringing effect and wave propagation in the transmission line. The value of 'ε_{reff}' would be slightly less than the 'ε_r' of the dielectric substrate because the fringing field around the periphery of the patch are not completely confined in the dielectric substrate but are also present in the air as shown in the Fig. 3.4 above. Thus the expression for the effective relative permittivity 'ε_{reff}' is given in Eq. 3.1 by Balanis [43] as:

$$\varepsilon_{reff} = \frac{\varepsilon_r + 1}{2} + \frac{\varepsilon_r - 1}{2}\left[1 + 12\left(\frac{h}{W}\right)\right]^{-1/2} \tag{3.1}$$

Here, 'ε_{reff}' is the effective relative permittivity of the transmission line structure, 'ε_r' is the relative permittivity of the substrate, 'h' is the height of the dielectric substrate and 'W' is the width of the transmission line.

The Fig. 3.5 shows a rectangular patch antenna having a length 'L' and width 'W' on the dielectric substrate which is generally made up of copper and the substrate height 'h'. The co-ordinate axis of the antenna is selected in such a way that the length of the patch is along the X-direction, width of the patch is along the Y-direction and the height of the substrate along the Z-direction.

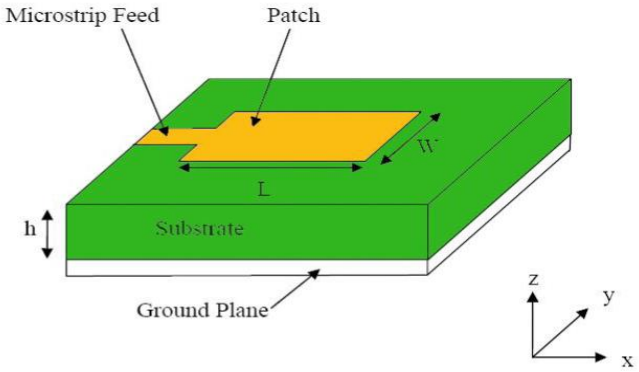

Fig. 3.5: *Microstrip patch antenna. (taken from Ref. [43])*

For the patch to operate in the fundamental mode of TM_{10} in which the length of the patch is made slightly less than $\lambda/2$, where 'λ' is the wavelength in the dielectric substrate and is equal to $\lambda_o/\sqrt{\varepsilon_{reff}}$ where λ_o is the wavelength in free space. The TM_{10} mode means that the field varies one half-wavelength cycle along the length and having no variation in the field along the width of the patch. In the Fig. 3.6 shows a microstrip patch antenna having two slots which are separated by a transmission line of length 'L' and is open circuited at the both ends. Along the width of the patch, the voltage is maximum and the current attains a minimum value due to open ends. The fields at the edges of the patch can be defined and resolved into its normal and tangential component with respect to the ground plane.

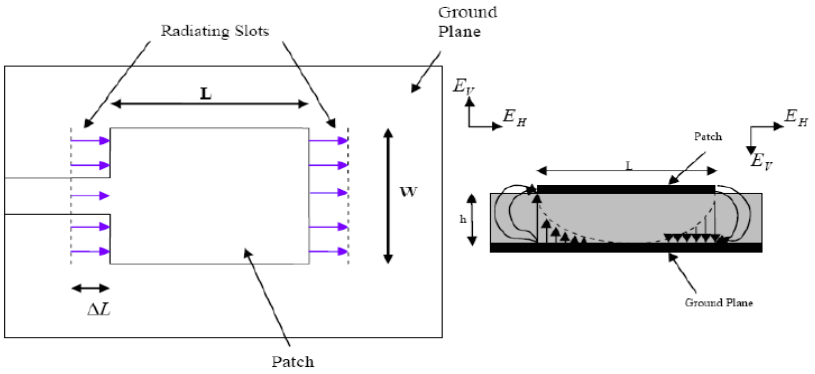

Fig. 3.6: *Top and side view of a microstrip patch antenna.*

From the Fig. 3.6, it can be seen that the normal components of the electric field along the width of the patch are in opposite direction and hence are out of phase since the patch is considered to be *λ/2* long and hence they cancel each other in the broadside direction. The tangential components which can be seen in the Fig. 3.6 are in phase and thus the resulting fields combine to give a maximum radiation field in the direction normal to the surface of the structure. Thus we can say that the edges along the width of the patch can be treated as the two radiating slots which are λ/2 apart and excited in phase. The fringing fields can be modeled as radiating slots and thus the patch of the antenna seems to be greater that its actual physical dimension. The patch dimension along its length is extended by some distance of ΔL which is given in the Eq. 3.2 as [43]:

$$\Delta L = 0.412h\frac{\left(\varepsilon_{reff}+0.3\right)\left(\frac{W}{h}+0.264\right)}{\left(\varepsilon_{reff}-0.258\right)\left(\frac{W}{h}+0.8\right)} \tag{3.2}$$

The effective length increases by twice the extension in length which is at the both sides of the patch and is given in Eq. 3.3 as [43]:

$$L_{eff} = L + 2\Delta L \tag{3.3}$$

For a resonance frequency of 'f_o', the effective length is given by the Eq. 3.4 as [43]:

$$L_{eff} = \frac{c}{2f_o\sqrt{\varepsilon_{reff}}} \tag{3.4}$$

Here 'c' is the speed of light in free space.

For a rectangular microstrip patch antenna, the resonant frequency for TM_{mn} mode is given in the Eq. 3.5 as [43]:

$$f_o = \frac{c}{2\sqrt{\varepsilon_{reff}}}\left[\left(\frac{m}{L}\right)^2+\left(\frac{n}{W}\right)^2\right]^{\frac{1}{2}} \tag{3.5}$$

Where 'm' and 'n' are the modes along the length and width of the patch respectively. For efficient radiation, the width 'W' is given by Eq. 3.6 as [43]:

$$W = \frac{c}{2f_o\sqrt{\frac{\varepsilon_r+1}{2}}} \tag{3.6}$$

(b) Cavity model

The cavity model helps in giving an insight of the radiation mechanism of the patch antenna as it provides a mathematical solution for electric and magnetic fields of a patch antenna. It uses a dielectric loaded cavity which is representing the antenna. This technique models the antenna as a substrate material and considers that the material is truncated at the patch edge. The ground plane and the patch are represented with a perfect electric conductor and the edges of the substrate are modeled as a perfect magnetic conductor.

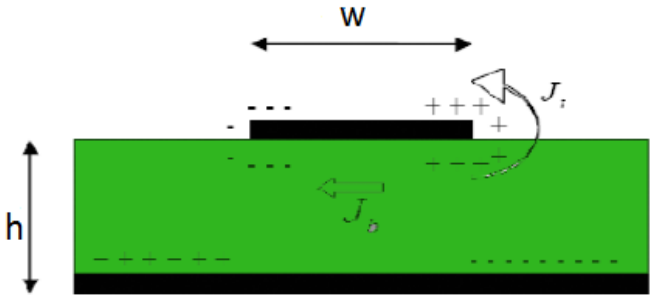

Fig. 3.7: *Charge distribution and current density creation on the microstrip patch. (Ref. [43])*

Looking at the Fig. 3.7 shown above. The microstrip patch antenna which provides radiation power, a charge distribution on its lower and upper surfaces of the patch and also at the bottom of the ground plane. The charge distribution is controlled by attractive and repulsive mechanism in the patch and the substrate. The attractive mechanism is between the opposite charges at the bottom side of the patch and the ground plane for the patch which allows the charge concentration to be intact at the bottom of the patch. The repulsive mechanism is between the like charges below the patch which causes charge to be pushed from bottom to the top of the patch. As a result, this charge movement causes a current flow at the bottom and top surface of the patch. The cavity model assumes that the height of the substrate to the width of the patch ratio is negligible and thus the attractive mechanism dominates and causes the charge concentration and current to flow below the patch surface. Therefore, the four sidewalls could be modeled as a perfect magnetic conductor. Therefore, we consider TM_z modes to propagate inside the cavity. The expressions for the magnetic and electric fields within the cavity in terms of vector potential '*Az*' [48] are given below in Eq. 3.7 through Eq. 3.12.

$$E_x = -j\frac{1}{\mu\varepsilon\omega}\frac{\partial^2 A_z}{\partial_x \partial_y} \tag{3.7}$$

$$E_y = -j\frac{1}{\mu\varepsilon\omega}\frac{\partial^2 A_z}{\partial_y \partial_z} \tag{3.8}$$

$$E_z = -j\frac{1}{\mu\varepsilon\omega}\left(\frac{\partial^2}{\partial z^2} + K^2\right)A_z \tag{3.9}$$

$$H_x = \frac{1}{\mu}\frac{\partial A_z}{\partial y} \tag{3.10}$$

$$H_y = \frac{1}{\mu}\frac{\partial A_z}{\partial x} \tag{3.11}$$

$$H_z = 0 \tag{3.12}$$

Since the vector potential satisfies the wave equation for homogenous medium, a variable separable method can be used to find the general solution. Thus the general solution for electric and magnetic fields inside the cavity are written in Eq. 3.13 through Eq. 3.18:

$$E_x = -j\frac{K_x K_y}{\mu\varepsilon\omega} A_{mnp}\, sin(K_x x)\, cos\big(K_y y\big)\, sin(K_z z) \tag{3.13}$$

$$E_y = -j\frac{K_y K_z}{\mu\varepsilon\omega} A_{mnp}\, cos(K_x x)\, sin\big(K_y y\big)\, sin(K_z z) \tag{3.14}$$

$$E_z = -j\frac{K^2 - K_z^2}{\mu\varepsilon\omega} A_{mnp}\, cos(K_x x)\, cos\big(K_y y\big)\, cos(K_z z) \tag{3.15}$$

$$H_x = -\frac{K_y}{\mu} A_{mnp}\, cos(K_x x)\, sin\big(K_y y\big)\, cos(K_z z) \tag{3.16}$$

$$H_y = -\frac{K_x}{\mu} A_{mnp}\, sin(K_x x)\, cos\big(K_y y\big)\, cos(K_z z) \tag{3.17}$$

$$H_z = 0 \tag{3.18}$$

Here, 'K_x', 'K_y' and 'K_z' are the propagation constant along X-direction, Y-direction and Z-direction respectively.

Also, the propagation constants are expressed in terms of length, width and height respectively along their direction of propagation.

$$K_x = \frac{m\pi}{L}\ , m = 0,1,2, \ldots \tag{3.19}$$

$$K_y = \frac{n\pi}{W}\ , n = 0,1,2, \ldots \tag{3.20}$$

$$K_z = \frac{p\pi}{h}\ , p = 0,1,2, \ldots \tag{3.21}$$

Where m=n=p≠0 and 'A_{mnp}' is the amplitude coefficient.

The resonant frequency 'f_r' of the cavity is given in the Eq. 3.22.

$$(f_r)_{mnp} = \frac{1}{2\pi\sqrt{\mu\varepsilon}}\left[\left(\frac{m\pi}{L}\right)^2 + \left(\frac{n\pi}{W}\right)^2 + \left(\frac{p\pi}{h}\right)^2\right]^{\frac{1}{2}} \tag{3.22}$$

Where m, n and p defines the modes in the designed cavity.

3.1.4 Microstrip feed techniques

There are various methods which can be used to feed a microstrip patch antenna. These can be categorized into two parts, first being the contacting type feeds and other being the non-contacting type feeds. In contacting method, the radio frequency power is directly fed to the radiating patch using a connecting element like a microstrip line. In non-contacting method, electromagnetic field coupling is employed to feed the power from the microstrip

line to the radiating patch. The four techniques which are used for feeding are microstrip line method and coaxial probe method which comes under contacting type scheme, while aperture coupling method and proximity coupling method comes under non-contacting type schemes. These four methods of feeding are discussed in the section below.

(a) Microstrip line feed

Microstrip line feed method is also called as offset microstrip line feed which uses a conducting strip connected directly to the edge of the patch to fed RF power as shown in the Fig. 3.8. The width of the conducting strip is much smaller than the patch width and this type of feed has an advantage that the feed is etched on the same substrate as that of the patch to provide a planar structure to the antenna.

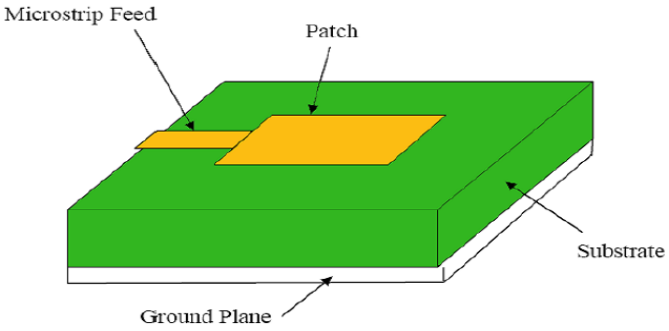

Fig.3.8: *Microstrip line feed. (Taken from Ref. [43])*

An inset cut is generally used to obtain a good impedance matching without the need of any additional matching elements. This can be done by a proper selection of inset position and hence this provides an easy technique for feeding, as well as an easy way for fabrication and allows simple modeling. However, the surface waves and spurious radiation increases as the thickness of the substrate is increased which affects the bandwidth of the patch antenna. This type of feeding technique suffers a drawback of cross polarization effects.

(b) Coaxial feed

The coaxial feed method which is also called as the probe feed is a common technique for feeding the microstrip patch antennas. The Fig. 3.9 shows the inner conductor of the coaxial cable or connector is extended to the radiating patch through the dielectric substrate while the outer conductor of the coaxial cable is connected to the ground plane of the patch.

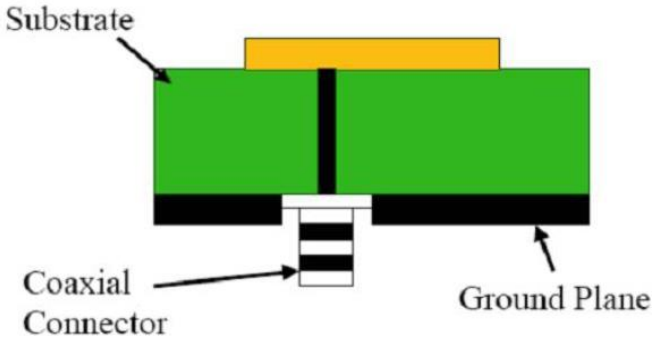

Fig. 3.9: *Coaxial feed technique. (Taken from Ref. [43])*

The major advantage of this type of feeding technique is that it can be placed at any desired position inside the patch to obtain impedance matching. Thus this type of feed method is easy to fabricate and has low spurious radiation. This type of feeding technique has

a disadvantage of a narrow bandwidth and difficult modeling as a hole has to be drilled into the substrate. For thick substrates, as the probe length increases the impedance gets more inductive and hence matching problems arises in such feeding technique.

(c) Aperture coupled feed

The aperture coupling is shown in the Fig. 3.10 which has a radiating microstrip patch element etched on the top of the antenna substrate and the microstrip feed line etched at the bottom of the feed substrate so that aperture coupling is achieved. Thus the dielectric constant and the thickness of the two substrates are chosen independently to optimize the electrical functions of circuit and its radiation. The coupling aperture is placed at the center below the patch, which reduces the cross-polarization effect due to the symmetry of configuration. The amount of coupling to the patch from the feed line is dependent on the size, shape and the position of the aperture. Since the patch and the feed line is separated by a ground plane, the spurious radiation is minimized in this type of feeding technique.

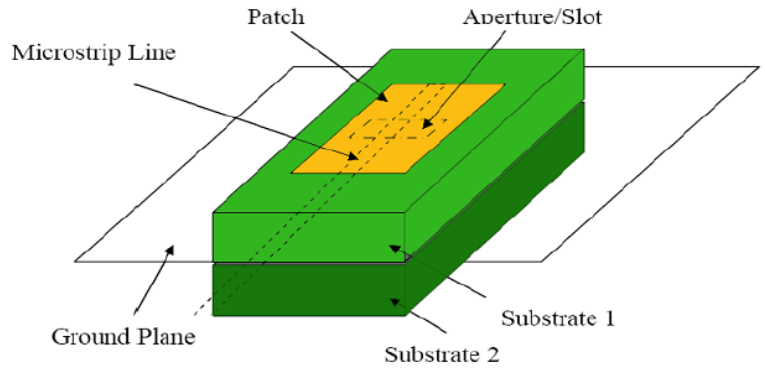

Fig. 3.10: *Aperture couple feed. (Taken from Ref. [43])*

Usually, a thick material with a high dielectric constant is used for the bottom substrate and a material with low dielectric constant is used for the top substrate to optimize the radiation pattern from the patch of the antenna. This type of non-contacting method of feed can provide a very high bandwidth and also the effect of spurious radiation is very less compared to other feeding techniques. The major disadvantage of this type of feeding mechanism is that it is difficult to fabricate due to the presence of multiple layers of dielectric and also increases the thickness of the antenna.

(d) Proximity coupled feed

Proximity coupled feed method is also called as electromagnetic coupling technique is shown in the Fig. 3.11. The figure shows two dielectric substrate placed in such a way that a feed line is used between the two substrates and the radiating patch is etched on the top of the upper substrate. The main advantage of this type of feeding technique is that it provides a very high bandwidth and completely eliminates the spurious feed radiation and is because of the increase in the thickness of the microstrip patch antenna. This feeding technique also provides a choice between the dielectric material, one used for the patch and the other is used for the feed line to optimize the performance of the antenna.

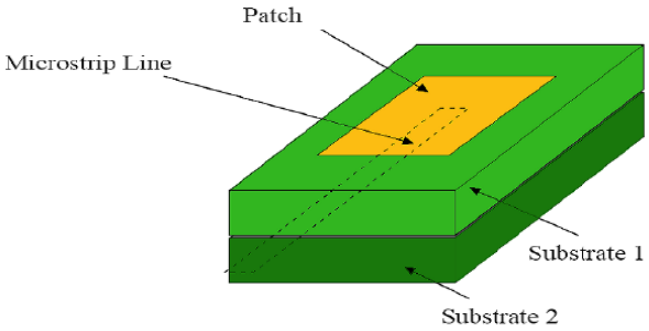

Fig. 3.11: *Proximity coupled feed technique. (Taken from Ref. [43])*

This scheme has major disadvantage that it is very difficult to fabricate as two dielectric layers are need with a proper alignment and also increases the thickness of the antenna.

The table 3.1 gives a comparison among the various feeding techniques used for a microstrip patch antenna based on their characteristic such as reliability, spurious radiation, impedance matching, bandwidth and ease of fabrication.

Table 3.1 Comparison of different feeding techniques for a patch antenna.

Characteristics	Microstrip Line Feed	Coaxial Feed	Aperture Coupled Feed	Proximity Coupled Feed
Spurious Radiation	High	High	Low	Very Low
Impedance matching	Very Easy	Easy	Easy	Easy
Reliability	Good	Poor	Very Good	Very Good
Bandwidth	2-5%	2-5%	7-10%	13%
Ease of Fabrication	Easy	Difficult	Difficult	Difficult

3.2 Design and simulated results of a conventional microstrip patch antenna at 4 GHz

In this section, a conventional method for designing a microstrip patch antenna has been used and is designed on an FR-4 (Lossy) substrate having relative permittivity 'ε_r'= 4.4, and relative permeability 'μ_r' = 1.0 with a loss tangent '$tan\delta$' value equal to 0.025 and having substrate height 'h' of 1.6 mm. The copper is used as ground plane and designing a patch whose dimension, i.e the length and the breadth is calculated in the design section. The copper conductor is a lossy metal with 'μ_r'= 1.0 (dielectric permeability) and electrical conductivity 'σ' = 5.8×10^7 S/m. The copper thickness 't' has a value equal to 0.035mm for both the patch and the ground plane. The inset microstrip feeding technique is used for the impedance matching of the antenna with the RF power source which is normalized to 50Ω of transmission line. The width, notch width and the cut depth of the feed is also calculated during the design of the patch antenna. The dimensions of the patch on the substrate are calculated very accurately for the antenna to resonate at its desired resonant frequency. The feed line dimensions are also calculated very accurately for the proper matching of the impedance of the source and the antenna and therefore allowing the maximum transfer of power from the source to the patch of the radiating antenna. The designing and simulation of

the conventional microstrip patch antenna is done in CST Microwave Studio and various simulation results like far-field directivity, far-field gain, main lobe power, 3-dB angular width, bandwidth, voltage standing wave ratio (VSWR) and the side lobe level are computed.

3.2.1 Design specification of a conventional microstrip patch antenna

There are three essential parameters which are used in designing of microstrip patch antenna. These are the frequency of operation, i.e. the resonant frequency 'f_o' of the patch antenna, dielectric constant for the substrate 'ε_r' and the height 'h' of the substrate on which the patch is designed. The patch antenna in this design has a resonant frequency of 4 GHz, the relative permittivity of 4.4 and the substrate height of 1.6 mm. Now after choosing the resonant frequency, substrate height and the dielectric constant of the substrate, we calculate the other parameters like the width and length of the patch antenna along with the feeding technique parameters used in the current design. This section shows the various steps which needs to be followed for designing a patch antenna with accurate results.

Step 1: Calculating the width of the patch.

The width 'W' of the patch is calculated using the Eq. 3.23 given below.

$$W = \frac{c}{2f_o\sqrt{\frac{\varepsilon_r + 1}{2}}} \tag{3.23}$$

Here, 'c' is the speed of light equal to 3×10^8 m/s, 'f_o' is the desired resonant frequency of the antenna which is selected to be 4.0 GHz and 'ε_r' is the relative permittivity of the substrate and is equal to 4.4. Substituting the values in the above equation, we get the width of the patch equal to **22.82 mm**.

Step 2: Calculating the effective dielectric constant.

The effective dielectric constant 'ε_{reff}' is calculated using the Eq. 3.24 given below.

$$\varepsilon_{reff} = \frac{\varepsilon_r + 1}{2} + \frac{\varepsilon_r - 1}{2}\left[1 + 12\left(\frac{h}{W}\right)\right]^{-\frac{1}{2}} \tag{3.24}$$

Here, 'h' is the height of the substrate and 'W' is the width of the patch calculated using Eq. 3.23. Substituting the value of relative permittivity, height of the substrate and the width of the patch in the above equation, we get the effective relative permittivity equal to **3.952**. This value of effective dielectric constant is used to calculate the effective length and the extension in length of the patch due to fringing effect.

Step 3: Calculating the effective length of the patch.

The effective length 'L_{eff}' of the patch is calculated using the Eq. 3.25 given below.

$$L_{eff} = \frac{c}{2f_o\sqrt{\varepsilon_{reff}}} \tag{3.25}$$

Substituting the value of speed of light, the resonant frequency and the effective dielectric constant calculated using Eq. 3.24 in the above expression, we get the effective length of the patch equal to **18.86 mm**.

Step 4: Calculating the extension in the length.

The extension in the length 'ΔL' of the patch is due to the fringing effect and is calculated using the Eq. 3.26 given below.

$$\Delta L = 0.412 \times h \times \frac{\left(\varepsilon_{reff} + 0.3\right)\left(\frac{W}{h} + 0.264\right)}{\left(\varepsilon_{reff} - 0.258\right)\left(\frac{W}{h} + 0.8\right)} \tag{3.26}$$

Substituting the value of effective relative permittivity, width of the patch and the height of the substrate in the above expression gives the extension length equal to **0.925 mm**. This extension in length is used to find the actual length of the patch which has a resonating frequency of 4 GHz.

Step 5: Calculating the actual length of the patch.

The actual length of the patch is less than the effective length of the patch because of the fringing fields which is encountered along the length of the patch. Thus the physical dimension of the patch is less than the electrical length of the patch and is given by the Eq. 3.27 below.

$$L = L_{eff} - 2\Delta L \tag{3.27}$$

Substituting the value of effective length and the extension in length in the above equation gives the value of the actual length of the patch and is equal to **17.01 mm**.

Step 6: Calculating the edge impedance of the patch.

The impedance of the patch antenna at the edge 'Z_a' is calculated using the Eq. 3.28 which is used further to calculate the cut depth in the inset feed technique used so that proper impedance matching is achieved between the patch and maximum transfer of power takes place from the RF source to the patch of an antenna.

$$Z_a = 90 \times \frac{{\varepsilon_r}^2}{\varepsilon_r - 1} \times \left(\frac{L}{W}\right)^2 \tag{3.28}$$

Substituting the value of the length and width of the patch, and the relative permittivity of the substrate, the impedance at the edges is found using the above equation. The edge impedance of the designed antenna comes out to be **284.42Ω**.

Step 7: Calculating the cut depth of the inset feed technique.

Since the current is low and the voltage is maximum at the ends of a half-wave patch of the antenna, the voltage decreases and current increases in magnitude as we move towards the center of the patch, thus the input impedance *(Z=V/I)* could be reduced if the patch is fed closer to the center. One method to do this is by using the inset feed (a distance R from the end of the patch) as shown in Fig. 3.12.

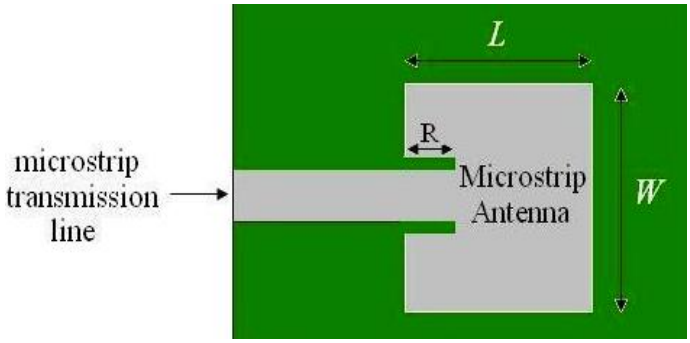

Fig. 3.12: *Microstrip patch antenna with inset feed.*

Since the current has a sinusoidal distribution, moving a distance '*R*' from the edge will vary the sinusoidal current by a factor cos(π×R/L), and so does the phase difference vary by the (π×R/L). The voltage also decreases in magnitude by the same amount as that the current increases, hence using Z=V/I relation, the input impedance at the distance '*R*' is given by the Eq. 3.27 given below.

$$Z_{in}(R) = Z_{in}(0)cos^2\left(\frac{\pi R}{L}\right) \tag{3.29}$$

Here, 'Z_{in} *(0)*' is the edge impedance of the patch which is calculated in the step 6, while '$Z_{in}(R)$' is the characteristic impedance of the patch antenna at the depth R. The impedance of the patch is kept equal to 50Ω so that maximum transfer of power takes place from the transmission line to the patch for radiating the EM wave whose characteristic impedance is normalized to 50Ω. Substituting the value of edge impedance and the length of the patch in the Eq. 3.29, we calculate the value of the cut depth '*R*' where the value of the edge impedance is equal to the value of the transmission line impedance. The value of the cut depth comes out to be **20.239 mm**.

Step 8: Calculating the width and length of the feed line.

The microstrip transmission line is used for the impedance matching and has the characteristic impedance of the 50Ω. The width and the length of the transmission line is calculated by using a line calculator which depends upon the height of the substrate, the dielectric constant of the substrate, the operating frequency and the electrical length, i.e. βl.

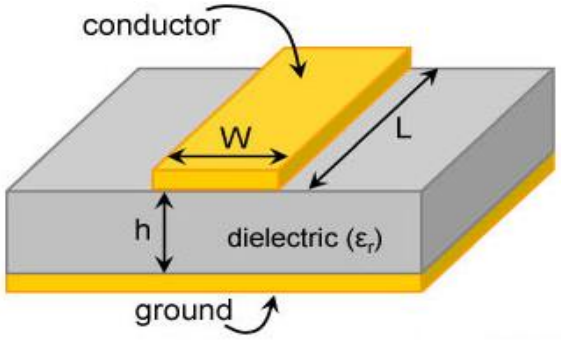

Fig. 3.13: *A schematic of a microstrip line.*

$$Z_o = \frac{120\pi}{\sqrt{\varepsilon_{reff}}}\left\{\frac{w_f}{h} + 1.393 + 0.677 * ln\left[\frac{w_f}{h} + 1.444\right]\right\}^{-\frac{1}{2}} \tag{3.30}$$

The Eq. 3.30 in the above expression is used to find the feed width of the transmission line whose characteristic impedance is 50 Ω. Substituting the value of substrate height,

effective permittivity and the characteristic impedance of the transmission line, the feed width 'w_f' is calculated using the above equation and is equal to **3.11 mm**. The length of the feed is considered at a electrical length $\beta l = 180^o$, i.e. at the length equal to λ/2. The length of the feed line 'L_f' comes out to be equal to **17.54 mm**.

A schematic for the designed patch antenna is shown in the Fig. 3.14.

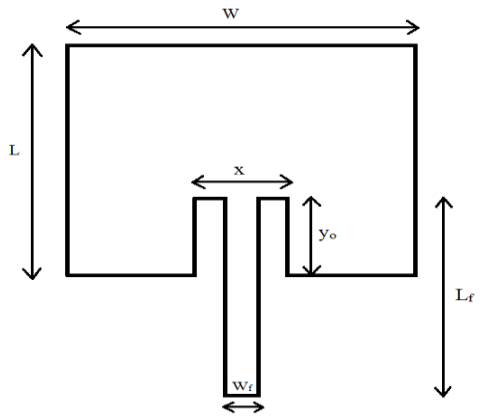

Fig. 3.14: *Schematic of a patch antenna.*

The table 3.2 given below summarizes the design parameters for the patch antenna having a resonant frequency of 4 GHz.

Table 3.2 Antenna design parameters for conventional patch antenna at 4 GHz.

Antenna Parameters	Dimension
Width (W)	22.82 mm
Length (L)	17.01 mm
Cut depth (y_o)	5.74 mm
Feed width (w_f)	3.11 mm
Feed length (L_f)	17.54 mm
Cut width (x)	5.00 mm

Step 9: Designing the waveguide port for the patch antenna.

The width of the waveguide port should be six times the width of the microstrip line and the height of the waveguide port should be the sum of the five times the height of the substrate and twice the height of copper thickness for proper power feeding.

Length of the port = $(5\times h+2\times t)$

Width of the port = $(6\times w_f)$

Substituting the value of the height and the thickness of the substrate and the copper respectively in the above expression of the length and width of the port, the length of the waveguide port comes out to be **8.07 mm** and the width of the port comes out to be **18.66 mm** which is symmetrically place along the width of the transmission line.

3.2.2 Simulation and simulated results for a conventional patch antenna

The microstrip patch antenna designed in CST Microwave Studio is simulated and the various performance parameters for the antenna like the reflection coefficient, far field gain, far field directivity, main lobe power pattern, 3-dB angular width, VSWR and the bandwidth

are computed during the simulation. The top view of the designed patch antenna is shown in the Fig. 3.15 (a) and the orientation of the designed patch antenna in the 3-D space is shown in the Fig. 3.15 (b).

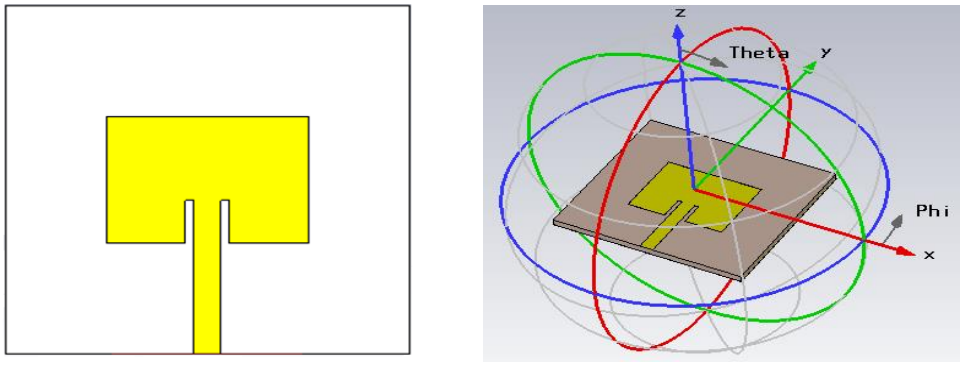

(a) ***(b)***

Fig.3.15: (a) *Top view,* ***(b)*** *Orientation of the designed patch antenna.*

From the above figure, it can be seen that the patch antenna lies in the XY-plane of the simulation and Z-axis being normal to the plane of an antenna.The Fig. 3.16 shows the waveguide port connected to the transmission line to feed the power to the patch.

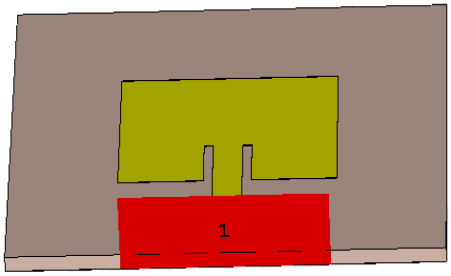

Fig. 3.16: *Waveguide port 1 connected to the transmission line of the patch antenna.*

The orientation of the feed signal is along the positive Y-direction of the patch and has a fundamental mode of TM_{10}. The reflection coefficient of the patch antenna is simulated at the waveguide port 1. The S-parameter S(1,1), i.e. the reflection coefficient of the microstrip patch antenna measure at the port 1 and hence find the resonant frequency of the patch is shown in the Fig. 3.17.

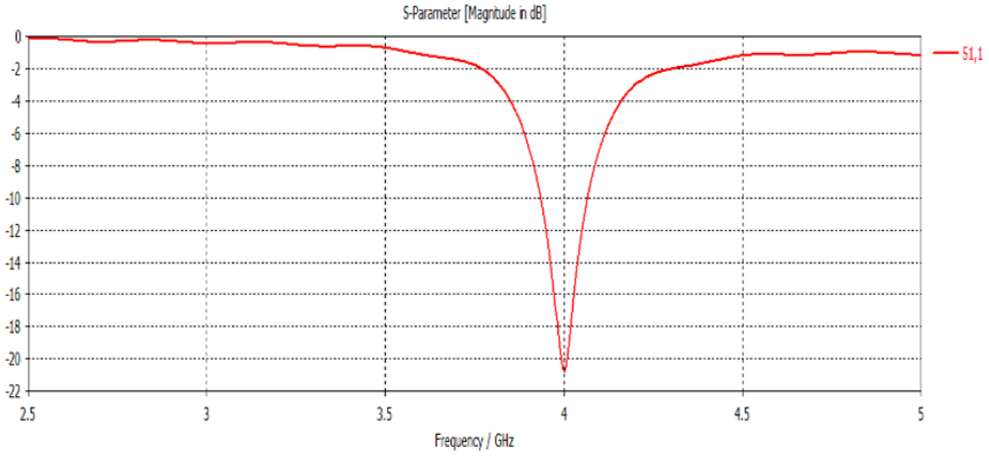

Fig. 3.17: *S(1,1) parameter result of a conventional patch antenna.*

The S(1,1) parameter which is the reflection coefficient of the antenna shows that the patch antenna has the resonant frequency at **4 GHz** and having a magnitude of **-20.5 dB**. The S(1,1) parameter which varies as a function of frequency can also be used to calculate the bandwidth of the antenna with the help of a -10 dB line. The Fig. 3.18 shows S-parameter with the two -10 dB points.

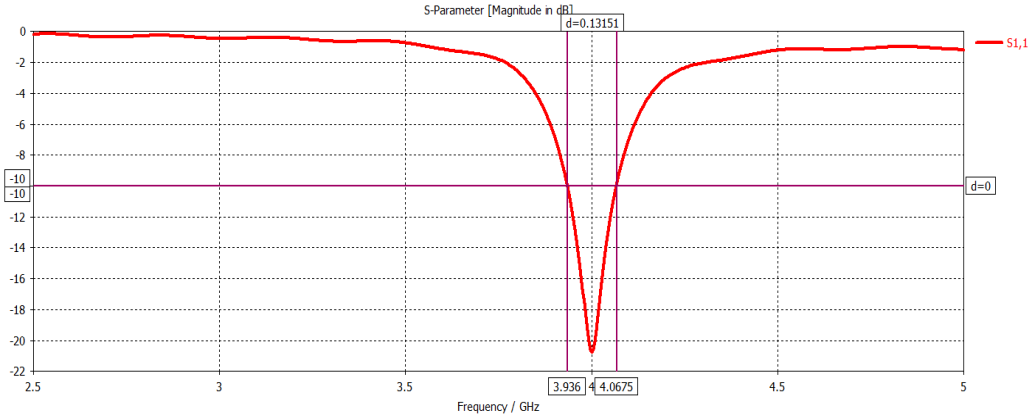

Fig. 3.18: *S(1,1) parameter with -10 dB points.*

From the above diagram it is evident that the two -10 dB points are at **3.936 GHz** and **4.0675 GHz** which gives the bandwidth of the patch antenna equal to the difference between these two frequency points. The bandwidth of this conventianal patch antenna is found out to be **131.5 MHz**.

The directivity of the patch antenna is defined as the figure of merit which measures the power density of the antenna in the direction of main lobe versus the power density of the ideal isotropic antenna radiating the same amount of total power. The Fig. 3.19 shown below shows the far field directivity of the designed patch antenna at 4 GHz at phi = 0 plane, i.e. the E-plane of the antenna.

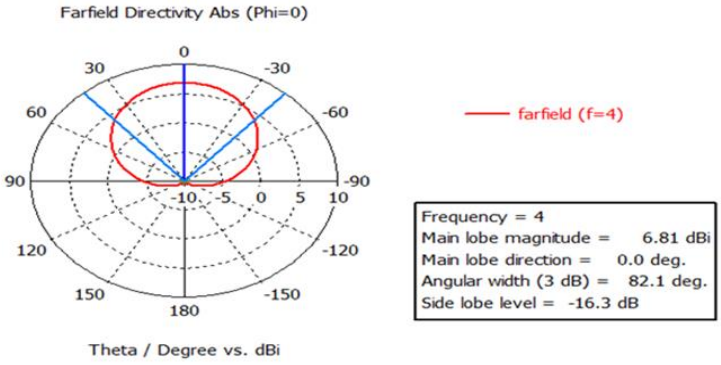

Fig. 3.19: *Farfield directivity of a conventional patch antenna at phi = 0 plane.*

From the above figure, it can be seen that the directivity of the designed conventional patch antenna is **6.81 dBi** and has an angular beamwidth (3-dB) of **82.1º** and a side lobe level of **-16.3 dB**. The main lobe direction is along **Theta = 0º** , i.e. along the z-direction of the patch antenna and normal to the surface of the patch.

The gain of the antenna gives a relative measure of the antenna's ability to direct or concentrate the radiated energy in a particular direction. The Fig. 3.20 shows the far field gain of the designed patch antenna at 4 GHz at phi = 0 plane.

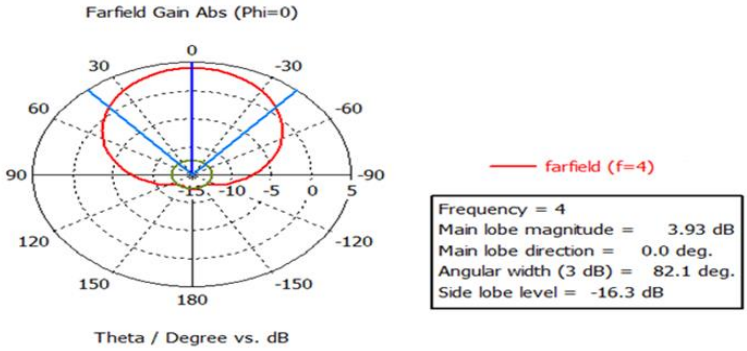

Fig. 3.20: *Farfield gain of a conventional patch antenna at phi = 0 plane.*

From the far-field gain figure, it can be seen that the gain of the designed conventional patch antenna is equal to **3.93 dB** which is respect to the gain of the isotropic antenna for the same amount of input power.

The farfield power pattern of the designed conventional patch antenna is shown in the Fig. 3.21 at phi = 0 plane at the resonant frequency of 4 GHz.

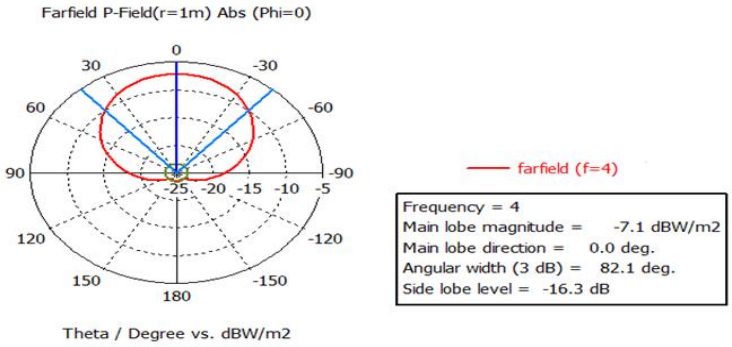

Fig. 3.21: *Power pattern of a conventional patch antenna at Phi = 0 plane.*

From the figure, it is seen that the power of the main lobe magnitude for the designed patch antenna is **-7.1 dBW/m^2**.

The voltage standing wave ratio (VSWR) is the function of reflection coefficient and defines the power reflected from the antenna due to mismatch between the load impedance and the impedance of the antenna. The Fig. 3.22 shows the VSWR of the designed antenna as a function of frequency.

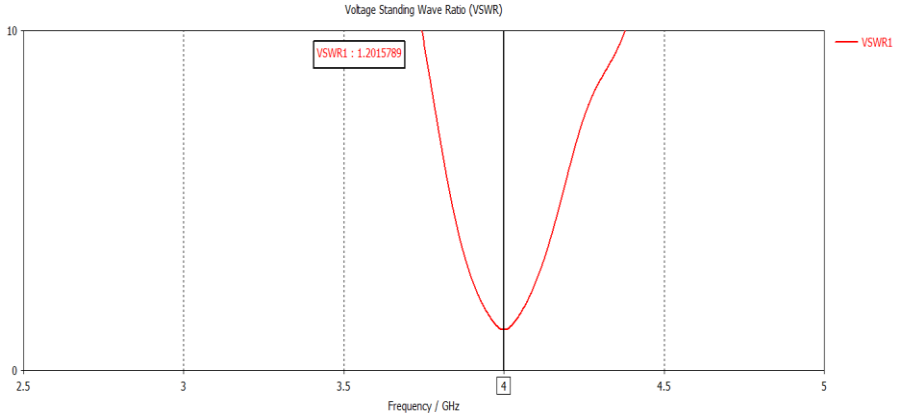

Fig. 3.22: *Variation of VSWR of a conventional patch antenna as a function of frequency.*

From the above plot of VSWR, it is seen that the VSWR is minimum at the resonant frequency of the designed antenna and is equal to **1.201**.

3.3 Design and simulated results of a microstrip patch antenna using complementary split ring resonators at 4 GHz

As the technology is rapidly growing, the needs for better patch antennas are being proposed with better performance and compact size. Nowadays, metamaterial based patch antennas have become very popular wireless communication. Many techniques have been proposed for the size reduction of the microstrip patch antenna which are like embedded tails along the edges [48], loading a substrate with high dielectric [49], employing shorting pins and wall at the patch [50,51] and making cutting slots on the radiating patch [52] which are different from the metamaterial based technique for size miniaturization. In this section, metamaterial based concept is used for reducing the size of the patch and hence achieves a compact size antenna with higher packing efficiency. Complementary split ring resonator (CSRR) which is the dual of split ring resonator (SRR) is etched at the ground plane of the patch antenna. The microstrip patch antenna with an array of complementary split ring resonator is designed on a FR-4 (Lossy) substrate with relative permittivity 'ε_r' value equal to 4.4 and relative permeability 'μ_r' value equal to 1.0. The height of the substrate 'h' has a value equal to 1.6 mm and having a loss tangent '$tan\delta$' value equal to 0.025. The patch is designed using the Eq. 3.21 through Eq. 3.28 using copper and has the electrical conductivity 'σ' equal to 5.8×10^7 S/m. The copper has a thickness of 0.035 mm for both the patch and the ground plane of the designed antenna. The dimension of the CSRR is given in the coming part of this section and the results for the designed CSRR loaded patch antenna are simulated. The inset feed technique is used for impedance matching of the antenna with a transmission line having a characteristic impedance of 50 Ω. The various parameters like S-parameter, far-field gain, far-field directivity, main lobe power pattern, bandwidth and VSWR for the designed CSRR loaded patch antenna are shown in the result part of this section.

3.3.1 Design of a CSRR loaded microstrip patch antenna

The complementary split-ring resonator which is also called as the slotted split-ring resonator or dual split-ring resonator comprises of slots corresponding to the SRR structure. These slots have the exact dimension which corresponds to the SRR to introduce capacitance in the rings. By using the principle of duality, the CSRRs exhibit the properties that are dual to that of the SRRs. The SRRs shows the property of magnetic point dipole, and by using the duality principle as proposed by Babinet [53], the CSRR can behave as an electric point dipole with the negative polarizability. Thus the fields scattered by the CSRR are given by the fields which are produced by the electric dipole. Since the CSRR is the dual of SRR, the CSRR is not excited by the magnetic field but is excited by the electric field. The electric field is kept parallel to the axis of the CSRR and thus CSRR are etched on the ground plane of the patch antenna such that they are easily excited by the electric field which is parallel to the axis. The CSRR unlike SRR will not affect the relative permeability of the material but will affect the relative permittivity of the medium. The equation used for designing the SRR can also be used for designing the CSRR. The schematic for the split ring resonator and its dual complementary split ring resonator is shown in the Fig. 3.23.

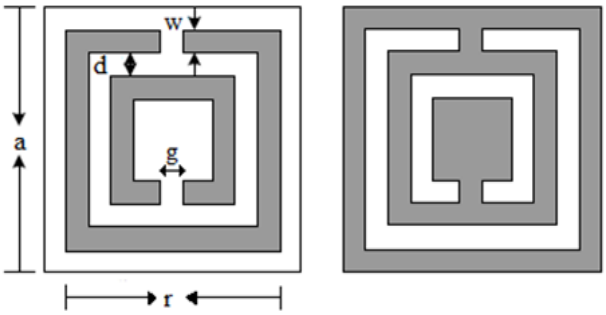

Fig. 3.23: *SRR (left) and CSRR (right) and its relevant dimension.*

Here, '*a*' is the lattice dimension for the designed CSRR, '*r*' is the length of the outer ring, '*d*' is the distance between the two concentric rings, '*w*' is the width of the ring and '*g*' is the slit gap in the rings. The grey portion in the above figure represents the copper while the white portion is the substrate which is exposed after etching the copper from the substrate. The relevant dimension of the designed CSRR is given in the table 3.3.

Table 3.3 Dimension of the designed CSRR.

CSRR Parameters	Dimension
Lattice Dimension (*a*)	6.00 mm
Outer length of ring (*r*)	5.00 mm
Width of ring (*w*)	0.65 mm
Distance between two rings (*d*)	0.50 mm
Slit gap (*g*)	0.40 mm

The simulated result of relative permittivity for the designed CSRR as a function of frequency is shown in the Fig. 3.24.

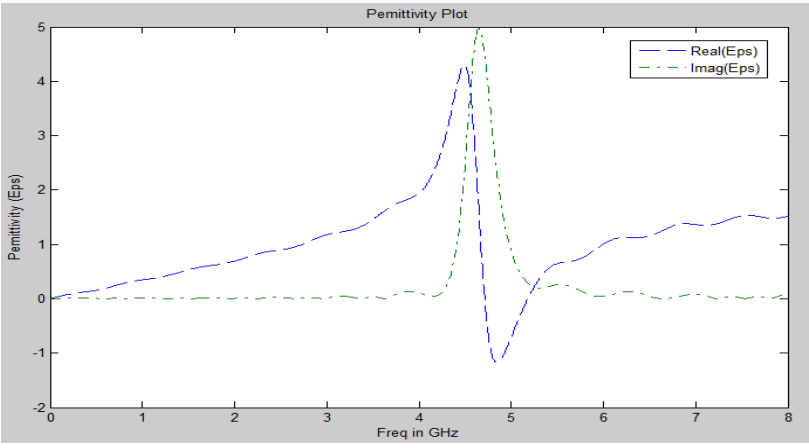

Fig. 3.24: *Variation of permittivity as a function of frequency for a designed CSRR.*

The simulated result for the CSRR shows that the real part of permittivity is negative in the frequency range from 4.7 GHz to 5.3 GHz while the imaginary part of the permittivity takes a value in frequency range from 4.3 GHz to 5.2 GHz. The real part of the permittivity continuously increases from DC frequency to resonant frequency of the CSRR and then attains a negative value till plasmonic frequency and thereafter again starts to increase. The real part of the permittivity attains a maximum value of 4 at 4.6 GHz while the imaginary part of the permittivity attains a maximum value at 4.8 GHz. Here, the complementary split ring

resonator has a resonant frequency of 4.5 GHz where the relative permittivity attains a negative value and continues to be negative till 5.3 GHz which is the plasmonic frequency for the designed CSRR. The simulated result for the designed CSRR can be verified mathematically using the Eq. 2.30 through Eq. 2.34 as proposed in the previous chapter of metamaterials.

In our proposed work, a microstrip patch antenna is designed whose resonant frequency is in the range of 4.4 GHz to 4.7 GHz where the CSRR exhibits a positive and large value of permittivity. In this work, a microstrip patch is designed whose resonant frequency is equal to 4.62 GHz.

The dimensions of the patch antenna with resonant frequency equal to 4.62 GHz are calculated using the Eq. 3.21 through Eq. 3.28. The dimensions for the patch antenna are formulated in the form of a table and are given in the table 3.4.

Table 3.4 Antenna parameters for CSRR loaded microstrip patch antenna.

Antenna Parameters	Dimension
Width (W)	17.50 mm
Length (L)	14.86 mm
Cut Depth (y_o)	5.64 mm
Feed Width (w_f)	3.11 mm
Feed Length (L_f)	17.79 mm
Cut Width (x)	5.00 mm

3.3.2 Simulation and simulated results of CSRR loaded microstrip patch antenna

The CSRR loaded microstrip patch antenna designed in CST Microwave Studio is simulated and the various parameters like reflection coefficient, far-field gain, far-field directivity, main lobe power pattern, 3-dB angular width, VSWR and the bandwidth are computed during the simulation are their plot are shown. The designed microstrip patch antenna has an array of CSRR etched at the ground plane of the patch antenna. The Fig. 3.25 (a) shows the top view of the designed patch antenna, while Fig. 3.25 (b) is the bottom view of the designed patch antenna which contains three CSRR etched at the ground plane of the antenna just behind the patch.

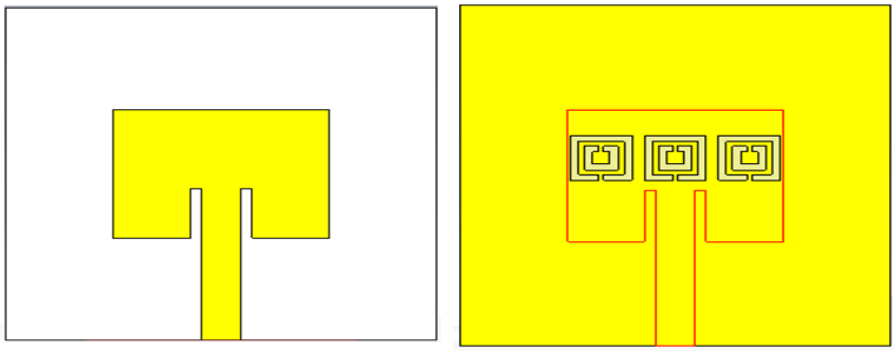

(a) **(b)**

Fig. 3.25: (a) *Top view,* ***(b)*** *Bottom view of a designed microstrip patch antenna with CSRRs at the ground plane.*

The Fig. 3.26 (a) gives the orientation of the designed patch antenna while the Fig. 3.26 (b) shows the waveguide port connected to the transmission line feed of the microstrip patch antenna.

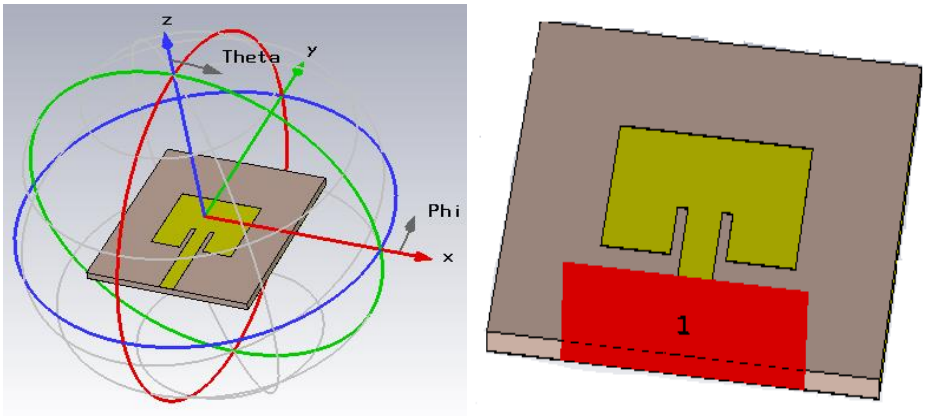

(a) **(b)**

Fig. 3.26: (a) *Orientation,* ***(b)*** *Waveguide port of the CSRR loaded patch antenna.*

The feed signal for the CSRR loaded patch antenna is oriented along the Y-direction and has a fundamental mode of TM_{10}. The reflection coefficient is simulated at the waveguide port 1 for the microstrip patch antenna. The S-parameter S(1,1) which is the reflection coefficient of the patch is shown in the Fig. 3.27.

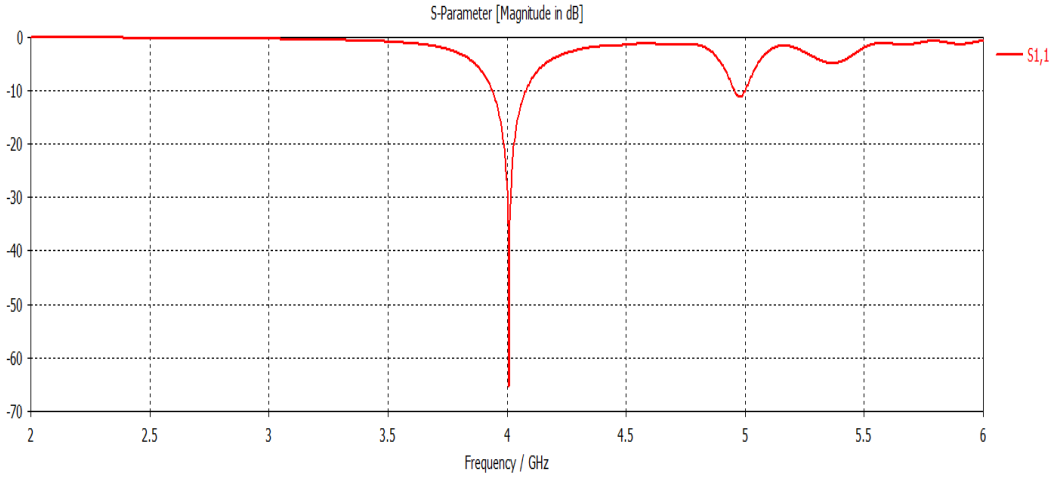

Fig.3.27: *S(1,1) parameter result for a CSRR loaded patch antenna.*

The reflection coefficient for the patch antenna shows that the resonant frequency of the CSRR loaded patch antenna is **4 GHz** and has a magnitude of **-65 dB**.

The reflection coefficient which varies as a function of frequency is also used to calculate the bandwidth of the antenna using a -10 dB points. The Fig. 3.28 shows S-parameter plot with two -10 dB frequency points.

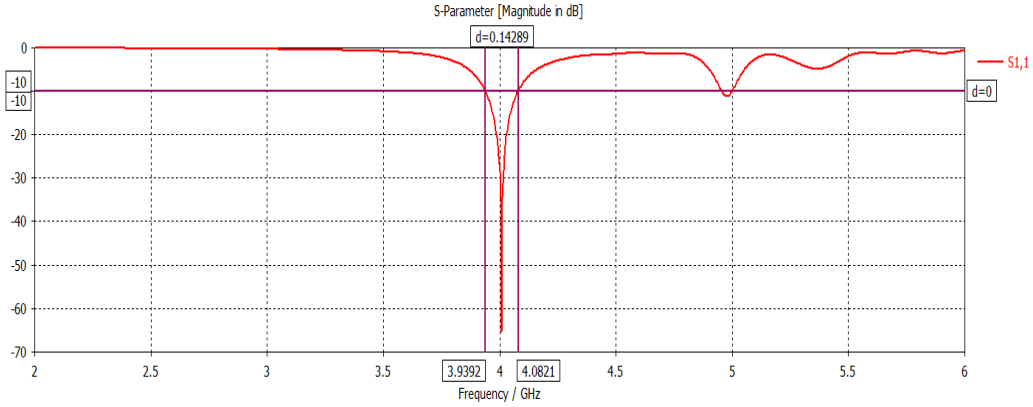

Fig. 3.28: *S(1,1) parameters with -10 dB points.*

From the above diagram it is seen that the two -10 dB points are at **3.9392 GHz** and **4.0821 GHz** which gives the bandwidth of the patch antenna equal to the difference between these two points. The bandwidth of this CSRR loaded patch antenna is found out to be **142.89 MHz.**

The Fig. 3.29 shown below shows the far-field directivity of the designed CSRR loaded microstrip patch antenna at 4 GHz at phi = 0 plane, i.e. the E-plane of the antenna.

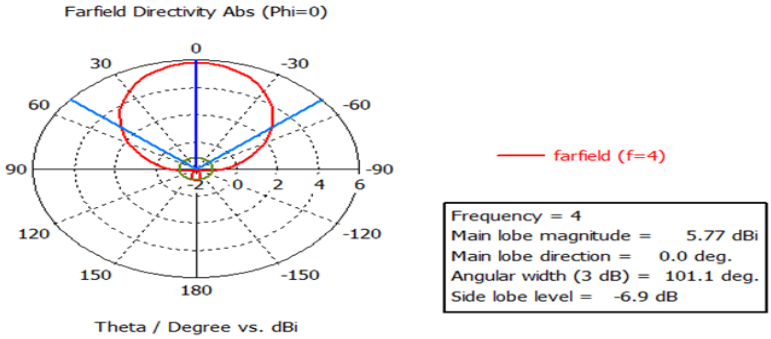

Fig. 3.29: *Farfield directivity of a CSRR loaded patch antenna at phi = 0 plane.*

From the simulation result of farfield directivity of a patch antenna, it is seen that the designed antenna has a directivity equal to **5.77 dBi**, angular 3-dB width equal to **101.1º** and a side lobe level of **-6.9 dB**. The main lobe direction is along **Theta = 0º** , i.e. normal to the surface of the patch.

The Fig. 3.30 shows the far-field gain of the CSRR loaded patch antenna at 4 GHz for phi = 0 plane.

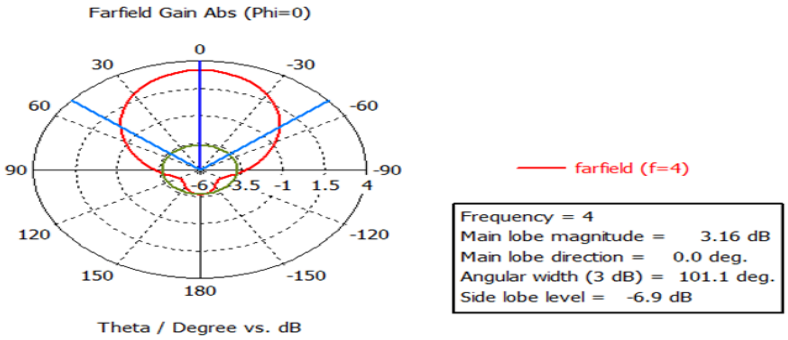

Fig. 3.30: *Farfield gain of a CSRR loaded patch antenna at phi = 0 plane.*

From the figure, it is seen that the farfield gain of the CSRR loaded patch antenna has a value of **3.16 dB** which is with respect to the isotropic antenna for the same amount of input power.

The farfield power pattern of the designed CSRR loaded patch antenna is shown in the Fig. 3.31 at phi = 0 plane having a resonant frequency of 4 GHz.

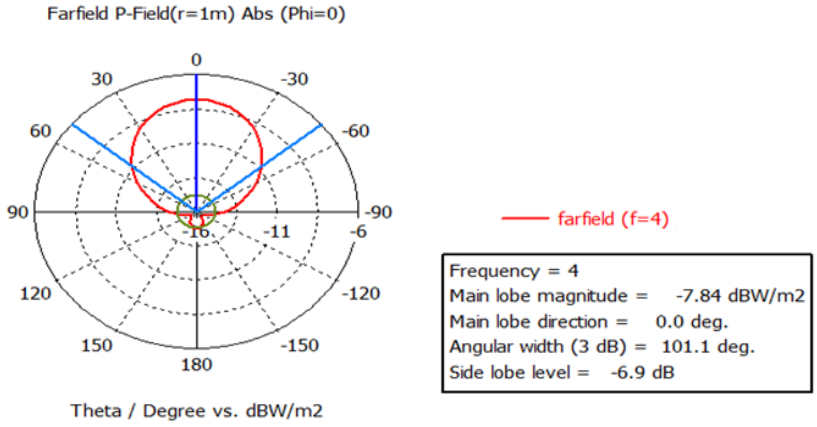

Fig. 3.31: *Power pattern of a CSRR loaded patch antenna at Phi = 0 plane.*

From the figure shown for the far-field power pattern, it is seen that the designed CSRR loaded patch antenna has a main lobe magnitude of **-7.84 dbW/m^2**.

The figure 3.32 shows the VSWR for the designed CSRR loaded microstrip patch antenna as function of frequency.

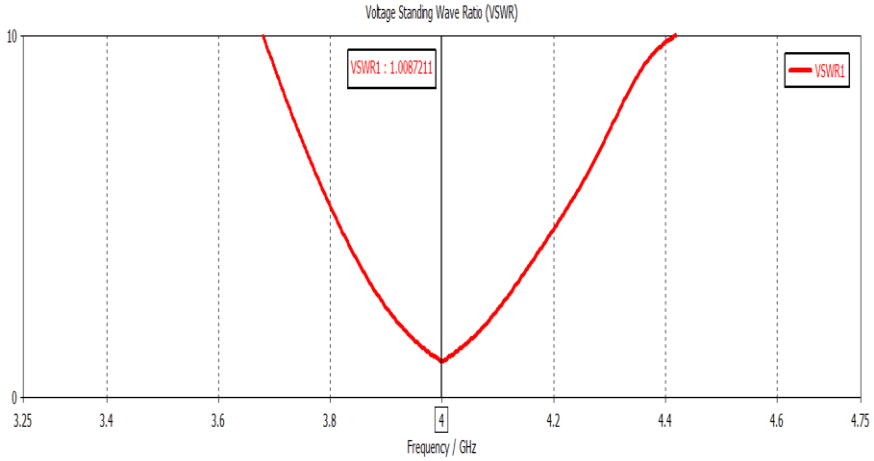

Fig. 3.32: *Variation of VSWR of a CSRR loaded patch antenna as a function of frequency.*

From the above plot of VSWR, it is seen that the VSWR is minimum at the resonant frequency of the designed antenna and is equal to **1.008**.

From the simulated result of the CSRR loaded patch antenna and conventional patch antenna, it can be concluded that the resonant frequency of the conventional microstrip patch antenna decreases when the ground plane of the antenna is loaded with an array of CSRR with appropriate dimensions. Thus the CSRR loaded patch antenna helps in miniaturization of the patch antenna. Also from the above results of conventional patch antenna and CSRR loaded patch antenna, it is seen that the far-field directivity, far-field gain and the magnitude of main lobe power pattern slightly decreases as the size of the patch is reduced while there is an increase in its bandwidth, 3-dB angular width and side lobe level.

3.4 Gain and directivity enhancement of the CSRR loaded microstrip patch antenna using double-superstrate configuration.

In the previous section, we simulated a CSRR loaded patch antenna which suffered a drawback of reduced directivity, gain and main lobe power pattern. These drawbacks need to be overcome as nowadays antennas with high directivity, high gain and main lobe power are required for wireless communication system. High directivity and gain antennas are required to direct the power in a particular direction and for transmitting more power towards the receiver respectively. Many techniques like spiral-shaped electromagnetic bandgap structures antennas [54], Fabry-Perot cavity antenna [55] and parasitic patch small patch antenna [56] are used to increase the directivity and gain of the designed patch antenna.

In this section, a double-superstrate configuration is used to enhance the directivity and gain of the designed CSRR loaded patch antenna. The two dielectric superstrates are used above the patch which are separated by the air gaps and acts like an aperture to the antenna and thus increases the effective aperture size which further enhances the directivity of the patch antenna when compared to a conventional patch antenna [57]. Dielectric superstrates over the ground plane of the patch uses the concept of multiple reflection phenomenon [58-60] in order to improve the directivity, gain and the main lobe power pattern of the microstrip patch antenna. The two dielectric layers which are used as superstrates have some finite thickness and are separated to each other by an air gap. The thickness of the superstrates and the thickness of the air gaps are the key parameters for controlling the directivity and gain enhancement for the patch antenna. The structure of the double-superstrate configuration (DSC) over the designed CSRR loaded patch antenna is shown in the Fig. 3.33.

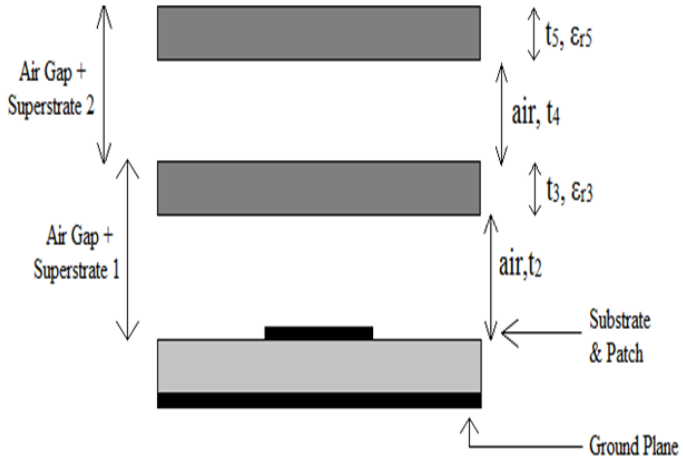

Fig. 3.33: *Structure of a double-superstrate configuration over a microstrip patch antenna.*

The superstrate 1 in the figure shown for the structure of DSC has a relative permittivity of 'ε_{r3}' and the thickness of 't_3' which is separated by an air gap of thickness 't_4' with the superstrate 2 which is placed above the superstrate 1. The superstrate 2 has a thickness of 't_5' and the relative permittivity of 'ε_{r5}'. The patch of the antenna is separated from the superstrate 1 by an air gap of thickness 't_2'. The thickness of the air gaps and the superstrates are optimized to give the maximum directivity and gain of a designed patch antenna [57]. The thickness of the superstrates is given in the Eq. 3.29.

$$t_i = \frac{\lambda_o}{4\sqrt{\varepsilon_{ri}}} \qquad i = 3,5 \tag{3.29}$$

The thickness of the two superstrates is calculated using the above expression where 'λ_o' is the wavelength in free space. The resonant frequency of the designed CSRR loaded patch antenna is 4 GHz, thus the free space wavelength 'λ_o' is equal to 75 mm. The relative permittivity of both the superstrates has the same value, i.e. $\varepsilon_{r3} = \varepsilon_{r5} = 3.0$. In order to maximize the directivity and gain of the antenna, the thickness of the air gap 2, i.e. 't_4' is optimized to a value equal to $0.27\lambda_o$ and the thickness of the air gap 1, i.e. 't_2' is optimized to value equal to $0.44\lambda_o$ as proposed by Kaymaram [57]. The dimension of the two superstrates, i.e. the length and the width of the superstrates are kept equal to the length and the width of the substrate respectively on which a patch antenna is designed. The parameters for the thickness of the superstrates and the air gaps of the double-superstrate configuration are given in the table 3.5 shown below.

Table 3.5 Design parameters for double-superstrate configuration.

Parameter	Thickness (mm)
Superstrate 1 (t_3)	10.82
Air Gap 1 (t_2)	33.00
Superstrate 2 (t_5)	10.82
Air Gap 2 (t_4)	20.75

The 3-D view of the CSRR loaded patch antenna with the double-superstrate configuration designed in CST Microwave Studio with the calculated superstrates thickness and the thickness of the air gaps is shown in the Fig. 3.34.

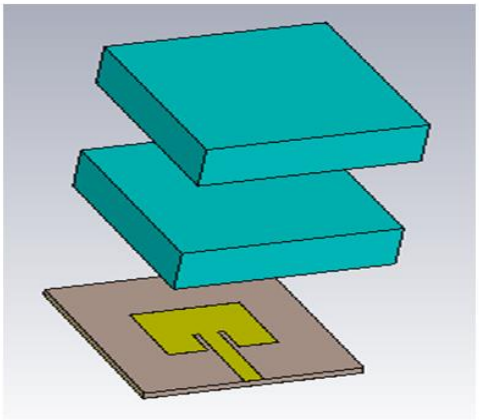

Fig. 3.34: *3-D view of a CSRR loaded patch antenna with two layers of superstrates.*

The dimensions of the designed patch antenna is kept same, thus the above antenna has the same frequency of operation, i.e. at 4 GHz. The simulation of the above designed patch antenna is done in CST Microwave Studio to verify the results of the proposed CSRR loaded patch antenna with DSC. The various parameters like S-parameter, far field gain, far field directivity, main lobe power pattern, bandwidth and VSWR are computed.

The S-parameter S(1,1), i.e. the reflection coefficient of the CSRR loaded patch antenna with DSC is shown in the Fig. 3.35.

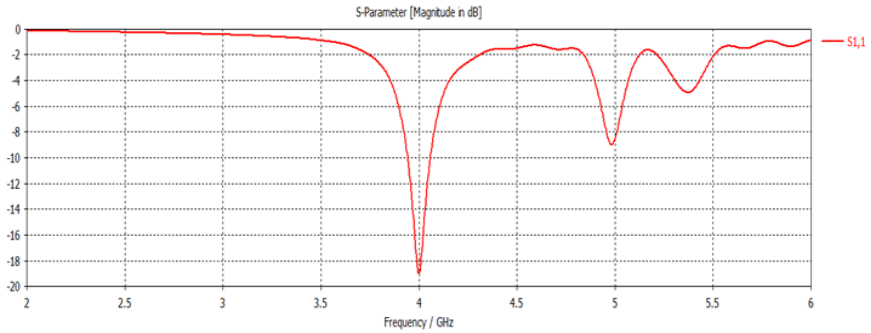

Fig. 3.35: *S(1,1) result of a CSRR loaded Patch Antenna with DSC.*

The reflection coefficient for the patch antenna shows that the resonant frequency of the CSRR loaded patch antenna with DSC is **4 GHz** and has a magnitude of **-19 dB**. The reflection coefficient which varies as a function of frequency is also used to calculate the bandwidth of the antenna using a -10 dB points. The Fig. 3.36 shows S-parameter plot with two -10 dB frequency points.

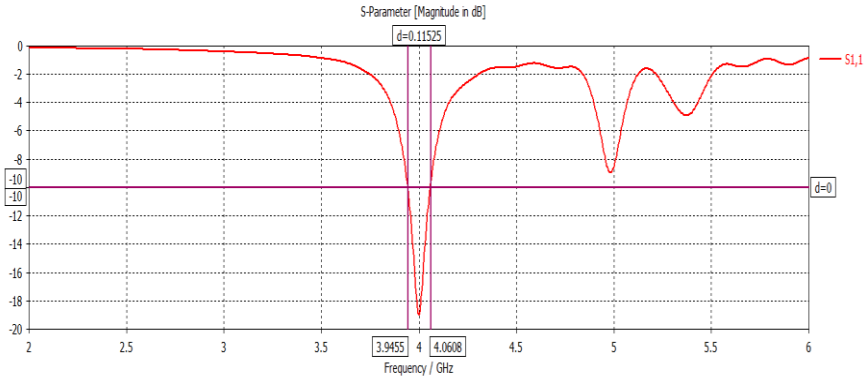

Fig. 3.36: *S(1,1) parameters with -10 dB points.*

From the above diagram it is seen that the two -10 dB frequency points are at **3.9455 GHz** and **4.0608 GHz** which gives the bandwidth of the patch antenna equal to the difference between these two points. The bandwidth of this CSRR loaded patch antenna is found out to be **115.25 MHz**.

The Fig. 3.37 shown below shows the farfield directivity of the designed CSRR loaded microstrip patch antenna with DSC at 4 GHz at phi = 0 plane, i.e. the E-plane of the antenna.

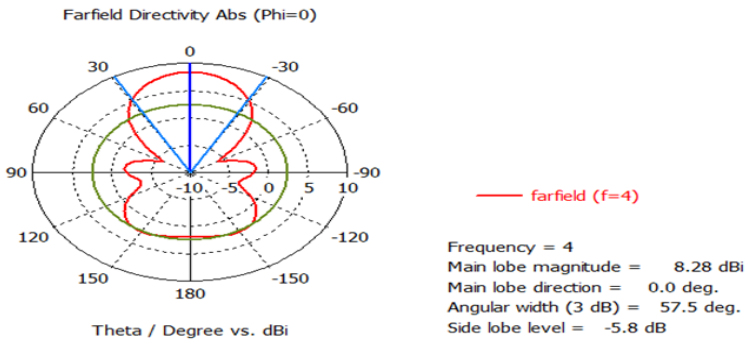

Fig. 3.37: *Farfield directivity of a CSRR loaded patch antenna with DSC at phi = 0 plane.*

From the simulation result of far-field directivity of a patch antenna with DSC, it is seen that the designed antenna has a directivity equal to **8.28 dBi**, angular 3-dB width equal

to **57.5º** and a side lobe level of **-5.8 dB**. The main lobe direction is along **Theta = 0º**, i.e. normal to the surface of the patch.

The Fig. 3.38 shows the far-field gain of the CSRR loaded patch antenna with DSC at 4 GHz for phi = 0.

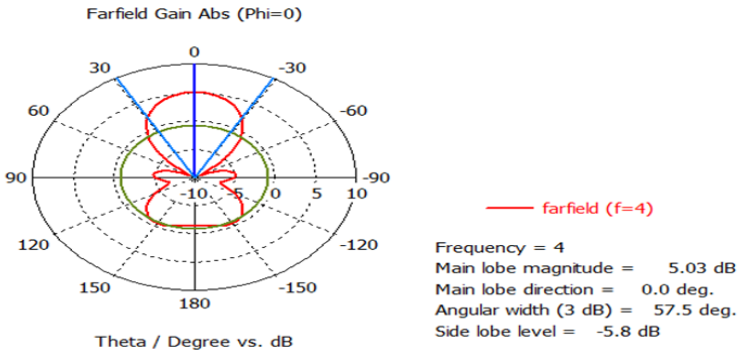

Fig. 3.38: *Farfield gain of a CSRR loaded patch antenna with DSC at phi = 0 plane.*

From the above figure, it is seen that the farfield gain of the CSRR loaded patch antenna has a value of **5.03 dB** which is with respect to the isotropic antenna.

The farfield power pattern of the designed CSRR loaded patch antenna with DSC is shown in the Fig. 3.39 at phi = 0 plane having a resonant frequency of 4 GHz.

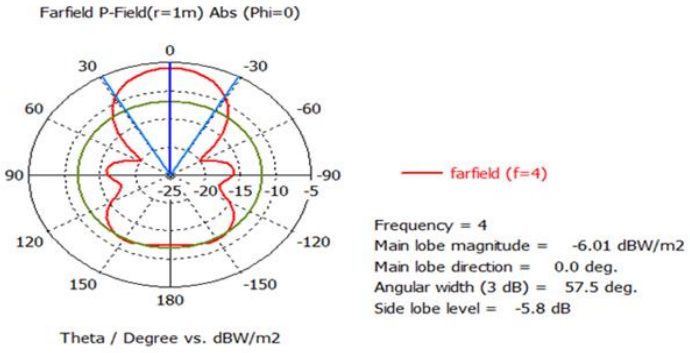

Fig. 3.39: *Power pattern of a CSRR loaded patch antenna with DSC at Phi = 0 plane.*

From the far-field power pattern figure, it is seen that the power of the main lobe magnitude is **-6.01dBW/m^2**.

The figure 3.40 shows the VSWR for the designed CSRR loaded microstrip patch antenna with DSC as function of frequency.

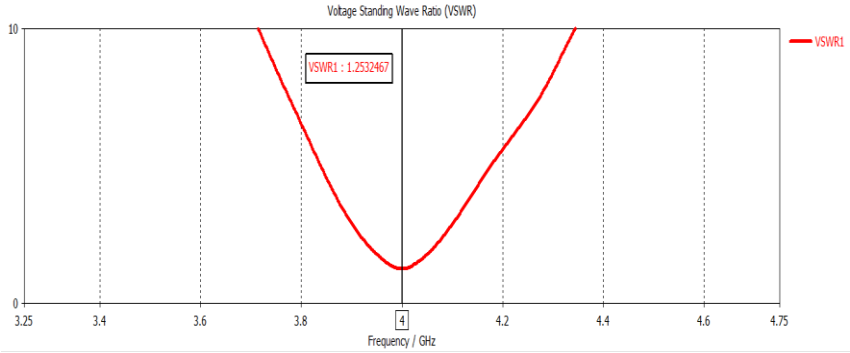

Fig. 3.40: *Variation of VSWR of a CSRR loaded patch antenna with DSC as a function of frequency.*

From the above plot of VSWR, it is seen that the VSWR is minimum at the resonant frequency of the designed antenna and is equal to **1.2532**.

3.5 Comparative analysis of various performance parameter for the designed patch antennas

In this section, the comparison between the performance parameters of the conventional microstrip patch antenna, CSRR loaded microstrip patch antenna and CSRR loaded microstrip patch antenna with double-superstrate layer is shown and formulated in the form of a table. The table 3.6 summarizes the comparison of various type of patch antennas having the same resonant frequency. The comparison table has performance parameters like dimensions (width×length), area of the patch antennas, far-field directivity, far-field gain, main lobe power magnitude, bandwidth, 3-dB angular beamwidth and side-lobe level. The percentage miniaturization of the CSRR loaded patch with respect to conventionally designed patch antenna is calculated in terms of the area using the Eq. 3.30 given below.

$$\%\, Size\ miniaturization = \frac{Area\ of\ CPA - Area\ of\ CSRRPA}{Area\ of\ CSRRPA} \times 100 \qquad (3.30)$$

Here, 'CPA' stands conventionally designed patch antenna and 'CSRRPA' stands for CSRR loaded patch antenna.

Table. 3.6 Comparitive analysis of performance parameters for designed patch antennas.

Parameter	Conventional Patch Antenna	CSRR loaded Patch Antenna	CSRR loaded Patch Antenna with DSC
Dimensions (Width×Length) (mm×mm)	22.82 × 17.01	17.50 × 14.86	17.50 × 14.86
Area (mm^2)	388.1682	260.05	260.05
Farfield Directivity (dBi)	6.81	5.77	8.28
Farfield Gain (dB)	3.93	3.16	5.03
Main Lobe Power (dBW/m^2)	-7.1	-7.84	-6.01
Bandwidth (MHz)	131.5	142.89	115.25
VSWR	1.201	1.008	1.253
Angular Width (3dB) (deg.)	82.1	101.1	57.5
Side Lobe Level (dB)	-16.3	-6.9	-5.8

From the above table we can conclude that the CSRR loaded patch antenna has smaller dimension than the dimensions of a conventional patch antenna having the same resonant frequency of 4 GHz. The CSRR loaded patch antenna showed a significant improvement in its bandwidth but suffered a drawback of reduced far-field directivity, far-field gain and magnitude of main lobe power which was overcome by using double-superstrate layers over a microstrip patch. The CSRR loaded patch antenna with DSC showed

a significant improvement in the performance parameters of the antenna which had the same dimensions to that of a CSRR loaded patch antenna. From the above table, it is seen that the directivity of the CSRR loaded patch antenna with DSC has increased by **2.51 dBi** and its gain improved by **1.87 dB**. The proposed CSRR loaded patch antenna with DSC helped us achieve a size reduction of **33%** with better performance parameters to that of a conventionally designed patch antenna.

3.6 Fabrication and testing of a designed CSRR loaded patch antenna

The CSRR loaded microstrip patch antenna is designed on a printed circuit board (PCB) with a copper as the perfect electrical conductor (PEC) of height 0.035 mm on a FR-4 substrate having a dielectric constant of 4.4 and thickness equal to 1.6 mm. The layout of the designed patch and the CSRR is designed in Coral Draw graphic design software for preparing the masks. Once the mask is printed on the transparent sheet, the patch and the CSRR at the ground plane is fabricated using conventional photolithography process. Photolithography method is a chemical etching process which is used to remove the unwanted metal regions of the PCB. Photolithography method produces highly accurate etched pattern for a microstrip patch. The fabrication accuracy is very important and critical as the microstrip patch antennas are narrow band resonant structure in which the errors in the patch dimensions will shift the resonant frequency of the antenna. The front and the back view of the fabricated patch antenna are shown in the Fig. 3.41.

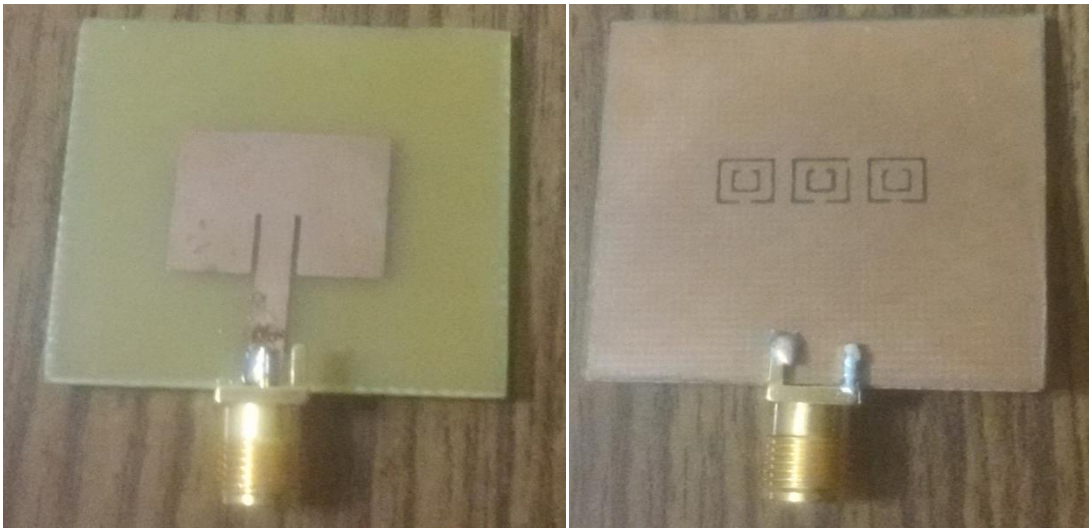

(a) ***(b)***

Fig. 3.41: (a) *Front view,* ***(b)*** *back view of fabricated patch antenna*

The measurement and testing of the fabricated CSRR loaded patch antenna is done using a Scalar Network Analyzer, Model No.: HP8757A having a sweep oscillator to control the display of the analyzer, Model No.: HP8350B. A RF Plug-In, Model No.: HP83525A is used to feed power to the patch antenna which is connected to it via Directional Bridge, Model No.: HP85027C. The figure 3.42 shows the setup for measuring the reflection the reflection coefficient for the designed patch antenna.

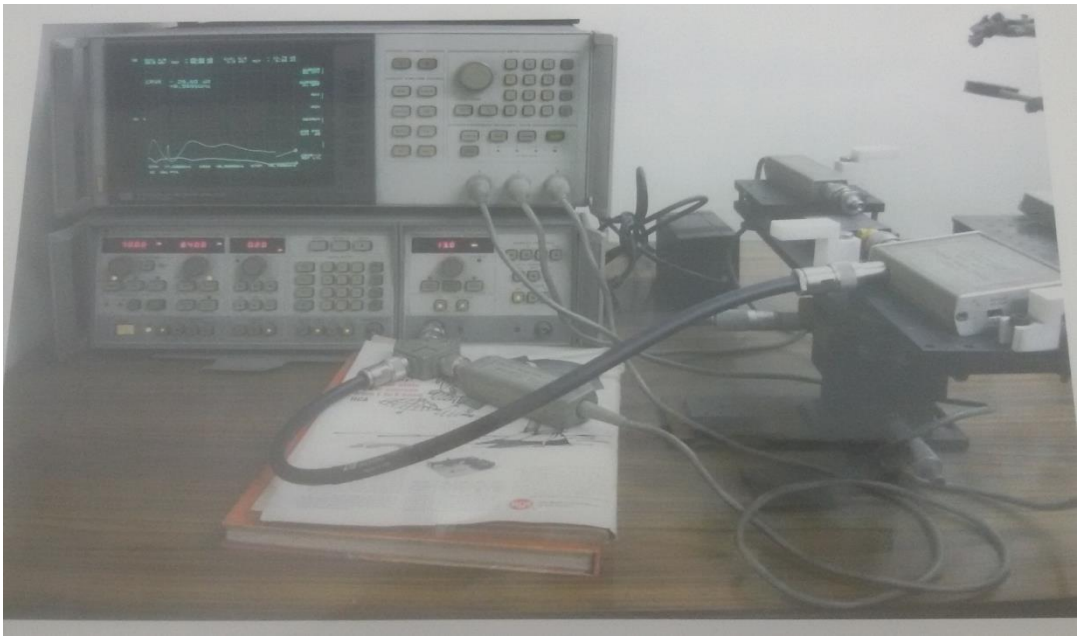

Fig. 3.42: *Experimental setup for measuring the reflection coefficient for the patch antenna.*

The Fig. 3.43 shows the result obtained during testing on the scalar network analyzer.

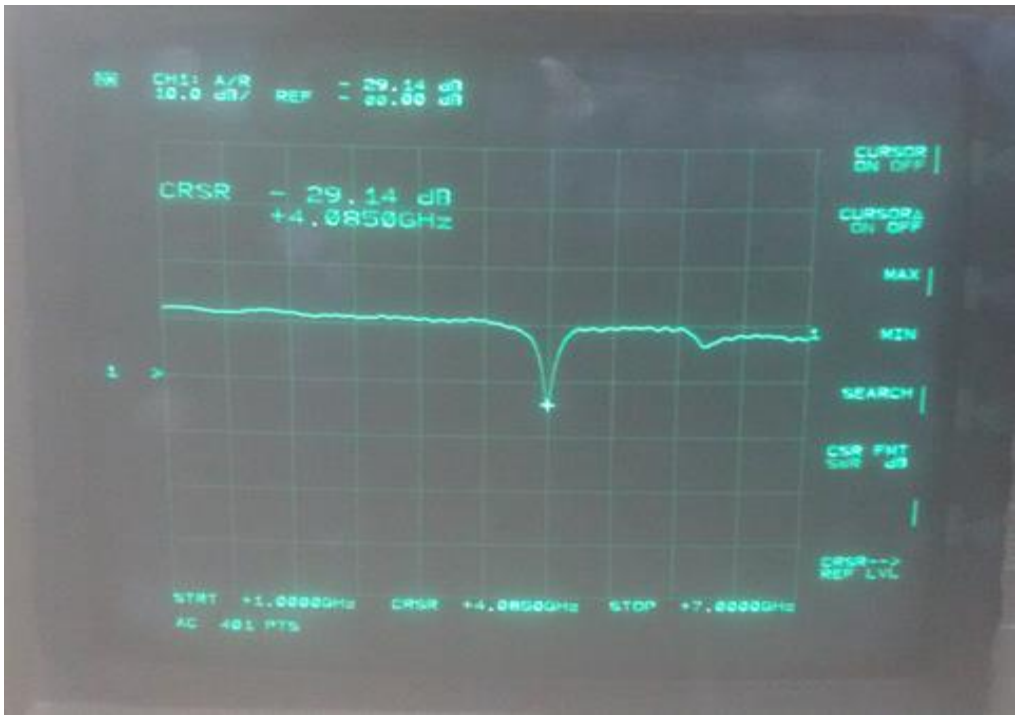

Fig. 3.43: *Tested result of the CSRR loaded patch antenna on network analyzer.*

The tested result shows that the designed CSRR loaded patch antenna has a resonant frequency of **4.0850 GHz** which is very close to the resonant frequency of the proposed design.

CHAPTER 4
Microstrip bandpass filter based on metamaterials

4.1 Introduction to filters

A basic review of some of the microwave filters are presented in this section before designing a bandpass filter. A filter is a device which removes the undesired frequency components from a signal while allowing the desired signal components to pass through them, or in other words we can say that a filter is a two port device which attenuates unwanted frequency component and allows transmission of the desired frequency component of an electrical signal. For the microwave filters, the range of frequency lies from ~300 MHz to ~300 GHz. The ability of the filter to reject the unwanted frequencies in a signal and pass the desired frequency find its application in several areas in wireless communication and signal processing field. For designing a microwave filters, certain important factors like cost for the device, fabrication difficulty, size of the filter and the ability of the component to be easily integrated with the other technologies are considered. These filters can be classified into three types: active filters which require an external power for its operation, passive filters which requires no external power and hybrid filters which is the combination of active and passive filters. In addition to it, filters can be classified into four types based on the frequency response: low-pass, high-pass, band-stop and band-pass filter.

A microwave filter can be represented as a two-port network which has two pairs of terminals that connects the network to the external circuit. This pair of terminal is known as ports and has a condition that the current entering in one terminal is equal to the current exiting the second terminal. The two-port network can be analyzed with the help of several performance measures like scattering (S) parameters, ABCD parameters, impedance (Z) parameters, admittance (Y) parameters, etc. In this work, S-parameters are used for analyzing the designed filter.

The passive RF and microwave filters are often represented by the lumped element models in which the circuits is made up of series and parallel or shunt combination of capacitors and inductor components. The lumped components can be usually represented in dual types of network configuration, first is the T-section network and second is the π-section network.

The Fig. 4.1 shows the T-section and the π-section of the lumped element.

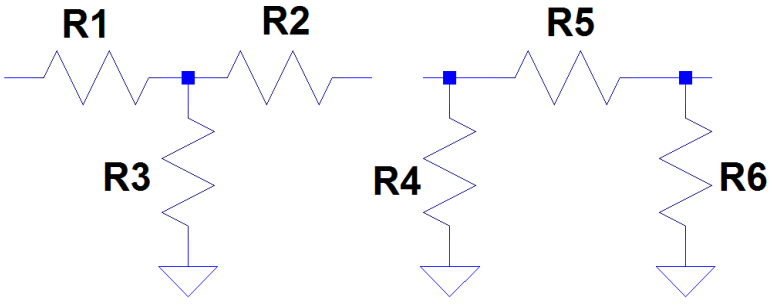

Fig. 4.1: (a) *T-section and,* ***(b)*** *π-section of the lumped elements. (Taken from Ref. [61])*

The T-section has a series element that is connected to a single end of the shunt element and thus making a '*T*' shape. Similarly, the π-section has two shunt elements connected to a series element in between the shunt elements thus making a '*π*' shape. Both the T-section and π-section are symmetric and contains odd number of elements in order to have symmetry during analysis.

The microwave components are classified into four categories depending upon the characteristics of their frequency response. First is the low-pass filter in which the lower frequency components of the signal are passed through the network while the higher frequency components of the signal get attenuated. The lumped element T-section and the π-section of the low-pass filter are shown in the Fig. 4.2.

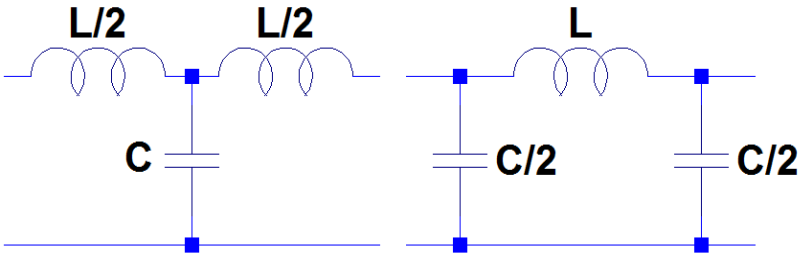

Fig. 4.2: *T-section and the π-section of the low-pass filter. (Taken from Ref. [61])*

The Fig. 4.3 shows the response of a low-pass filters where '*f*' is the cutoff frequency of the filter after which the stopband region starts and provides attenuation to the frequency components of the signal. The normalized output power in the stopband region is less than the half.

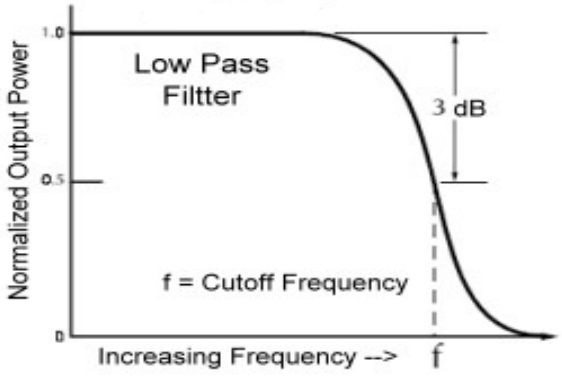

Fig. 4.3: *Response of a low-pass filter as a function frequency.*

In the low-pass filter, the inductor serves as a series element while capacitance acts a shunt element. At lower frequencies below the cutoff frequency, the capacitance acts like open circuit and current flows through the inductor. At higher frequencies above the cutoff frequency, currents flows through the capacitor and effectively short circuiting the line to ground. Thus a very low amount of power is transmitted through the device at the higher frequencies and hence the signal gets attenuated.

The opposite of the low-pass filter is a high-pass filter in which the lower frequency components below the cutoff frequency are attenuated and the higher frequency components of the signal are passed through the network. The T-section and the π-section of the high-pass filter is shown in the Fig. 4.4 below.

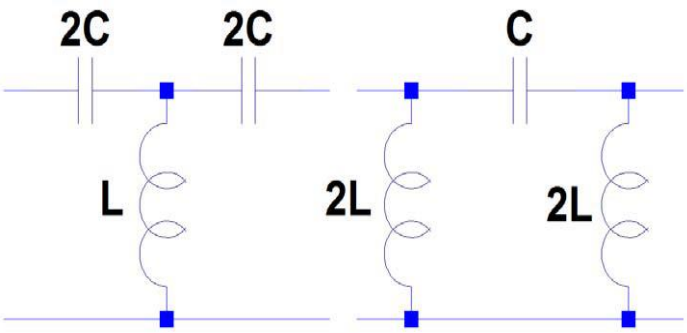

Fig. 4.4: *T-section and the π-section of the high-pass filter. (Taken from Ref. [61])*

In a high-pass filter, the capacitance is a series element while the inductance is a shunt element. At lower frequencies below the cutoff frequency, the inductor acts like a short circuit to the ground thus preventing the signal to pass through the network. At the higher frequencies greater than the cutoff frequency, the inductor acts as an open circuit and capacitance acts as a shirt circuit which allows the signal to propagate through the network. The low-pass and high-pass filters are duals in nature can be transformed from one to another by replacing the inductance with the capacitance and capacitance with the inductance. The Fig. 4.5 shows the response of a high-pass filter.

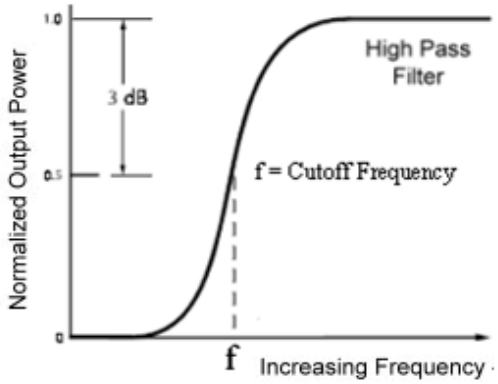

Fig. 4.5: *Response of a high-pass filter as a function frequency.*

Apart from low-pass and high-pass filter, there exist band-stop and band-pass filter. The band-stop filter is a filter which is designed to allow frequencies from DC onward except a certain band of frequencies. This band is called as the stopband of the signal in which the signal gets attenuated and allows propagation to take place in other frequency range. In the band-pass filter, a single band of frequency components is passed while the region outside the passband is attenuated by the network.

The Fig. 4.6 shows the T-section and π-section of the band-stop filter using lumped elements.

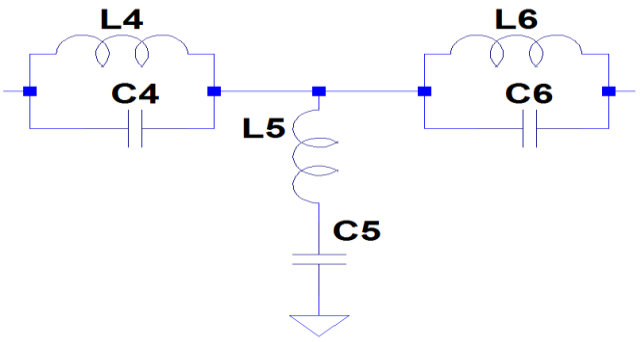

Fig. 4.6: *T-section and the π-section of the band-stop filter. (Taken from Ref. [61])*

The series element of the band-stop filter has a parallel combination of an inductor and capacitor which forms an ideal tank circuit, while the shunt element of the stop-band filter has a series combination of an inductor and capacitor. At the lower and higher frequencies, the capacitance provides very high impedance while the inductor provides very low impedance in the series combination and this provides very low impedance and allows the frequency components of the signal to pass through it. At lower and higher frequencies, the shunt combination acts as an open circuit and thus preventing the signal from being shorted to ground. In the medium frequency range, the shunt elements provide very low impedance which shorts the signal to the ground and hence the medium frequency component of the signal does not pass through the network and forms a stopband.

The Fig. 4.7 below shows the response of the band-stop filter.

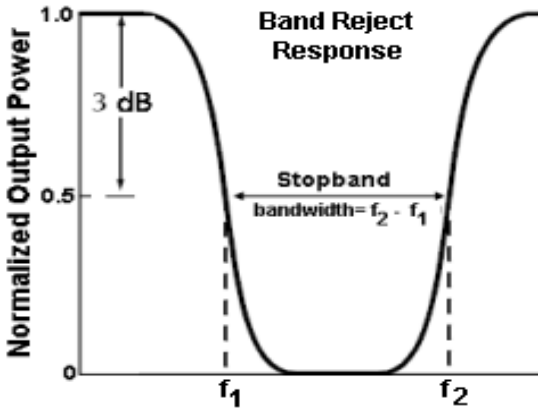

Fig. 4.7: *Response of a band-stop filter as a function frequency.*

Here, 'f_1' is the lower cutoff frequency and 'f_2' is the higher cutoff frequency and the stopband lies between the upper and lower cutoff frequency in which the normalized output power is below the 0.5. Thus the frequency components between the higher and lower cutoff frequency components get attenuated while other frequency components pass through the network.

The Fig. 4.8 shows the T-section and π-section of the band-pass filter using lumped elements.

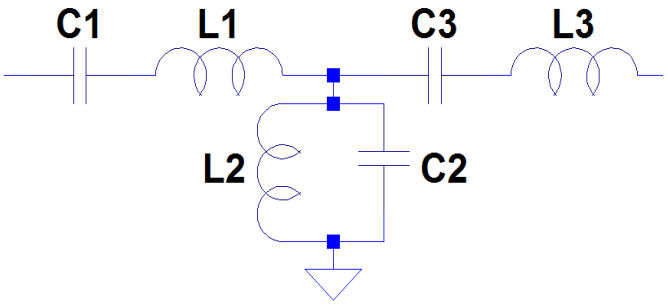

Fig. 4.8: *T-section and the π-section of the band-stop filter. (Taken from Ref. [61])*

The series elements of the band-pass filter has a series combination of inductor and capacitor while the shunt element of the network has parallel combination of inductor and capacitor. The series element offers high impedance at lower and higher frequencies which attenuates the signal to pass through the network. While at medium frequencies, the series elements provide medium impedance which allows signal to propagate through the network while the parallel combination of inductor and capacitor provides high impedance and thus avoiding short circuited condition.

The Fig. 4.9 shown below is the response of the band-pass filter.

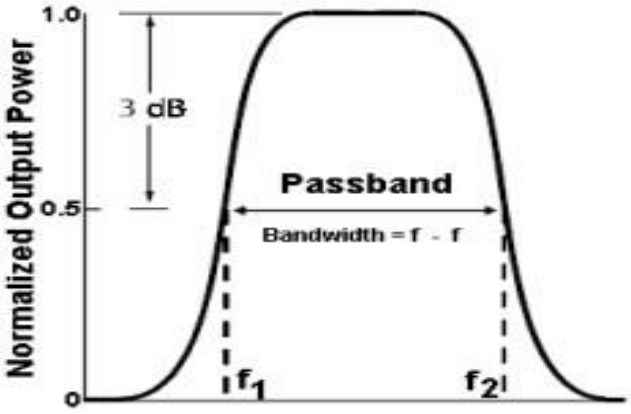

Fig. 4.9: *Response of a band-pass filter as a function frequency.*

Here, 'f_1' is the lower cutoff frequency and 'f_2' is the higher cutoff frequency and the passband lies between the upper and lower cutoff frequency in which the normalized output power is above the 0.5. The frequency components outside the passband get attenuated by the system.

To realize microwave filters, a planar microstrip transmission line design approach is used to design a filter. Microstrip offers several engineering advantages which includes ease to integrate with active and passive devices, small size, low cost and light weight. For designing a microstrip filters various methods have been proposed. The image parameter method on one of the method is conventionally used for designing a microwave filter in which the specification of the passband and the stopband characteristic is defined and the cascade combination of the two-port networks is used for designing a filter. This method is relatively simple but suffers a drawback of arbitrary frequency response of a system and hence not practically used. The image parameter method has various methodologies like constant f-filter section, m-filter section and composite filter structures which are used to design a low pass and high pass filter based on passband and stopband characteristics

specified. The cascade of lowpass and highpass filter designed can be used to design a bandstop and bandpass filter by selecting proper cutoff frequencies of the low-pass and high-pass filters. The insertion loss method is another method which is practically used for designing filters with high degree of freedom to control the passband and the stopband amplitude and phase characteristic and hence synthesize a desired frequency response. The filter response in this method depends upon the power loss ratio and uses some practical response like maximally flat (Butterworth), equal ripple (Chebyshev) and elliptical function for designing a filter. In insertion loss method, first a low-pass filter prototype is designed and then with proper scaling and frequency conversion, other high-pass, bandstop or bandpass filter is designed using this low-pass filter prototype. The filters designed are lumped element filters applicable at lower frequencies. Thus to implement them for microwave range, Richard's transformation and Kuroda's identity are applied to the lumped element filters designed. The Richard's transformation is used to convert the lumped elements into a transmission line section and Kuroda's identity is used to separate this transmission line section and thus makes the microwave filter design more realizable. Impedance and admittance inverters is also used for designing microwave filters. The stepped impedance approach of designing the filters can also be used for designing a lowpass, highpass, bandpass and stopband filter. A parallel coupled transmission line is another approach which can be used to design many types of filters.

Fabrication of bandpass and bandstop filter using coupled line techniques is easy in microstrip lines with a bandwidth less than 20%. The bandpass filters can also be designed using coupled line resonators which includes quarter-wave resonators, capacitively coupled series resonators, capacitively coupled shunt resonator. All the above method provide a narrow bandwidth in its designing thus to achieve a greater bandwidth a new approach of designing a bandpass filter with greater bandwidth is proposed. The wideband bandpass filter is proposed in the next section.

4.2 Design and simulated result of microstrip bandpass filter using CSRR

In this section, a wideband bandpass filter has been designed for wireless communication system. Nowadays, wideband bandpass filter with low insertion loss, low cost and high performance are being desired for its application in various communication fields. A planar bandpass filter are fabricated on printed circuit board by pattern forming which is a very attractive feature for practical use and has a easy method to fabricate it. The planar wideband bandpass filters are usually formed with the help of a transmission lines and requires some proper resonator circuits which may acquire a large area in the communication devices. Thus a compact size wideband bandpass filters are needed to be designed. Complementary split-ring resonators which exhibits negative permittivity and exhibit the characteristics of left-handed metamaterials in planar configuration [62] are proposed in this section for the designing of a wideband bandpass filter. Some of the attractive features of the designed CSRRs are their compact size, high quality factor (Q), low radiation loss and low cost of designing it in a planar structure [63]. Many compact filters using the CSRRs with different structures have been proposed to achieve a wide passband. These includes cascading highpass and lowpass CSRR filters [64], stepped impedance resonators and an open-circuited

stub [65], coupled square loop [66], odd-even modes CSRR bandpass filter [67], dual mode open loop microstrip filters [68], etc. In this proposed work, a improved structure for wideband bandpass filter is designed by changing the crucial design parameters of the filters. A parameter optimizing procedure and a numerical computation were used as proposed by K.T Kim et al [69] for designing a wideband bandpass filter with a compact size and good performance characteristics.

The Fig. 4.10 shows the design of a CSRR loaded transmission line with a capacitive gap and its equivalent lumped element model which is used to design a bandpass filter. This first left-handed transmission line based on the concept of CSRR above it was implemented in the year 2004 [62] with a series gap in the transmission line.

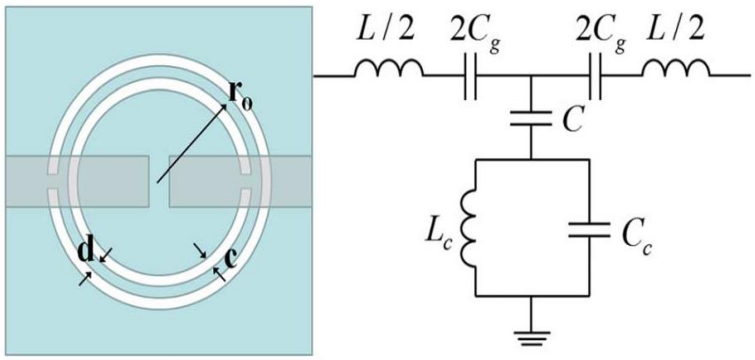

(a) ***(b)***

Fig. 4.10: (a) *CSRR loaded transmission line* ***(b)*** *Lumped element model. (Taken from Ref [69])*

From the equivalent circuit of the complementary split-ring resonators at the ground plane of the substrate, the CSRR can expressed as a resonant tank circuit with 'L_c' as the inductance and 'C_c' as the capacitance of the CSRR tank circuit. 'L' models the line inductance of the transmission line above the CSRR and 'C_g' represents the gap capacitance in the designed transmission line. Here 'C' is the capacitance due to the electrical coupling between the transmission line and the CSRR [70]. In the CSRR circuit shown in the above figure, 'L_c' is the parallel inductance of the two rings and is given by the equation Eq. 4.1 given below [71].

$$L_c = \frac{L_o}{4} \tag{4.1}$$

Here each inductance of the parallel rings is given by $L_o/2$ where 'L_o' is defined in the Eq. 4.2 given below [71].

$$L_o = 2\pi r_o L_{pul} \tag{4.2}$$

Here, 'L_o' is obtained for a single ring of average radius 'r_o' and the width of the ring 'c'. Here 'L_{pul}' is called as the inductance per unit length of the coplanar waveguide which connects the inner wall of the rings to the ground [71]. The capacitance 'C_c' of the CSRR resonant circuit can be approximated by the average radius, width of the wire and the dielectric [62]. The 'C_g' which is the total capacitance of the transmission line for designing a bandpass filter can be expressed in terms of 'C_s' and the 'C_{par}'. Here the 'C_{par}' is the parasitic capacitance which is given in the Eq. 4.3 [71].

$$C_{par} = C_f + C_L \tag{4.3}$$

Here 'C_f' is the fringing capacitance of the gap due to fringing of the fields and 'C_L' is the inductance of the transmission line. The capacitance 'C_g' is expressed in Eq. 4.4 given below [71].

$$C_g = 2C_s + C_{par} \tag{4.4}$$

Here, 'C_s' is the series capacitance of the gap. The series gap introduced in the transmission line on the phase opposite to the CSRR is mainly responsible for negative permittivity in the filter design. Thus combining the gaps and the CSRRs in the structure, a narrow band with simultaneously negative permeability and permittivity appears in the region close to the resonance frequency of the designed CSRR and hence exhibit a left-handed behavior in that band [72]. From the design of the bandpass filter, it can be said that the 'L_c' is useful for determining the central frequency of the filter and 'C_c' is used to the varying the bandwidth of the filter. The total capacitance 'C_g' of the transmission line is the key factor for varying the passband of the filter. The increase in the line capacitance increases the passband of the bandpass filter. As shown in the Eq. 4.4, the gap capacitance which is the sum of fringing capacitance, line capacitance and series gap capacitance can vary the bandwidth of the filter, but in our design model we do not restrict the variation to only series gap capacitance but also use a parallel line gap capacitance in the series gap in order to design a simple and better bandpass filter which has higher degree of freedom to vary the passband characteristic of the filter. The schematic of the proposed wideband bandpass filter with a parallel transmission line stub on it with a series gap on one side of the substrate and the CSRR in the opposite side of the substrate [69] is shown in the Fig. 4.11 below. There are eight design parameters for a bandpass filter which controls the central frequency and the bandwidth of the filter.

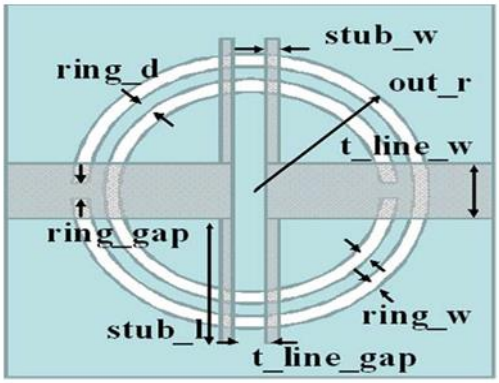

Fig. 4.11: *Design of a CSRR loaded bandpass filter. (Taken from Ref. [69])*

The eight design parameters crucial for designing a bandpass filter are the width of the ring '*ring_w*', ring distance between the two concentric rings '*ring_d*', ring gap in the rings '*ring_gap*', radius of the outer ring '*out_r*', the capacitance stub width '*stub_w*', the capacitance stub length '*stub_l*', transmission line width '*t_line_w*' and the transmission line gap '*t_line_gap*'.

The wideband bandpass filter (WBPF) is designed on a FR-4 (Lossy) substrate having its relative permittivity 'ε_r' equal to 4.4 and the height of the substrate '*h*' equal to 1.6 mm. The transmission line and the ground plane of the filter is made up of copper whose

conductivity 'σ' is equal to 5.8×10^7 S/m and the thickness of the copper 't' equal to 0.035 mm. The design parameters for the WBPF are formulated in the Table 4.1 given below.

Table 4.1 Design parameters of a CSRR loaded bandpass filter.

Parameters for CSRR loaded bandpass filter	Dimensions
Outer Ring radius (out_r)	5.0 mm
Ring Width (ring_w)	0.5 mm
Ring distance (ring_d)	0.35 mm
Ring gap (ring_g)	0.75 mm
Transmission line Width (t_line_w)	3.05 mm
Transmission line Length (t_line_l)	7.0 mm
Transmission line Gap (t_line_gap)	0.75 mm
Capacitance stub width (stub_w)	0.5 mm
Capacitance stub length (stub_l)	4.5 mm

The transmission line designed has width of 3.05 mm in order to have a characteristic impedance normalized to 50Ω so that maximum power is transferred from the waveguide port to the filter. The top view of the WBPF containing the transmission line having the capacitive gap and parallel stub capacitance is shown in the Fig. 4.12 (a) while the bottom view containing the CSRR which is etched on the substrate of the proposed WBPF is shown in the Fig. 4.12 (b).

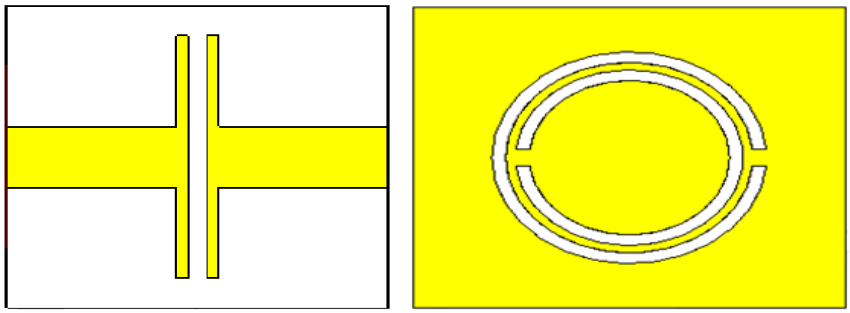

(a) ***(b)***

Fig. 4.12: (a) *Top view of designed bandpass filter,* ***(b)*** *Back view of CSRR containing CSRR.*

The Fig. 4.13 shows the two waveguide ports of the designed filter across which the S-parameters of the filter are measured.

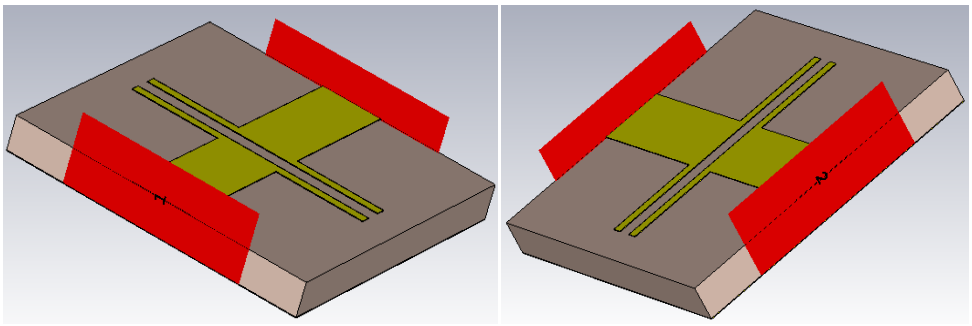

Fig. 4.13: *The waveguide ports for a microstrip bandpass filter.*

The frequency domain solver is used in CST Microwave Studio for obtaining the S-parameter of the designed bandpass filter. The Fig. 4.14 shows the simulated S(2,1) result of the filter.

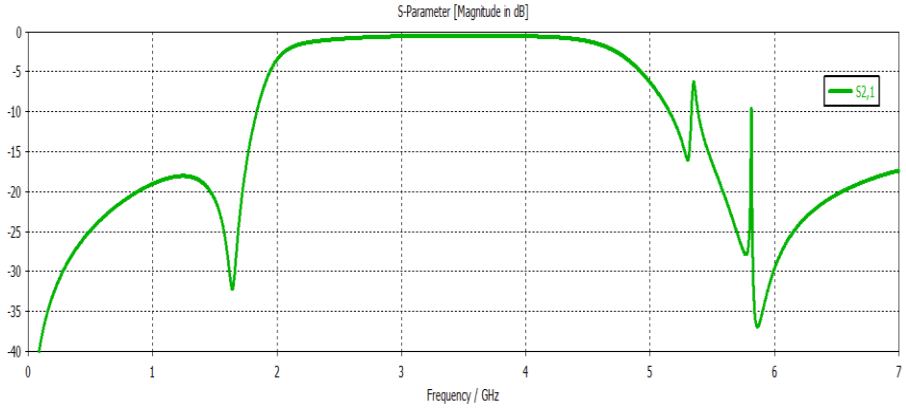

Fig. 4.14: *S(2,1) result of the designed bandpass filter.*

The S(2,1) result which is the transmission coefficient from port 1 to port 2 of the filter can be used to find the bandwidth of the filter with the help of -3dB points where the power of the of wave received at the port 2 becomes half the power inputted at the port 1. The Fig. 4.15 (a) and Fig. 4.15 (b) shows the upper and lower -3dB cutoff frequencies respectively. The difference between these -3dB cutoff frequencies gives the bandwidth of the designed filter.

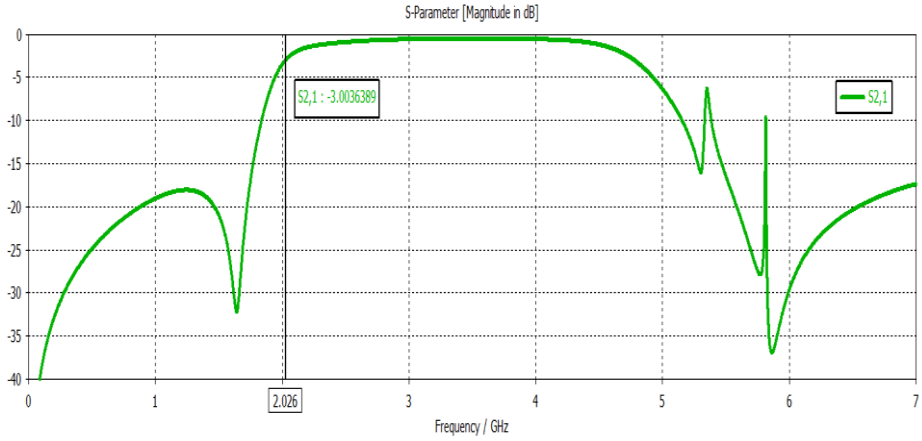

(a)

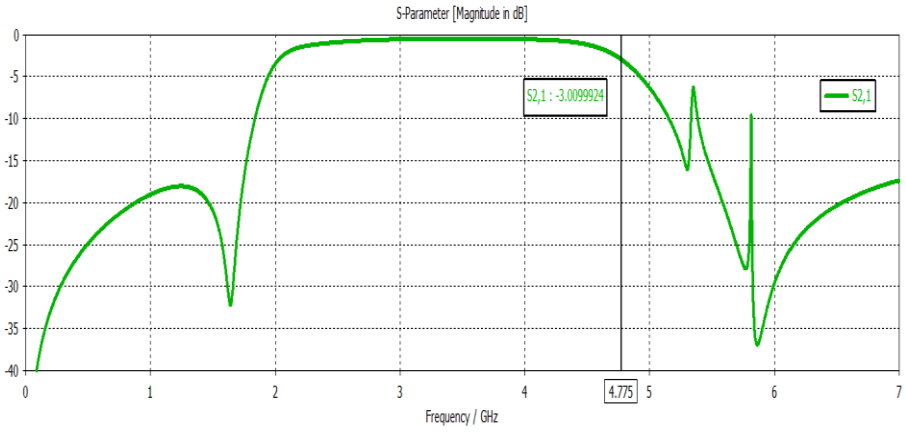

(b)

Fig. 4.15: (a) *Lower -3dB cutoff frequency,* ***(b)*** *Upper -3dB cutoff frequency.*

From the above graph it can be seen that the lower -3dB cutoff frequency of the bandpass filter is at **2.026 GHz** while the upper cutoff -3dB cutoff frequency of the designed filter is at **4.775 GHz**. The difference between the upper and lower cutoff frequency of the bandpass filter gives the bandwidth of the designed filter. Thus the bandwidth of the designed filter is approximately equal to **2.750 GHz**. From the S(2,1) parameter variation as a function of frequency, it can be seen that the central frequency of the designed filter is **3.375 GHz**. The quality factor 'Q' of the designed filter can be determined using the Eq. 4.5 as shown below.

$$Q = \frac{f_o}{BW} = \frac{f_o}{f_h - f_l} \tag{4.5}$$

Here, 'f_o' is the central frequency of the bandpass filter, 'f_h' is the -3dB upper cutoff frequency and 'f_l' is the -3dB lower cutoff frequency of the filter. From the above expression, the quality factor of the bandpass filter comes out to be **1.227**. Thus a compact size wideband bandpass filter is designed using the CSRR at the ground plane of the substrate and its passband and stopband plots are simulated in the software.

4.3 Fabrication and testing of the designed CSRR loaded bandpass filter

The CSRR loaded bandpass filter is designed on a printed circuit board (PCB) with a copper as the perfect electrical conductor (PEC) of height 0.035 mm on a FR-4 substrate having a dielectric constant of 4.4 and thickness equal to 1.6 mm. The layout of the designed transmission line and the CSRR is designed in Coral Draw graphic design software for preparing the masks. Once the mask is printed on the transparent sheet, the patch and the CSRR at the ground plane is fabricated using conventional photolithography process. The front and the back view of the fabricated CSRR loaded bandpass filter are shown in the Fig. 4.16.

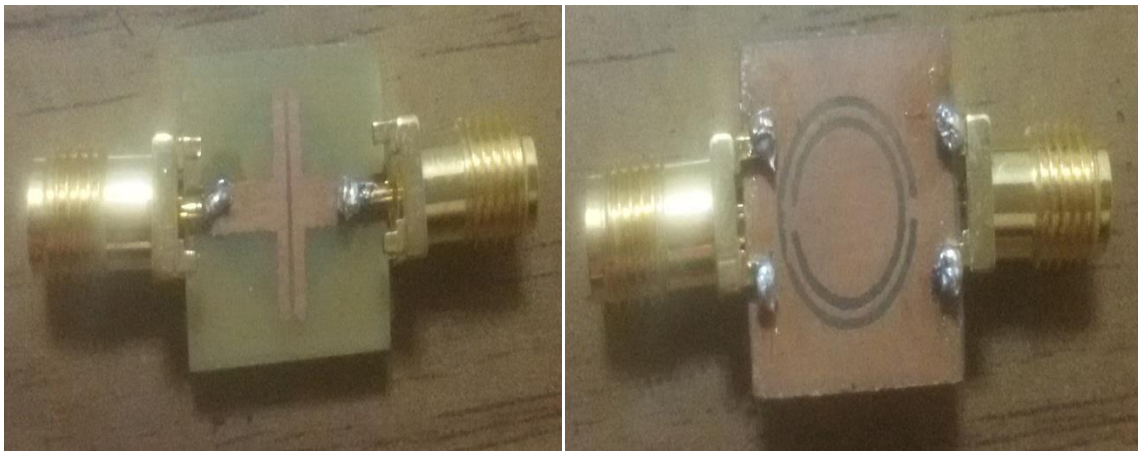

(a) ***(b)***

Fig. 4.16: (a) *Front view,* ***(b)*** *back view of fabricated CSRR loaded bandpass filter.*

The measurement and testing of the fabricated CSRR loaded bandpass filter is done using a Scalar Network Analyzer, Model No.: HP8757A having a sweep oscillator to control the display of the analyzer, Model No.: HP8350B. A RF Plug-In, Model No.: HP83525A is used to feed power to one of the port of the designed filter which is connected to it via Directional Bridge, Model No.: HP85027C. The Fig. 4.17 shows the tested result of the CSRR loaded bandpass filter.

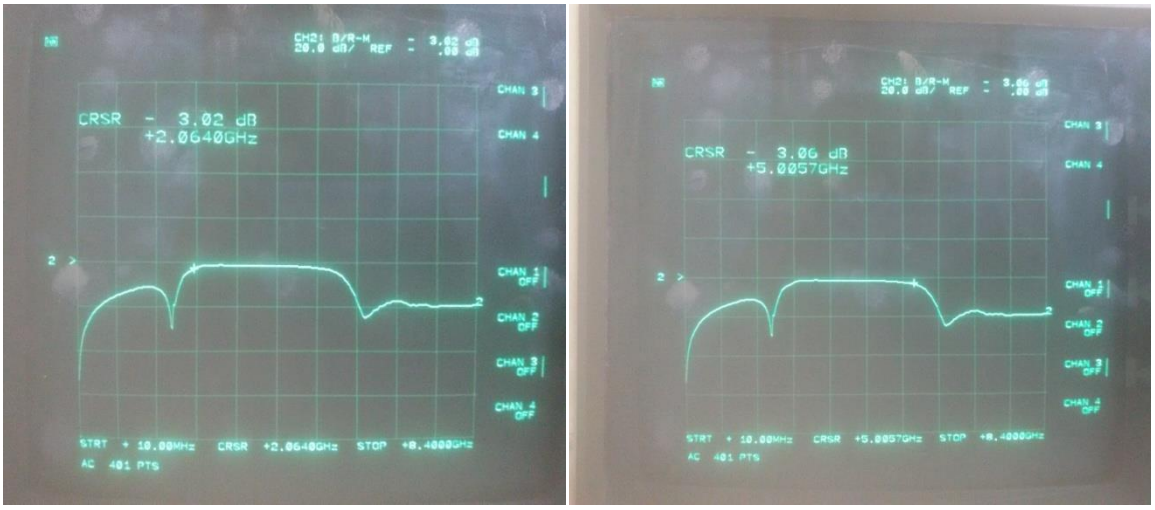

(a) ***(b)***

Fig. 4.17: *Tested result of CSRR loaded bandpass filter showing* ***(a)*** *lower cutoff frequency,* ***(b)*** *upper cutoff frequency*

The tested result of the CSRR loaded bandpass filters shows that the lower 3dB cutoff frequency of the fabricated component is equal to 2.0640 GHz and the upper 3dB cutoff frequency is equal to 5.0057 GHz which is nearly equal to the cutoff frequencies of the proposed bandpass filter. Thus the bandwidth of the fabricated filter is equal to 2.9417 GHz with a central frequency of 3.53485 GHz. The results obtained by testing the fabricated bandpass filter is in accordance with the proposed design with some error which is encountered during the fabrication of the component.

CHAPTER 5
Conclusion and Future Scope

5.1 Conclusion

In this thesis work, basic knowledge of the left-handed materials is studied, i.e. how these left-handed materials are different from the materials which are naturally found and follow a backward propagation of the wave in the material. The various progress and advancement in the field of metamaterials were studied and the property of the metamaterials to show a negative refractive index was also analyzed. The thesis analyzed the basic concept of metamaterials and how the combination of the wire array and the split ring resonator acts as a basic cell structure for the implementation the metamaterials. The wire array geometry placed at certain distance apart confines the electric field in it and showed a negative permittivity to a certain range called the plasma frequency, and the split ring resonator which confines the magnetic field around it produces a negative permeability in a certain range of frequency. The design geometry of the wired array and split ring resonators were also studied. With the basic knowledge of a metamaterials, a unit cell structure for a metamaterial was designed and simulated in CST Microwave Studio and the S-parameters results were obtained from the simulation and using S-parameter retrieval technique in the MATLAB, the range of frequencies in which the basic cell structure was computed which showed a negative refractive index and hence behaving as a metamaterial. The unit cell structure is designed on a FR-4(lossy) substrate having a height of 1.6 mm and relative permittivity of 4.4, and on it we designed a split ring resonator having its thickness t = 0.035 mm, lattice dimension a = 12.5 mm, the width of the ring w = 1.0 mm, the distance between the two rings d = 0.75 mm, the slit gap g = 1.5 mm and the length of the outer ring r = 10 mm. The results of the MATLAB show that this split ring resonator which confines the magnetic field around it showed a negative permeability in the range of 2.2 GHz to 2.6 GHz. The back side of the substrate was loaded with a symmetric wire geometry which had a width w = 1 mm and the thickness t = 0.035 mm which showed a negative permittivity to a range of 3.0 GHz. The program code for calculating the negative refractive index and the impedance for the unit cell structure were written in the MATALB using the S-parameter retrieval technique and its result showed that the refractive index of the unit cell has its negative refractive index in the range of 2.25 GHz to 2.5 GHz. Thus a basic unit cell metamaterial structure showing a negative refractive index in a particular range of frequency was designed and simulated in CST Microwave Studio and the results for impedance and refractive index were plotted in MATLAB.

This knowledge of basic unit cell structure was used to design a CSRR loaded microstrip patch antenna. The next chapter of this thesis introduced the basic knowledge of a microstrip patch antenna. A conventional microstrip patch antenna was designed on CST Microwave studio on a FR-4 (Lossy) substrate with a relative permittivity of 4.4 and height of 1.6 mm with a resonant frequency of 4 GHz, and the various performance parameters of the designed patch were computed during simulation. Then a CSRR loaded microstrip patch antenna was designed on the same substrate, i.e. the FR-4 (lossy) with the same height of the

substrate. The CSRR etched at the ground plane of the patch antenna has its lattice dimension a = 6.0 mm, outer ring length r = 5.0 mm, width of the ring w = 0.65, distance between the two rings d = 0.5 mm and the slit gap g = 0.4 mm. The CSRR designed showed a negative permittivity in the frequency range 4.5 GHz to 5.3 GHz. The CSRR loaded patch antenna was designed and simulated in CST Microwave Studio which had a resonant frequency of 4 GHz. The dimensions (width×length) of the patch for a designed CSRR loaded patch antenna are 17.50 mm and 14.86 mm and an area of 260.05 mm^2, while the conventional patch antenna designed has the dimensions (width×length) as 22.82 mm and 17.01 mm and an area of 388.1682 mm^2. Thus the CSRR loaded patch antenna operating at the same resonant frequency had its dimensions reduced by 33%. The CSRR loaded patch antenna with double-superstrate configuration was designed in order to improve the performance parameters of the patch antenna. The CSRR loaded patch antenna with DSC had the same operating frequency of 4 GHz and was designed on the same substrate. The proposed patch antenna with DSC had its directivity increased by the 2.51 dBi and its gain increased by 1.87 dB. Thus the proposed CSRR loaded patch antenna with DSC helped us in reducing the size of the patch antenna with better performance parameters when compared to a conventional patch antenna. The designed patch antenna was fabricated and tested to verify the simulation results obtained.

Further, the concept of this metamaterials where used to design a wideband band-pass filter. The equivalent model of the designed bandpass filter was also studied. The wideband band-pass filter was designed on a FR-4 (lossy) substrate with a height of 1.6 mm and the relative permittivity of 4.4. The filter designed has a CSRR etched at the ground plane with the dimensions of outer ring radius *out_r* = 5.0 mm, ring width *ring_w* = 0.5 mm, ring distance between the two rings *ring_d* = 0.35 mm and a ring gap *ring_g* = 0.75 mm which represented a parallel tank circuit for the bandpass filter to control the central frequency and bandwidth of the filter. The transmission line designed at the top of the substrate represents the series inductance and capacitance of the designed bandpass filter and has its dimensions of transmission line width *t_line_w* = 3.05 mm, *t_line_l* = 7 mm, *t_line_gap* = 0.75 mm, capacitance stub width *stub_w* = 0.5 mm and stub length *stub_l* = 4.5 mm. The designed bandpass filter has its lower cutoff frequency equal to 2.026 GHz and the upper cutoff frequency equal to 4.775 GHz. Thus the band-pass filter has bandwidth equal to 2.750 GHz and a central frequency of 3.375 GHz. The designed filter has the dimensions width equal to 15 mm and the length equal to 15 mm. Thus, a wideband bandpass filter with compact size is designed and simulated in CST Microwave Studio. The quality factor computed for the designed CSRR loaded bandpass filter has a value equal to 1.227. The wideband bandpass filter is fabricated and tested to verify the results obtained from the simulation.

5.2 Future work

The future work of this thesis includes the designing of a unit cell structure for metamaterials for different ranges of microwave frequency where the materials can exhibit negative permittivity and negative permeability and thus achieving negative refractive index for a composite medium. These metamaterial structures which exhibit left-handed properties in microwave band region can be used in designing the microwave components like antennas, filters, couplers, etc. The concept of unit cell metamaterial structure can also be used for designing the 2-D and 3-D structures for metamaterials which can be used as a composite

structure to enhance the properties of the microwave components. In recent technologies, the materials can also be used to design superlenses, absorbers for microwave radiation, cloaking devices, light and sound filtering and many passive microwave components.

The designed microstrip patch antenna with the concept of metamaterials and superstrate configuration can be used in future for designing small and compact microstrip antennas with enhanced performance characteristics. Hence the antenna size miniaturization can be used to reduce the size of the microwave components and pack more number of patch antennas onto a single device. Hence the packing efficiency as well as the performance of the designed antennas can be increased in the wireless communication systems. The superstrate configuration provides an easy and compatible way to improve the directivity and gain of the designed patch antennas based upon the applications of the microstrip patch antennas for microwave frequencies. The small size of patch antennas helps is reducing the cost and material used for fabricating the component.

The designed bandpass filter using CSRR at the ground plane can be used in future in the wireless communication systems for wideband and ultra-wideband applications where a certain microwave band like L-band, S-band, C-band, etc. is filtered out from the received signal in the various microwave systems. Moreover, the designed bandpass filters are compact and small in size as compared to the size of a conventional bandpass filters designed which makes a component more packing efficient and thus would help in future technology for making miniaturized components for wireless communication. Due to size miniaturization of the components, more number of microwave filters can be fabricated in a small region to reduce the cost and material used for the final fabricated microwave component.

References

[1] V. G. Veselago, "The electrodynamics of substances with simultaneously negative values of permittivity and permeability", Sov. Phys. USPEKHI, vol. 10, pp. 509, 1968.

[2] J. B. Pendry, A. J. Holden, W. J. Stewart and I. Youngs, "Extremely Low Frequency Plasmons in Metallic Mesostructures", Phys. Rev. Lett., vol. 76, pp. 4773, 1996.

[3] J. B. Pendry, A. J. Holden, D. J. Robbins, and W. J. Stewart, "Low frequency plasmons in thin-wire structures", Journal of Physics: Condensed Matter, vol. 10, pp. 4785, 1998.

[4] D. R. Smith, D. C. Vier, Willie Padilla, Syrus C. Nemat-Nasser, and S. Schultz, "Loop-wire medium for investigating plasmons at microwave frequencies", Appl. Phys. Lett., vol. 75, pp. 1425, 1999.

[5] J. B. Pendry, A. J. Holden, D. J. Robbins, and W. J. Stewart, "Magnetism from conductors and enhanced nonlinear phenomena", IEEE Trans. Microwave Theory Tech., vol. 47, pp. 2075, 1999.

[6] D. R. Smith, Willie J. Padilla, D. C. Vier, S. C. Nemat-Nasser, and S. Schultz, "Composite medium with simultaneously negative permeability and permittivity", Phys. Rev. Lett., vol. 84, pp. 4184, 2000.

[7] R. A. Shelby, D. R. Smith, S. C. Nemat-Nasser, and S. Schultz, "Microwave transmission through a two-dimensional, isotropic, lefthanded metamaterial", Appl. Phys. Lett., vol. 78, pp. 489, 2001.

[8] D. R. Smith, and N. Kroll, "Negative refractive index in left-handed materials", Phys. Rev. Lett., vol. 85, pp. 2933, 2000.

[9] R. A. Shelby, D. R. Smith, and S. Schultz, "Experimental verification of a negative index of refraction", Science, vol. 292, pp. 77, 2001.

[10] E. Cubukcu, K. Aydin, S. Foteinopolou, C. M. Soukoulis, and E. Ozbay, "Subwavelength Resolution in a Two-Dimensional Photonic Crystal Based Superlens", Phys. Rev. Lett., vol. 91, pp. 207401, 2003.

[11] Ertugrul Cubukcu, Koray Aydin, Ekmel Ozbay, S. Foteinopoulou, and Costas M. Soukoulis, "Electromagnetic waves: Negative refraction by photonic crystals", Nature, vol. 423, pp. 604, 2003.

[12] Kaan Guven, Koray Aydin, K. B. Alici, C. M. Soukoulis, and Ekmel Ozbay, "Spectral negative refraction and point focusing analysis of a two-dimensional left-handed photonic crystal lens", Phys. Rev. B, 2004.

[13] Chiyan Luo, Steven G., J. D. Joannopoulos, and J. B. Pendry, "All-angle negative refraction without negative effective index", Phys. Rev. B, vol. 65, pp. 104, 2002.

[14] M. Notomi, "Theory of light propagation in strongly modulated photonic crystals: Refractionlike behavior in the vicinity of the photonic band gap", Phys. Rev. B, vol. 62, pp. 10696, 2000.

[15] S. Foteinopoulou, E. N. Economou, and C. M. Soukoulis, "Refraction in Media with a Negative Refractive Index", Phys. Rev. Lett., vol. 90, pp. 107402, 2003.

[16] E. Cubukcu, "Subwavelength Resolution in a Photonic Crystal Superlens", Bilkent University M.Sc. Thesis, July 2003.

[17] N. Seddon and T. Bearpark, "Observation of the Inverse Doppler Effect", Science, vol. 302, pp. 1537, 2003.

[18] Jie Lu, Tomasz M. Grzegorczyk, Yan Zhang, Joe Pacheco, Jr., Bae-Ian Wu, Jin A. Kong, and Min Chen, "Cerenkov radiation in materials with negative permittivity and permeability", Optics Express, vol. 11, pp. 723, 2003.

[19] Anthony Grbic and George V. Eleftheriades, "Experimental verification of backward-wave radiation from a negative refractive index metamaterial", J. Appl. Phys., vol. 92, pp. 5930, 2002.

[20] P. Mondal, M. Mandal, A. Chakrabarty and S. Sanyal, "Compact bandpass filter with wide controllable fractional bandwidth", IEEE Microw. Wireless Component Lett., vol. 16, no. 10, pp. 540-542, 2006.

[21] J. C. Liu, D.-S. Shu, B. H. Zeng and D.-C. Chang, "Improved equivalent circuits for complementary split-ring resonator-based high-pass filter with c-shaped couplings", IET Microw. Antennas Propag., vol. 2, no. 6, pp. 622-626, 2008.

[22] Li, L.; Li, Y.; Yeo, T.S.; Mosig, J.R.; Martin, O.J.F. "A broadband and high-gain metamaterial microstrip antenna", Appl. Phys. Lett. 2010, pp. 96, 164101:1–164101:3.

[23] Wu, B.-I.; Wang, W.; Pacheco, J.; Chen, X.; Grzegorczyk, T.; Kong, J.A. "A study of using metamaterials as antenna substrate to enhance gain", Prog. Electromagn. Res. 2005, 51, pp. 295–328.

[24] Faruque, M.R.I.; Islam, M.T.; Misran, "N. Design analysis of new metamaterial for EM absorption reduction", Prog. Electromagn. Res. 2012, 124, pp. 119–135.

[25] Faruque, M.R.I.; Islam, M.T.; Misran, N. "Electromagnetic (EM) absorption reduction in a muscle cube with metamaterial attachment", Med. Eng. Phys. 2011, 33, pp. 646–652.

[26] Schurig, D.; Mock, J.J.; Justice, B.J.; Cummer, S.A.; Pendry, J.B.; Starr, A.F.; Smith, D.R. "Metamaterial Electromagnetic Cloak at Microwave Frequencies", Science 2006, 314, pp. 977–980.

[27] Landy, N.; Smith, D.R. "A full-parameter unidirectional metamaterial cloak for microwaves", Nat. Mater. 2013, 12, pp. 25–28.

[28] Cong, L.; Cao, W.; Zhang, X.; Tian, Z.; Gu, J.; Singh, R.; Han, J.; Zhang, W. "A perfect metamaterial polarization rotator", Appl. Phys. Lett. 2013, 103, pp. 171107:1–171107:4.

[29] M. C. K. Wiltshire, J. B. Pendry, I. R. Young, D. J. Larkman, D. J. Gilderdale, and J. V. Hajnal, "Microstructured magnetic materials for RF flux guides in magnetic resonance imaging," Science, vol. 291, pp. 849, 2001.

[30] R. W. Ziolkowski and E. Heyman, "Wave propagation in media having negative permittivity and permeability", Physical Review E., vol. 64, pp. 056625-1, Nov. 2001.

[31] J. B. Pendry, "Negative refraction makes a perfect lens", Phys. Rev. Lett., vol. 85, pp. 3966-3969, Oct. 2000.

[32] J. Pacheco Jr., T. M. Grzegorczyk, B. -. Wu, Y. Zhang and J. A. Kong, "Power propagation in homogeneous isotropic frequency-dispersive left-handed media", Phys. Rev. Lett., vol. 89, pp. 257401-1, Dec. 2002.

[33] C. L. Holloway, E. F. Kuester, J. Baker-Jarvis and P. Kabos, “A Double Negative (DNG) Composite Medium Composed of Magnetodielectric Spherical Particles Embedded in a Matrix,” IEEE Transactions on Antennas and Propagation, vol. 51, pp. 2596-2603, Oct. 2003.

[34] A. N. Lagar'kov and V. N. Kisel', “Electromagnetic properties of the simple bodies consisting of matter with negative permeability and permittivity”, Doklady Akademii Nauk, vol. 377, pp. 40-44, Jan. 2001.

[35] J. D. Baena, J. Bonache, F. Martin, R. M. Sillero, F. Falcone, T. Lopetegi, M. A. G. Laso, J. Garcia-Garcia, I. Gil, M. F. Portillo and M. Sorolla, “Equivalent-circuit models for split-ring resonators and complementary split-ring resonators coupled to planartransmission lines”, IEEE Trans. Microwave Theory Tech., vol. 53, pp. 1451-1460, Apr. 2005.

[36] C. L. Holloway, E. F. Kuester, J. Baker-Jarvis and P. Kabos, “A Double Negative (DNG) Composite Medium Composed of Magnetodielectric Spherical Particles Embedded in a Matrix”, IEEE Transactions on Antennas and Propagation, vol. 51, pp. 2596-2603, Oct. 2003.

[37] J. Pendry, A. Holden, W. Stewart, and I. Youngs, “Extremely low frequency plasmons inmetallic mesostructures”, Physical Review Letters, vol. 76, pp. 4773, Jun 1996.

[38] J. D. Jackson, “Classical Electrodynamics”, John Wiley, third ed., 1998.

[39] Ertugrul Cubukcu, Koray Aydin, Ekmel Ozbay, S. Foteinopoulou, andCostas M. Soukoulis, “Electromagnetic waves: Negative refraction by photonic crystals,” Nature, vol. 423, pp. 604, 2003.

[40] D. R. Fredkin and A. Ron, "Effectively left-handed (negative index) composite material," Appl. Phys. Lett., vol. 81, pp. 1753, Sep. 2002.

[41] C. Caloz, H. Okabe, T. Iwai, and T. Itoh, “ Transmission line approach of left handed (LH) materials,” Proc. USNC/URSI National Radio Science Meeting, San Antonio, TX, June 2002, vol. 1, p. 39.

[42] D. Smith, D.C. Vier, T. Koschny, C. Soukoulis, “Electromagnetic parameter retrieval from inhomogeneous metamaterials”, Phys. Rev. E 71, 036617, pp. 1-11, Mar. 2005.

[43] C. A. Balanis, “Antenna Theory, Analysis and Design”, John Wiley & Sons, New York, 1997.

[44] S. A. Schelkunoff, H.T.Friss, “Antennas: Theory and Practice”, New York: John Willy & Sons, 1952.

[45] JR James & P S Hall, “Handbook of Microstrip Antennas”, Peter Peregrinus Ltd., 1989.

[46] R Garg, P Bhartia, I Bahl, and A. Lttipiboon, “Microstrip antenna design handbook”, Artech House, 2000.

[47] C. A. Balanis, “Advanced Engineering Electromagnetics”, New York, John Wiley and Sons, 1989.

[48] M. Manteghi, Y. Rahmat-Samii, “Patch antennas using embedded lumped element delay line for size reduction”, Antennas and Propagation Society International Symposium, 2002.IEEE, vol. 4, pp. 2-5, 2002.

[49] T. Fukusako, T. Nakano, "A compact patch antenna using artificial ground structure with high permittivity substrate", Antennas and Propagation in Wireless Communication (APWC), 2015 IEEE-APS Tropical Conference, pp. 1548-1549, Sept., 2015.

[50] M Sanad, "Effect of the shorting posts on short circuit microstrip antennas", IEEE Antennas and Propagat. Society Int. Symposium Dig., vol. 2, pp. 794-797, Seattle, Washington, USA, Jun. 1994.

[51] K. F. Lee, Y. X. Guo, J. A. Hawkins, R. Chair, and K. M. Luk, "Theory and experiment on microstrip patch antennas with shorting walls", IEE Proc. Microw. Antennas Propagat., vol. 147, pp. 521-525, Dec. 2000.

[52] H. Iwasaki "A circularly polarized small-size microstrip antenna with a cross slot", IEEE Trans. Antennas Propagat., vol. AP-44, no 10, pp. 1399-1401 Oct, 1996.

[53] F. Falcone, T. Lopetegi, M. A. G. Laso, J. D. Baena, J. Bonache, M. Beruete, R. Marques, F. Martin and M. Sorolla, "Babinet principle applied to the design of metasurfaces and metamaterials", Phys. Rev. Lett., vol. 93, pp. 197401-1, Nov. 2004.

[54] A. A. Roseline, K. Malathi and A. K. Shrivastav, "Enhanced performance of a patch antenna using spiral-shaped electromagnetic bandgap structures for high-speed wireless networks", IET Microw., Antennas Propag., vol. 5, no. 14, pp. 1750-1755, 2011.

[55] B. Zhu, Z. N. Chen, and Y. Feng, "Fully substrate-integrated high-gain thin Fabry-Perot cavity antennas", Microwave Conference Proceedings (APMC), 2011 Asia-Pacific. 2011.

[56] S. Sakai and H. Arai, "Directivity gain enhancement of small antenna by parasitic patch", IEEE Antennas and Propagation Society International Symposium, vol. 1, 1998, pp. 320-323.

[57] F. Kaymaram and L. Shafai, "Enhancement of microstrip antenna directivity using double-superstrate configurations," Canadian J. Elect, Comput.Eng., vol.32, no. 2, pp.77-82, 2007.

[58] Y. Sugio, T. Makimoto, S. Nishimura, and H. Nakanishi, "Gain enhancement of dielectric covered antennas with a ground plane," in Proc. IEE Int. Conf. Antennas Propagat., Apr. 1983, pp. 289–293.

[59] Chi-Sen Lin, Shun-Shi Zhong, Jian-Hui Shi, and Yuan Wang, "Gain enhancement technique for microstrip antennas", in IEEE Int. Symp. Antennas Propagat., vol. 1, June 26–30, 1989, pp. 454–457.

[60] B.H. Sasser, "A highly thinned array using the image element", in Proc. IEEE Int.Symp. Antennas Propagat., Quebec, Que., 1980, pp. 150–153.

[61] J.D Rhodes, "Theory of Electrical Filters", Pitman Press Ltd, Bath, Great Britain. 1976.

[62] F. Falcome and M. Sorolla et al., "Effective negative stopband microstrip lines based on complementary split ring resonators", IEEE Microw. Wireless Compon. Lett., vol. 14, no. 6, pp. 280–282, Jun. 2004.

[63] J. Bonache, M.Gil, I. Gil, J. Garcia-Garcia, and F.Martin, "On the electrical characteristic of complementary metamaterial resonators", IEEE Microw. Wireless Compon. Lett., vol. 16, no. 10, pp. 543–545, Oct. 2006.

[64] P. Mondal, M. K. Mandal, A. Chaktabarty, and S. Sanyal, "Compact bandpass filters with wide controllable fractional bandwidth", IEEE Microw. Wireless Compon. Lett., vol. 16, no. 10, pp. 540–542, 2006.

[65] J.-F. Huang, J.-Y. Wen, and M.-C. Huang, "Design of a compact planar UWB filter for wireless communication applications", in 2009Int. Conf. WCSP, pp. 1–4.

[66] J.-G. Liu et al., "An improved equivalent circuit model for CSRR based bandpass filter design with even and odd modes", IEEE Microw. Wireless Compon. Lett., vol. 20, no. 4, pp. 193–195, Apr. 2010.

[67] J.-C. Liu, H.-C. Lin, B.-H. Zeng, K.-D. Yeh and D.-C. Chang, "An improved equivalent circuit model for CSRR-based bandpass filter design with even and odd modes", IEEE Microw. Wireless Compon. Lett., vol. 20, no. 4, pp. 193-195, 2010

[68] L. Athukorala and D. Budimir, "Compact dual-mode open loop microstrip resonators and filters", IEEE Mirow. Wireless Compon. Lett., vol. 19, no. 11, pp. 698-700, 2009

[69] Koon-Tae Kim , Jae-Hyeong Ko , Kyung Choi ,and Hyeong-Seok Kim, "Optimum Design of Wide band Bandpass Filter With CSRR-Loaded Transmission Line Using Evolution Strategy", IEEE Transactions On Magnetics, Vol. 48, No. 2, February 2012

[70] X. Luo, H. Qian, J.-G. Ma, and E.-P. Li, "Wideband bandpass filter with excellent selectivity using new CSRR-based resonator", Electron. Lett., vol. 46, no. 20, pp. 1390–1391, 2010.

[71] Marques, R.; Martín, F.; Sorolla, M., "Metamaterials with Negative Parameters: Theory, Design and Microwave Applications", John Wiley & Sons, Inc.: Hoboken, NJ, USA, 2008.

[72] J. D. Baena et al., "Equivalent-circuit models for split-ring resonators and complementary split-ring resonators coupled to planar transmission line", IEEE Trans. Microw. Theory Tech., vol. 53, no. 4, pp.1451–1461, 2005.